

DEVELOPMENT OF NON-INVASIVE AND BIOCOMPATIBLE THIN FILM
MICRO-EXTRACTION CONTACT LENS-TYPE DEVICES COMPATIBLE
FOR IN VIVO METABOLOMICS INVESTIGATIONS FROM EYE SURFACE

A THESIS SUBMITTED TO
THE GRADUATE SCHOOL OF NATURAL AND APPLIED SCIENCES
OF
MIDDLE EAST TECHNICAL UNIVERSITY

BY

ATAKAN ARDA NALBANT

IN PARTIAL FULFILLMENT OF THE REQUIREMENTS
FOR
THE DEGREE OF MASTER OF SCIENCE
IN
CHEMISTRY

SEPTEMBER 2020

Approval of the thesis:

**DEVELOPMENT OF NON-INVASIVE AND BIOCOMPATIBLE THIN
FILM MICRO-EXTRACTION CONTACT LENS-TYPE DEVICES
COMPATIBLE FOR IN VIVO METABOLOMICS INVESTIGATIONS
FROM EYE SURFACE**

submitted by **ATAKAN ARDA NALBANT** in partial fulfillment of the requirements for the degree of **Master of Science in Chemistry, Middle East Technical University** by,

Prof. Dr. Halil Kalıpçılar
Dean, Graduate School of **Natural and Applied Sciences** _____

Prof. Dr. Cihangir Tanyeli
Head of the Department, **Chemistry** _____

Assoc. Prof. Dr. Ezel Boyacı
Supervisor, **Chemistry, METU** _____

Examining Committee Members:

Prof. Dr. Bekir Salih
Chemistry, Hacettepe University _____

Assoc. Prof. Dr. Ezel Boyacı
Chemistry, Middle East Technical University _____

Prof. Dr. Ahmet Emin Erođlu
Chemistry, İzmir Institute of Technology _____

Prof. Dr. Gülay Ertaş
Chemistry, Middle East Technical University _____

Asst. Prof. Dr. Süreyya Özcan Kabasakal
Chemistry, Middle East Technical University _____

Date: 01.09.2020

I hereby declare that all information in this document has been obtained and presented in accordance with academic rules and ethical conduct. I also declare that, as required by these rules and conduct, I have fully cited and referenced all material and results that are not original to this work.

Name, Last name : Atakan Arda Nalbant

Signature :

ABSTRACT

DEVELOPMENT OF NON-INVASIVE AND BIOCOMPATIBLE THIN FILM MICRO-EXTRACTION CONTACT LENS-TYPE DEVICES COMPATIBLE FOR *IN VIVO* METABOLOMICS INVESTIGATIONS FROM EYE SURFACE

Nalbant, Atakan Arda
Master of Science, Chemistry
Supervisor: Assoc. Prof. Dr. Ezel Boyacı

September 2020, 153 pages

In this thesis, the aim was to develop biocompatible extractive thin films in contact lens geometries with application potential for *in vivo* sampling of small molecules from the eye surface with the ultimate goal of being suitable for untargeted metabolomics and biomarker discoveries. For this purpose, polydimethylsiloxane was functionalized with amine-containing groups using in situ modification approach and thin films were characterized with Fourier transform infrared spectroscopy, energy dispersive x-ray analysis, thermogravimetric analysis, and contact angle measurements. To investigate the thin films under representative conditions of eye surface contact lens geometries and *in vitro* agarose gel eye model were prepared in 3D printed molds. To investigate the extractive capabilities of the thin films, various metabolites found on the eye surface such as representative lipids, amino acids, neurotransmitters, and other metabolites were used. Extractive capabilities of modified and unmodified polydimethylsiloxane thin films were compared by extractions from aqueous solutions and *in vitro* eye models after separation and detection of the analytes with liquid chromatography/mass spectrometry. Extractions showed that modified extractive lenses had between 60 to 130% increased extractive capability towards polar analytes and similar extractive capability towards non-polar analytes compared to unmodified

polydimethylsiloxane extractive lenses. Composition of the desorption solvent and desorption time were optimized as ACN:MeOH:H₂O (40:40:20, v/v/v/) and 30 minutes, respectively. Extractions using modified extractive lenses from the agarose *in vitro* eye model showed good repeatability with RSD% values ranging between 5 to 18% and good linearity in the tested range of 50.0-500.0 ng mL⁻¹ for all analytes.

Keywords: thin-film microextraction, metabolomics, mass spectrometry, biocompatible materials

ÖZ

GÖZ YÜZEYİNDEN *İN VİVO* METABOLOMİKS ÇALIŞMALARI İÇİN KULLANILABİLECEK LENS ŞEKLİNDE TASARLANMIŞ İNVAZİF OLMAYAN VE BİYO-UYUMLU MİKROEKSTRAKSİYON İNCE FİMLERİNİN GELİŞTİRİLMESİ

Nalbant, Atakan Arda
Yüksek Lisans, Kimya
Tez Yöneticisi: Doç. Dr. Ezel Boyacı

Eylül 2020, 153 sayfa

Bu çalışmanın amacı, göz yüzeyinden küçük moleküllerin ekstraksiyonunda kullanılabilir ve kontakt lens geometrisine sahip ince filmlerin hazırlanması ve incelenmesidir. Hazırlanan ince filmlerin nihai amacı hedefsiz metabolomiks ve biyoışareyetlici keşfi çalışmalarında kullanılmak üzere ve potansiyel olarak *in vivo* çalışmalarında kullanılabilir özellikleri sahip olmalarıdır. Katı faz mikroekstraksiyon (SPME), analitlerin ince bir fiber ucuna kaplanmış ekstraktif faz ile numune arasında dağılım dengesi geliştirmesine dayanan örnekleme ve örnek hazırlama tekniğidir. Bu amaçlar doğrultusunda, polidimetilsiloksan bazlı ince filmler amin fonksiyonel gruplarına sahip olacak şekilde sentezlenmiş ve 3B baskılama ile hazırlanan kalıplar sayesinde kontakt lens şekline getirilmiştir. Hazırlanan ince filmler Fourier dönüşümlü kızılötesi spektroskopisi, enerji dönüşümlü x-ışını spektroskopisi, termogravimetrik analiz ve temas açısı ölçümleri ile karakterize edilmiştir. Hazırlanan ince filmlerin ekstraksiyon becerilerinin incelenmesi için göz yüzeyindeki ufak biyomolekülleri temsil edecek şekilde seçilen analitler yüksek performanslı sıvı kromatografi ve kütle spektrometresi kullanılarak incelenmiştir. Modifiye edilmiş ince filmlerin ekstraksiyon becerileri farklı analit derişimlerinde hazırlanmış su çözeltileri ve 3B baskılama tekniğiyle hazırlanmış *in vitro* agaroz hidrojel göz modellerinden gerçekleştirilen ekstraksiyonlar ile

incelenmiştir. Yapılan deneyler sonucunda modifiye edilmiş ince filmlerin, modifiye edilmemiş polidimetilsiloksan ince filmlere göre, polar analitleri %60 ila %130 arasında daha iyi ekstrakte ettiği ve apolar analitleri benzer oranlarda ekstrakte ettiği görülmüştür. Desorpsiyon solventi ve desorpsiyon süresi parametreleri incelenmiş, ACN:MeOH:H₂O (40:40:20, v/v/v) ve 30 dakika olarak optimize edilmiştir. *In vitro* göz modeli kullanılarak yapılan deneylerde, modifiye edilmiş ince filmlerin iyi tekrarlanabilirliğe ve lineerliğe sahip olduğu %5 ila %18 arasında değişen RSD değerleri ve 50.0 – 500.0 ng mL⁻¹ konsantrasyon aralığındaki ekstraksiyonlar ile gösterilmiştir.

Anahtar Kelimeler: ince film mikroekstraksiyon, metabolomiks, kütle spektrometre, biyo-uyumlu malzeme

“Don't Panic.”

— Douglas Adams, *The Hitchhiker's Guide to the Galaxy*

This thesis is dedicated to my mother, aunt and grandmother, they say it takes a village to raise a child, but three women were enough to raise me.

ACKNOWLEDGMENTS

The author wishes to express his deepest gratitude to his supervisor, Assoc. Prof. Dr. Ezel Boyacı for her patience, guidance, criticism, encouragement, and insight throughout the research.

The author would also like to thank Prof. Dr. Bekir Salih for his suggestions, comments, and generously allowing the use of their laboratory equipment. The author also extends his gratitude for Dr. Mehmet Atakay for his patient and supportive guidance.

The author also thanks Dr. Ceyhun Kırıklı for allowing the use of their 3D printer and his helpful insights in the development of the lens and eye model molds.

The author also wishes to thank Prof. Dr. Jale Hacalođlu and Nehir Utku for their help in the characterization of thin films by thermogravimetric analysis.

The author thanks Prof. Dr. Ahmet Emin Erođlu, Prof. Dr. Bekir Salih, Prof. Dr. Göluy Ertas, Asst. Prof. Dr. Süreyya Özcan Kabasakal for their corrections and valuable input.

The technical assistance of Ms. Selin Özesen, Ms. Kübra Kahremanođlu, Ms, Ezgi Rana Temel is much appreciated and acknowledged.

Last but not least, I would like to thank my family and friends for their kind support, and my wife Müge Özcan for her assuring and calm presence and her constructive criticisms.

This work is funded by the Scientific and Technological Research Council of Turkey under grant number TUBİTAK 118Z435.

TABLE OF CONTENTS

ABSTRACT.....	v
ÖZ vii	
ACKNOWLEDGMENTS	x
TABLE OF CONTENTS.....	xi
LIST OF TABLES.....	xiv
LIST OF FIGURES	xvi
LIST OF ABBREVIATIONS.....	xix
LIST OF SYMBOLS	xxi
CHAPTERS	
1 INTRODUCTION	1
1.1 Anatomy of the human eye	2
1.2 Chemical composition of human tears.....	3
1.3 Biomarkers in the human eye	6
1.3.1 Disease-specific biomarkers in the human eye and diagnostic approaches...	7
1.3.2 Techniques and technologies for biomarker identification in the tear film.	12
1.4 Sampling and sensing from the eye surface.....	15
1.5 Solid-phase microextraction	17
1.5.1 Fundamentals of SPME (and TFME)	18
1.5.2 Applications of SPME (and TFME)	22
1.6 Aim of the Study	33
2 EXPERIMENTAL	35
2.1 Reagents and Materials	35

2.2	Instruments	36
2.3	Design of extractive thin film molds	36
2.4	Design of the <i>in vitro</i> eye model mold	38
2.5	Synthesis of contact lens type thin films	39
2.5.1	Post-modification method	40
2.5.2	<i>In situ</i> modification method.....	41
2.6	Characterization of extractive thin films	48
2.7	Preparation of <i>in vitro</i> eye model	49
2.8	Development of LC-MS methods	51
2.9	Optimization of extraction parameters	55
2.9.1	Optimization of extractions from PBS buffer solutions	55
2.9.2	Optimization of extractions from <i>in vitro</i> eye model	57
3	RESULTS AND DISCUSSION.....	61
3.1	Evaluation of optimization of synthesis of extractive thin films.....	61
3.2	Characterization of extractive thin films	69
3.2.1	FTIR characterization of thin films	69
3.2.2	Contact angle measurements of thin films	72
3.2.3	Thermogravimetric analysis of thin films	74
3.2.4	Scanning electron microscopy and energy dispersive x-ray analysis	76
3.3	LC-MS analysis	77
3.3.1	HILIC-LC-MS method: chromatographic separation of polar analytes.....	79
3.3.2	Reverse phase LC-MS method chromatographic separation of non-polar analytes	81
3.4	Extraction of selected analytes with synthesized thin films	81

3.4.1	Comparison of extraction performances of thin films	81
3.4.2	Optimization of desorption solvent.....	84
3.4.3	Optimization of desorption time	88
3.4.4	Extractions from <i>in vitro</i> eye model	92
4	SUMMARY AND CONCLUSION	105
	REFERENCES	109
	APPENDICES	
A.	Chromatograms and mass spectra of analytes	147
B.	Instrumental calibration curves for analytes	152

LIST OF TABLES

TABLES

Table 1.1 Biomarkers associated with ocular and systematic diseases and disorders reproduced with additions and with permission from [35] and Springer (continued for next two pages).	9
Table 1.2 Applications of SPME. Reproduced with permission from [203] and ACS (continued for next six pages).....	23
Table 1.3 Summary of skin sampling methods. Reproduced with permission from [205] and MDPI.....	32
Table 2.1 Parameters for -OH terminated PDMS modification reactions (continued on the next page).	44
Table 2.2 Parameters for -OH terminated PMHS (type II thin films) modification reactions.....	48
Table 2.3 LC parameters for HILIC method (polar analytes).....	52
Table 2.4 MS parameters used in HILIC LC-MS method for polar analytes	53
Table 2.5 LC parameters for reverse phase method (non-polar analytes).....	54
Table 2.6 MS parameters used in reverse phase LC-MS method for non-polar analytes	54
Table 2.7 Optimization of desorption parameters for extractive thin films (Extraction conditions; extraction time: 120 mins, extraction volume: 4.0 mL, extraction agitation: 1200 rpm)	56
Table 3.1 Physical and visual evaluation of type I thin films	62
Table 3.2 Physical and visual evaluation of type II thin films	68
Table 3.3 EDX analysis for unmodified PDMS, type I and type II thin films.....	77
Table 3.4 Physicochemical properties of analytes	78
Table 3.5 Observed m/z and calculated LOQ and LOD values for polar analytes .	80
Table 3.6 Observed m/z and calculated LOQ values for non-polar analytes.....	81
Table 3.7 Calculated $t_{experimental}$ values for non-polar analyte desorptions with ACN:MeOH:H ₂ O and ACN:MeOH ($t_{critical} = 2.78$)	86

Table 3.8 Calculated $t_{experimental}$ values for non-polar analyte desorptions with ACN:MeOH and ACN:IPA:H ₂ O ($t_{critical} = 2.78$).....	86
Table 3.9 Calculated $t_{experimental}$ values for non-polar analyte desorptions with ACN:MeOH:H ₂ O and ACN:IPA:H ₂ O ($t_{critical} = 2.78$)	86
Table 3.10 Calculated $t_{experimental}$ values for amount of extracted analytes from 30 and 60-minute desorptions ($t_{critical} = 2.78$).....	89
Table 3.11 Recovery, (R%), values of all analytes for extractive contact lenses ...	95
Table 3.12 Repeatabilities of extraction of selected analytes by type II thin films	101

LIST OF FIGURES

FIGURES

Figure 1.1. Anatomy of the human eye.	3
Figure 1.2 Three diagrams of different models of the tear film,	5
Figure 1.3 The number of untargeted, case-control omics studies performed for multifunctional eye diseases up to date until 2017. Reproduced with permission from [34] and ARVO.....	7
Figure 1.4 Conceptual illustration of a contact lens biosensor. Reproduced with permission from [165] and MDPI.	16
Figure 1.5 (a) Schematic diagram of the “membrane sandwich” headspace sampling for skin volatiles sampling.	31
Figure 1.6 Schematic representation of the proposed extraction of analytes with the contact lens type devices from the eye surface	34
Figure 2.1 3D printed mold for contact lens type extractive thin films,	37
Figure 2.2 The conjoined form of the mold for contact lens type thin films,	38
Figure 2.3 Molds of the eye model designed for in vitro extraction experiments,..	39
Figure 2.4 Proposed schematic representation of PDMS surface functionalization	41
Figure 2.5 Preparation of type I thin films	42
Figure 2.6 Reaction scheme for modification of -OH terminated PDMS with APTES precursor.....	43
Figure 2.7 Molecular structures of PDMS (on the left) and PMHS (on the right)..	45
Figure 2.8 Reaction scheme for modification of PMHS with hydrolyzed APTES (hydrolysis of APTES is identical to one shown in Figure 2.6).....	46
Figure 2.9 Preparation of type II thin films.....	47
Figure 2.10 a) 3D printed mold (conjoined) b) two separate parts of the mold c) the in vitro eye model before being removed from the mold d) in vitro eye model after removed from the mold	50
Figure 2.11 Relative mass loss of <i>in vitro</i> eye models prepared with agarose hydrogels with different gel concentrations	51

Figure 2.12 A typical extraction from PBS solutions spiked with analytes by extractive thin films	56
Figure 2.13 A typical extraction and desorption scheme from <i>in vitro</i> eye models spiked with analytes by extractive lens type thin films	58
Figure 3.1 FTIR spectra of unmodified PDMS thin films before.....	69
Figure 3.2 FTIR spectra of type I (APTES modified -OH terminated PDMS) thin films	70
Figure 3.3 FTIR spectra of type II (APTES modified PMHS) thin films.....	72
Figure 3.4 Contact angle measurements for unmodified PDMS, type I, and type II thin films.	73
Figure 3.5 TGA curves of extractive thin films	75
Figure 3.6 SEM images of (a) unmodified PDMS ,(b) type I, and (c) type II thin films, 500x magnification	76
Figure 3.7 Comparison of PDMS, Type I, and Type II thin films from PBS solutions	82
Figure 3.8 Comparison of desorption solvent effectiveness for polar analytes	87
Figure 3.9 Comparison of desorption solvent effectiveness	88
Figure 3.10 (a) Comparison of the effect of desorption times on extracted amount of polar analytes	90
Figure 3.11 (a) Comparison of the effect of desorption times on extracted amount of non-polar analytes.....	91
Figure 3.12 Comparison of extractive thin films for polar analytes by extractions from <i>in vitro</i> eye model.....	93
Figure 3.13 Comparison of extractive thin films for non-polar analytes by extractions from <i>in vitro</i> eye model	94
Figure 3.14 Extraction time profile for polar analyte extractions from <i>in vitro</i> eye model.....	97
Figure 3.15 Extraction time profile for non-polar analyte extractions from <i>in vitro</i> eye model	98
Figure 3.16 Extraction calibration curves for type II lenses.....	102

Figure A.1 Mass spectrum of acetylcarnitine.....	147
Figure A.2 Mass spectrum of acetylcholine	147
Figure A.3 Mass spectrum of adenosine	148
Figure A.4 Mass spectrum of retinoic acid	148
Figure A.5 Mass spectrum of cholesterol.....	148
Figure A.6 Mass spectrum of citrulline.....	149
Figure A.7 Mass spectrum of creatine.....	149
Figure A.8 Mass spectrum of DHA.....	149
Figure A.9 Mass spectrum of GABA	150
Figure A.10 Mass spectrum of glutamine	150
Figure A.11 Mass spectrum of phenylalanine.....	150
Figure A.12 Mass spectrum of proline	151
Figure A.13 Mass spectrum of tryptophan	151
Figure B.1 Instrumental calibration curves for polar analytes (continued).....	152
Figure B.2 Instrumental calibration curves for non-polar analytes.....	153

LIST OF ABBREVIATIONS

ELISA	Enzyme-linked immunosorbent assay
EDX	Energy dispersive x-ray analysis
ESI	Electrospray ionization
FTIR	Fourier transform infrared spectroscopy
HPLC	High-performance liquid chromatography
LC	Liquid chromatography
MALDI	Matrix-assisted laser desorption ionization
MS	Mass spectrometry
MS/MS	Tandem mass spectrometry
MRM	Multiple reaction monitoring
SDS-PAGE	Sodium dodecyl sulfate-polyacrylamide gel electrophoresis
SELDI	Surface-enhanced laser desorption/ionization
SEM	Scanning electron microscopy
SPME	Solid-phase microextraction
TFME	Thin-film microextraction
TGA	Thermogravimetric analysis
TOF	Time-of-flight
TWA	Time-weighted average

LIST OF SYMBOLS

°C degree Celsius

CHAPTER 1

INTRODUCTION

The human eye is a complex and intricate organ, developed from the forebrain of the embryo, and made up of numerous layers of tissue, including all three embryological tissues. Naturally, the development of the eye involves many genes, and nearly 25% of all phenotypes linked to hereditary genetic disorders were associated with the eye [1]. Excess of 200 human loci that involve genetic ocular diseases has been mapped, including developmental eye disorders as well as disorders that involve other tissues [2,3]. The fact that the human eye is composed of different types and layers of tissue makes the eye susceptible to different types of diseases and disorders [4,5]. The spatial relationship of the eye to the brain creates a unique metabolomic window that can be used to peer into biomolecules related to diseases and disorders related to the brain. A large number of capillary vessels to keep the eye well supplied with blood also carry all types of metabolites that can be investigated for systemic disease and disorders. Therefore, it is of paramount importance that reliable sampling techniques that lead to reproducible results are employed while sampling from the human eye. The golden standard in clinical research for investigating eye diseases and disorders is tear sampling [6], and biopsies from patients (requires consent of patients during regular biopsies) as well as organ donors. However, a 2018 survey with 407 participants have shown that 57% of scientists find it difficult to obtain eye samples from local eye banks, 47% find it “difficult” or “very difficult” to find adequate tissue samples for their research, 43% regularly limit the scope of their research due to difficulty in obtaining samples that meet their study criteria and 43% reported to question their findings due to the quality of tissue samples they have obtained [7]. This thesis aims to prepare, characterize, and investigate the extractive performance of biocompatible and flexible thin films with contact lens geometries for extraction of small molecules that have different polarities and with the future aim to potentially

be used for non-invasive *in vivo* sampling from the human eye. It should be noted with an emphasis that actual *in vivo* investigations are outside the scope of this thesis, and *in vitro* experiments using eye models prepared with agarose hydrogel are carried out instead to compare the performances of prepared extractive lenses. In order for the extractive lenses to be suitable for *in vivo* applications, a biocompatible polymer, polydimethylsiloxane (PDMS) and its derivatives, were modified with polar functional groups to increase its extractive capabilities towards polar, hydrophilic analytes. Extracted analytes were analyzed using LC-MS to establish the extractive capabilities of synthesized contact lens extractive devices.

1.1 Anatomy of the human eye

The anatomy of the eye, albeit much more complex and in need of a detailed examination than the one offered in this thesis, can broadly be divided into two parts as the anterior (outer) and the posterior (inner) segments. The anterior segment includes the cornea, conjunctiva, aqueous humor, iris, ciliary body, and lens. Meanwhile, the posterior segment is composed of the sclera, choroid, retina, and vitreous [8]. Figure 1.1 shows the basic anatomy and of the human eye. The biomarkers that are contained or circulated in the anterior segment are of interest in this study, especially the integrated functional unit called as ‘lacrimal functional unit’ (LFU), which is comprised of the ocular surface (the cornea, conjunctiva, and meibomian glands), the lacrimal glands and the sensory and motor nerves. Major components of human tear come from secretory glands located in the eye, such as the lacrimal glands. However, conjunctival vessels can carry biomolecules from other parts of the body, which can pass to tears, allowing information on systemic diseases in other body parts to be gathered from the eye surface.

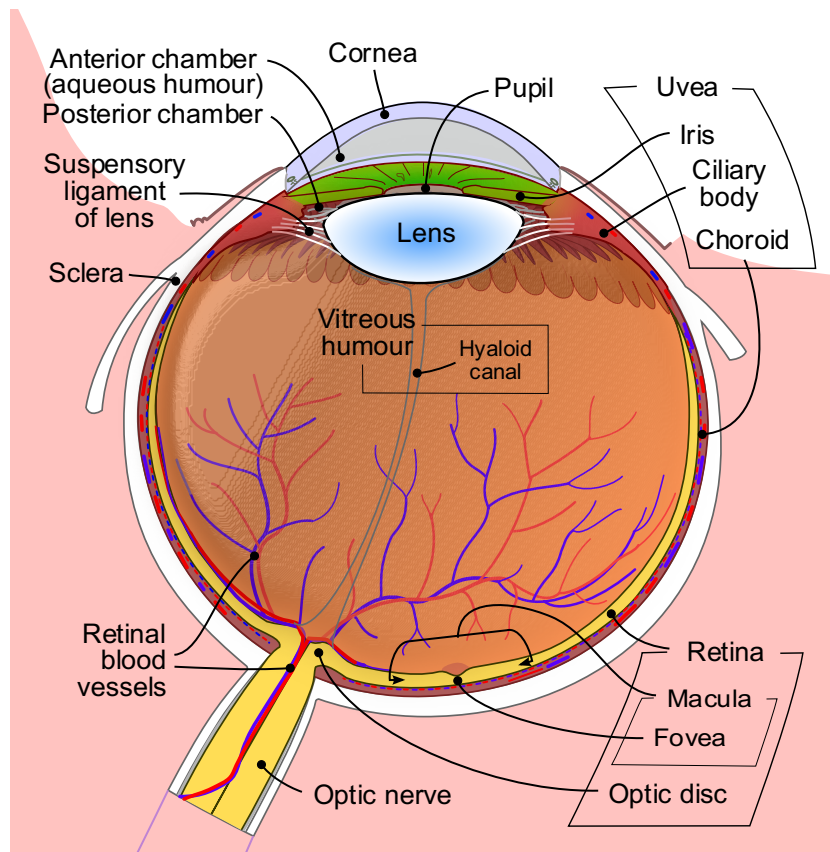


Figure 1.1. Anatomy of the human eye.

(Rhcasilhos and Jmarchn. 2007. Diagram of the human eye in English. It shows the lower part of the right eye after a central and horizontal section. Used under a Creative Commons Attribution-ShareAlike license: <http://creativecommons.org/licenses/by-sa/3.0/>. File accessed on 16/06/2020 from https://commons.wikimedia.org/wiki/File:Schematic_diagram_of_the_human_eye_en.svg)

1.2 Chemical composition of human tears

Tear fluid has a complex composition of proteins, lipids, mucins, water, and salts, and various small molecules; a 2015 proteomics study has identified 1526 proteins present in the human tear fluid employing two-dimensional LC-MS/MS analysis sampled via superior temporal sulcus (STS) [9], while other studies put the number of proteins between 1800-2000 [10–12] using relatively new analysis techniques

such as MALDI-TOF/TOF (validation with ELISA) and LC-nanoESI-MS/MS. A similar study identified and quantified over 200 lipids in tears extracted with microcapillary tubes (MCT) and analyzed using nanoESI-MS/MS, belonging to eight different lipid species such as cholesteryl esters, wax esters, fatty acids, phospholipids as well as free cholesterol [13]. The number of proteins, lipids, and other components of tears makes the tear matrix less complex compared to blood or plasma [14]. The concentration of proteins and lipids in tear fluid depends on the collection method and how the samples were processed and vary from $\text{mg}\cdot\text{mL}^{-1}$ level to $\text{pg}\cdot\text{mL}^{-1}$ level [15]. The relationship between proteins, lipids, and mucins in the human tear fluid has been studied over the years. Models with increasing complexity have been proposed. The current understanding is that the mucous layer formed by mucins and some glycoproteins forms the first layer directly on the ocular surface. This first layer is followed by an aqueous layer containing proteins, salts, and gel-forming mucins (MUC5AC). Lastly, a thin lipid layer with non-polar lipids on the outer surface and an inner surface made up of polar-lipids intercalated proteins [16–18]. Alongside proteins, lipids, and mucins, some small biomolecules such as amino acids and neurotransmitters can be found on the eye surface and in tear fluid [19–23]. Concentrations of amino acids range from $\text{mg}\cdot\text{mL}^{-1}$ to $\text{ng}\cdot\text{mL}^{-1}$ level with glutamic acid, glutamine, and taurine being the more dominant components compared to other amino acids [24]. Figure 1.2 shows three different models of the tear film, illustrating the thicknesses of the regions where different biomolecules can be found.

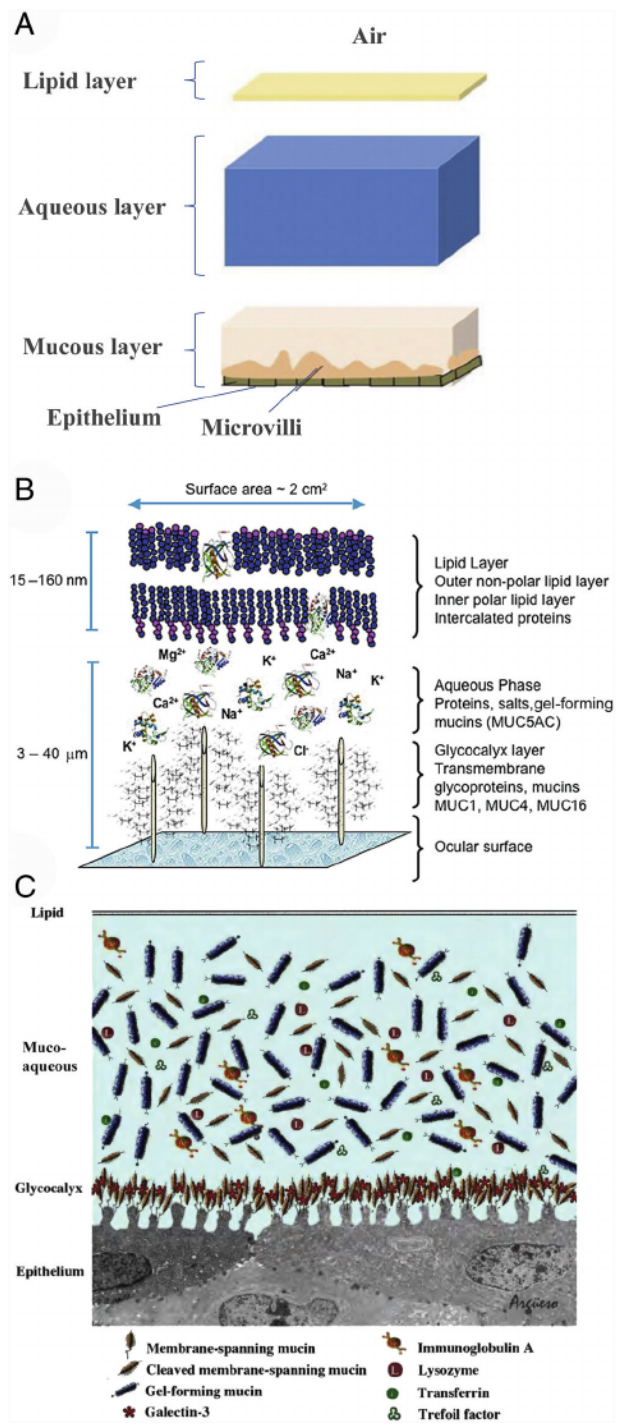


Figure 1.2 Three diagrams of different models of the tear film, A) a simplistic model showing three layers of human tear film, B) a more complex model that illustrates the proposed structure of the lipid layer, C) the interaction of proteins and mucins in human tears. Reproduced with permission from [15] and Wiley.

1.3 Biomarkers in the human eye

The National Institute of Health (NIH) defines a biomarker as,

A characteristic that is objectively measured and evaluated as an indicator of normal biological processes, pathogenic processes, or pharmacologic responses to therapeutic intervention [25]

Biomarkers play a crucial role in the field of predictive and preventive medicine by helping doctors and scientists to both discover and develop new drugs and to design new diagnostic tools for monitoring treatments clinically. Biomarkers specifically allow measurable ways of how a biological system changes when it is affected by a disease, disorder, or toxic chemical substances as well as to treatment. In this context, biomarkers act as indicators to detect disease risk and progression, predicting and monitoring the course of treatments and therapies.

The idea of looking for biomarkers in human tears is not that new. The earliest cases where tears were used for diagnosis go back to the 1950s. An article in 1951 used mucin stains to detect aqueous tear deficiency [26]. Another article dated 1958 showcases an attempt to diagnose diabetes by detecting glucose levels in tears [27]. The search for biomarkers in eye-related diseases and disorders is an active research field with the most effort being concentrated on examination and characterization of biomarkers present in human tear fluid for both ocular and non-ocular diseases [14,28–33]. Identifying and characterizing biomarkers associated with these diseases is an active and ongoing endeavor that spans multiple omics fields. Figure 1.3 presents an effort to display eye-related diseases that are studied in different omics fields [34].

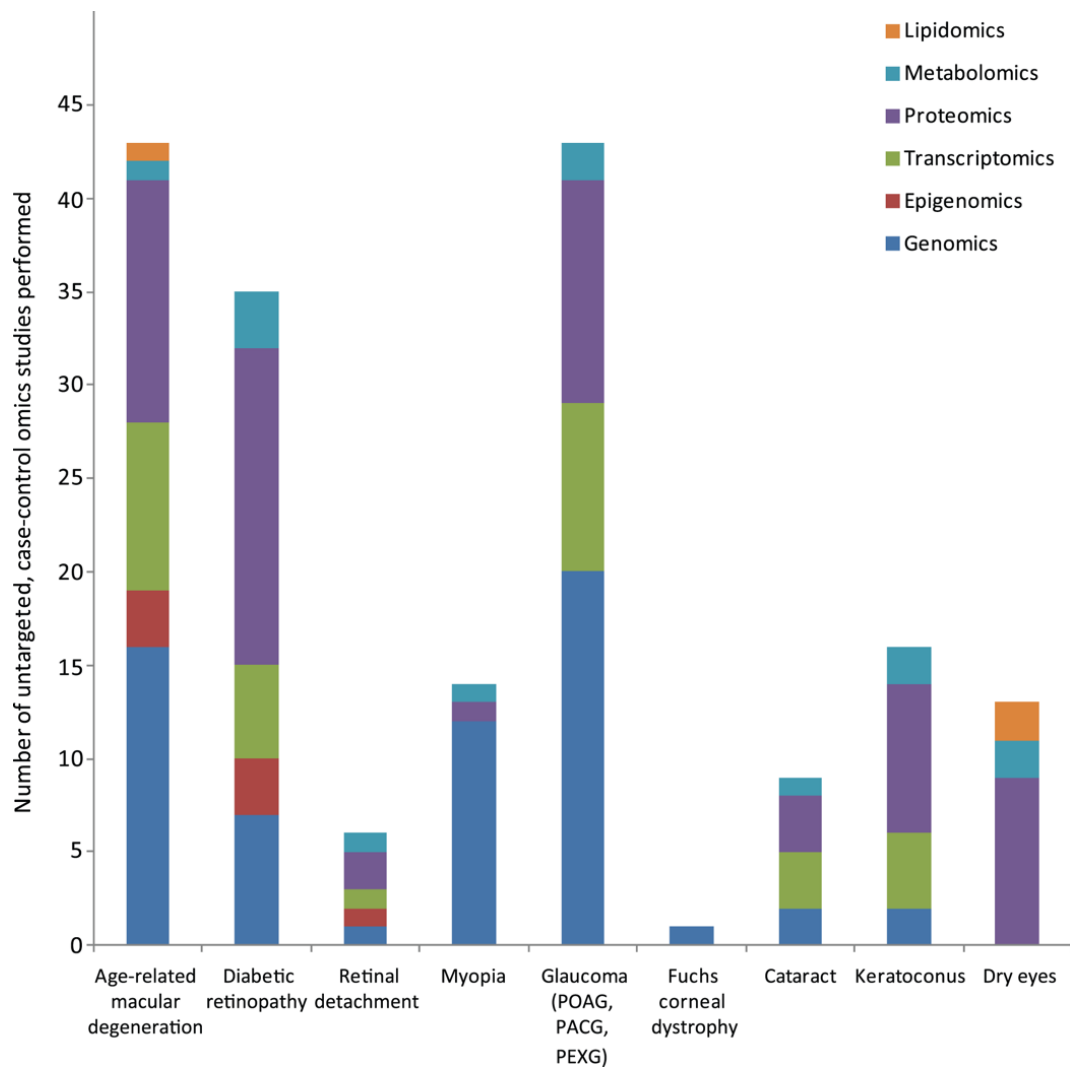


Figure 1.3 The number of untargeted, case-control omics studies performed for multifunctional eye diseases up to date until 2017. Reproduced with permission from [34] and ARVO.

1.3.1 Disease-specific biomarkers in the human eye and diagnostic approaches

An in-depth review of efforts to identify and quantify ocular and non-ocular biomarkers would be outside the scope of this thesis. However, in order to set the stage for potential application areas of a new method for ocular sampling, a summary

of current trends in the ocular omics field is presented. Biomarkers of interest, as well as sampling and analysis methods for some of the most common and well investigated ocular and non-ocular diseases that the ocular surface can provide information on, have been selected, a more comprehensive list of disease biomarkers that were found in tears are given in Table 1.1.

Table 1.1 Biomarkers associated with ocular and systematic diseases and disorders reproduced with additions and with permission from [35] and Springer (continued for next two pages).

Biomarkers	Disease/Disorder	References
Lactoferrin	Dry eye disease (DED)	[12,36–41]
MMP-9	DED, Sjögren’s Syndrome, Ocular graft versus host disease	[42–57]
Acetylcholine	Alzheimer’s disease, pesticide poisoning, cardiovascular diseases	[58–60]
Creatine	Rhabdomyolysis, Huntington’s disease, mitochondrial disease	[61–63]
γ -aminobutyric acid (GABA)	Multiple sclerosis, PTSD, osteoporosis	[64–66]
Acetylcarnitine	Major depressive disorder, mitochondrial disease, autism spectrum disorder	[67,68]
Adenosine	Macrophage activation syndrome, pleural tuberculosis	[69,70]
Eicosapentaenoic acid	Coronary heart disease	[71]
Docosahexaenoic acid	Cardiovascular disease	[72]
Cholesterol	Coronary artery disease	[73]
Retinoic acid	Leukoplakia, myeloid leukemia, neuroblastoma	[74,75]
Amino Acids		
Phenylalanine	Parkinson’s disease, Amyotrophic lateral sclerosis	[76].
Glutamine	Diabetic retinopathy, Alzheimer’s disease, depression	[77,78]
Proline	Chronic obstructive pulmonary disease, cystic fibrosis	[79]
Citrulline	Alzheimer’s, diabetes, sickle cell disease, hypertension	[80]
Tryptophan	Coronary heart disease, inflammatory bowel disease, depression	[81–83]

Biomarkers	Disease/Disorder	References
Proteins		
EGF	DD, SS, Stevens-Johnson syndrome	[39,49,84–87]
LPRR4, LPRR3, nasopharyngeal carcinoma associated PRP4 and α -1 antitrypsin	DED, SS, Meibomian gland dysfunction	[37,40,88–91]
PIP (prolactin- inducible protein)	DED	[33,40]
Lipocalin-1	DED	[10,33,37,40,41,89,91–93]
α -enolase	Pancreatic cancer, myeloid leukemia, rheumatoid arthritis. DED	[33,37,90,94–96]
S100 family of proteins:		
S100A8/Calgranulin A, S100A9/Calgranulin B, S100A4 and S100A11	DED	[12,33,37,88,90,91,93]
Annexin A1 (ANXA1), Annexin A11 (ANXA11)	DED	[12,90,91]
MUC5AC	DED, SS	[97–101]
Cathepsin S	SS	[98,102,103]
Neuromediators: substance P, NGF, VIP, CGRP	DED	[104,105]
Other biomarkers:		
IgE, Tryptase, Histamine, ECP	Ocular allergies	[93,106–108]
β -amyloid, microtubule-associated protein tau	Alzheimer disease	[109]

Biomarkers	Disease/Disorder	References
α -synuclein	Alzheimer disease, Parkinson disease	[109,110]
Inflammatory cytokines		
IFN- γ	DED, SS	[43,46,49,54,84,85,92,93,107,108,111–117]
TNF- α ,	DED, Parkinson disease	[49,54,56,85,87,92,107,111–115,117–119]
IL-1 α , IL-1 β	DED	[46,49,53,54,85,92,107,112,117,120]
Chemokines		
IL-8/CXCL8	DED	[49,56,84,85,87,92,107,112,115,117,121]
MIP-1 α / CCL3, MIP-1 β /CCL4, RANTES/CCL5, Fractalkine/CX3CL1, CXCL9, CXCL10, CXCL11, MCP- 1/CCL2	DED, SS	[49,56,84–86,107,112,117,122,123]

1.3.2 Techniques and technologies for biomarker identification in the tear film

The search for disease biomarkers in human tears is mostly focused on tear proteins. However, the dynamic concentration range and low sample volume present a challenge that warrants the use of highly sensitive detection methods. High-performance liquid chromatography (HPLC) and electrophoretical techniques are two tools that are successful in overcoming this challenge in tear proteome studies [124–128]. Although there are in-depth reviews [29,32] on the application of new and novel techniques to biomarker discovery from tear fluid, a summary of the most common and successful methods could provide a much-needed perspective.

1D and 2D SDS-PAGE can be employed to separate tear proteins [129–135], which can also be used for diagnostic purposes [136,137]. 2D electrophoresis, in which proteins are first separated based on their isoelectric points (1D) and later based on their molecular weights (2D), is a suitable separation method for developing tear film protein maps [127,133,135,138]. SDS-PAGE data have been used to diagnose diabetes [132], blepharitis [139], and dry eye disease [130,136,137] with multivariate statistical analysis, comparing protein patterns of healthy and sick patients. The main drawback of SDS-PAGE separation is low gel to gel reproducibility and its large sample volume requirement [140].

Electrophoretic techniques can also be used for small molecule detection from the eye when they are combined with a suitable sampling method. In a recent study, phenol red threads were employed for collecting mice tear fluid samples, and small molecules containing primary-amines were separated and identified using capillary electrophoresis[141]. Fifteen small molecules were identified: arginine, histamine, lysine, ornithine, citrulline, threonine, glutamine, asparagine, methionine, serine, alanine, taurine, glycine, glutamic acid, and aspartic acid.

Several HPLC techniques such as size exclusion HPLC [126,142], reverse phase HPLC [143], ion exchange HPLC [143], and nano-LC [144] have been employed for identification of tear protein analysis. HPLC has two crucial advantages, low sample volume requirement and its compatibility with mass spectrometric techniques. However, the complexity of the tear matrix is known to cause ion suppression, where several biomolecules can coelute with the analyte of interest [145–147]. This problem can sometimes be overcome by using an elution gradient but still clean-up steps before LC-MS analysis is required.

Developments in the mass spectrometry field translated well into many omics fields, tear composition has also been successfully analyzed with many MS approaches. Methods like MALDI and ESI are increasingly employed in high-throughput protein analyses [124,148–151]. MALDI-MS and ESI-MS methods can also be coupled with TOF and ion trap analyzer for enhanced sensitivity and resolution [152–154]. The development of such sensitive techniques has allowed MS methods to overcome the difficulties mentioned above, such as ion suppression, by analyzing specific fractionation patterns [155]. Another development in MS techniques that have been employed in proteomics studies is SELDI-TOF-MS, where surfaces with specific chromatographic properties (i.e., H50 reverse phase, CM10 cation exchange, and Q10 anion exchange), these so-called “ProteinChip”s were used to develop protein profiles for patients with dry eye disease [89,156] and breast cancer [150]. Aside from proteins, mass spectrometry has also been employed in identifying amino acids in human tear fluids. In a 2013 study, amino acid levels in tear fluids of 31 healthy volunteers and 33 afflicted patients were investigated and profiles using HPLC and ESI-MS [24].

Another commonly used analysis technique for the identification of eye-related biomarkers is the microarray platforms. Microarrays are mainly used in proteomics research, where protein-specific antibodies can be placed onto nitrocellulose-coated slides. This highly specific and sensitive method can be employed for high-throughput analyses and can also serve as a validation tool for MS-based proteomics studies. The potential of this method can also be realized by coupling its high-

throughput capacity with multivariate statistical tools to look for patterns in disease biomarkers [92,157–159]. The limitations of the microarray method are due to its specificity where only pre-selected proteins can be investigated, availability of commercial antigen/antibodies, and the hydrophilic nature of the surface, which makes investigating hydrophobic biomolecules such as protein-lipid interactions difficult.

ELISA is another method for quantitative investigations and can be employed in sensitive and reliable tear film analyses [160]. ELISA is also commonly used for clinical studies and validation of global proteomics studies as a complementary method [155]. ELISA has been employed in the determination of inflammatory cytokine concentration in human tears [120] as well as analyzing changes to mucin levels [161]. Recently, ELISA has also been used to measure and compare dopamine levels in human tear fluids; samples were collected using Schirmer's strips and microcapillary tubes, and plasma [162]. Dopamine levels were reported as $97.2 \pm 11.8 \text{ pg}\cdot\text{mL}^{-1}$ in tear fluid using Schirmer's strips, $279 \pm 14.8 \text{ pg}\cdot\text{mL}^{-1}$ using microcapillary tubes, and $470.4 \pm 37.64 \text{ pg}\cdot\text{mL}^{-1}$ in plasma. In another study, ELISA was used to determine serotonin levels in 62 volunteers (control group included) suffering from various degrees of dry eye syndrome, which showed a correlation between dry eye syndrome and increased serotonin levels in human tear fluid [163].

It can be surmised from the summary above that the advent of sensitive analysis techniques has allowed the identification of thousands of biomarkers and the investigation of their role in many different diseases and disorders. As the sensitivity of analytical instruments increases, it becomes possible to design less invasive techniques as the sample size requirements become smaller. It becomes paramount, then, to come up with new techniques that allow easy, fast, reliable sampling from biological surfaces so that medical personnel can take full advantage of the technological developments in these instruments.

1.4 Sampling and sensing from the eye surface

Although there are many methods currently employed in the collection of human tear samples and it is a relatively non- or low-invasive process, the complex nature of the human tear as a biological fluid makes the sampling step crucial due to the potentially unstable compounds it contains. The low volume of the samples makes it difficult for detecting low concentration biomarkers [6]. Tear collection is usually a straightforward process via either capillary tubes or adsorbent materials; microcapillary tubes (MCT), Schirmer test strips (STS), or ophthalmic sponges are three of the most common materials that can be employed to collect non-stimulated, stimulated, or washout (flush) tears [6]. Each collection method has its advantages and disadvantages; for example, STS has been found to cause irritation and underestimate protein concentration due to increased tear flow during sampling [6]. MCT is considered a less invasive procedure than STS. However, sampling with MCT often takes longer than the STS method since the tube has to be physically held in/under the eye for the whole duration of the sampling, and the process can be interrupted by blinking and cause discomfort to patients [6]. A 2008 comparing tear samples collected with STS and MCT methods have detected 13 MCT specific, 54 STS specific, and 30 overlapping proteins using in-gel tryptic digestion followed by liquid chromatography-tandem mass spectrometry [37]. In order to compensate for the low sample volumes, several researchers employed the washout method, in which an exogenous fluid, usually sterile physiological saline solutions are used to force out tear samples. However, this has been found to dilute even the most abundant biomolecules in the eye, even dropping some low concentration biomarkers below LOD levels [6].

Over the last decade, wearable devices equipped with various sensors that can detect a single or several analytes to gather information about specific diseases/disorders have been a rapidly increasing area of research. Wearable devices operate in many different ways and can be divided into four categories based on their mode of operation; mechanical, electrical, chemical, and optical [164]. Such wearable devices

have also been developed with contact lens geometries, as shown in Figure 1.4 below, employing chemical and electrochemical sensors and have been recently reviewed [165]. Most contact lens biosensors were developed for glucose sensing employing various detection methods such as fluorescence detection [166–171], photodetectors [172–180], and electrochemical sensors [181–183]. A similar contact lens biosensor was employed for monitoring L-lactate levels equipped with an electrochemical sensor [184]. It can be expected that such wearable sensors will continue to be developed for various diseases and their related biomarkers. Such designs can be equipped with sensors to detect multiple biomarkers as well. However, sensors inherently limit the amount of information that can be gathered from the eye surface as they can only be used to detect a handful of biomolecules at best, which limits their application.

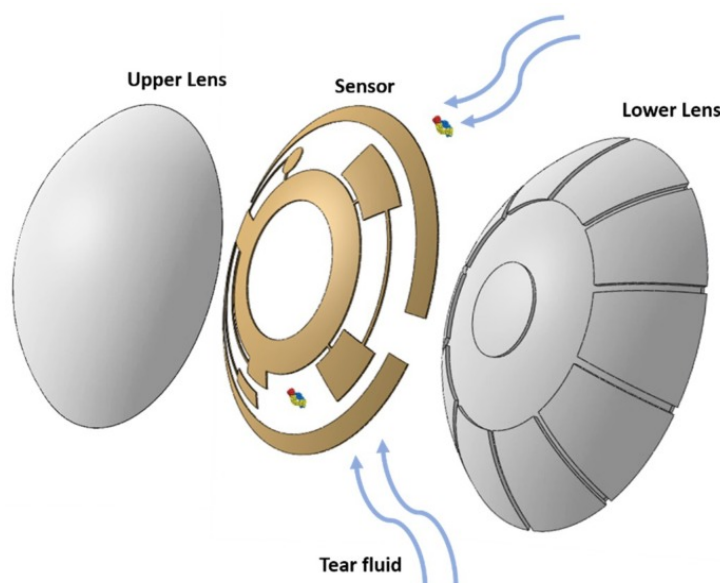


Figure 1.4 Conceptual illustration of a contact lens biosensor. Reproduced with permission from [165] and MDPI.

Ocular related omics research needs new sampling techniques that allow the researchers to take advantage of the analysis techniques and instruments that are

available. Wearable sensors have been gathering interest, and it can be surmised that they have not reached their full potential in terms of design and application areas. However, in order to conduct an untargeted metabolomics survey, a new approach that can work with a wide range of biomolecules is necessary.

1.5 Solid-phase microextraction

Solid-phase microextraction (SPME) is a non-exhaustive extraction method that is a versatile tool that has been employed in the analyses of a wide range of compounds in a variety of different fields since its inception by Pawliszyn and Belardi in 1989 [185–194]. SPME has many advantages over traditional extraction methods, solid-phase extraction (SPE) and liquid-liquid extraction (LLE), such as applicability to small and large sample volumes, ability to perform well in complex matrices due to its proper matrix clean up procedures as well as its ability to be made selective towards selected analytes, suitability to *in vivo* and on-site applications, adaptation to automation processes and being environmentally friendly just to name a few [195]. SPME extractive phases can be prepared with different materials and modifications to cover a wide range of analytes or target specific analytes and in different geometries to better suit the unique problems posed by the system to be sampled from [196–202]. Most conventional, and the first developed, SPME extractive phase geometry is the so-called fiber coatings, in which a thin fiber or needle is coated with a material that acts as the solid extractive phase. Different materials can be used for both the coating as well as the core fiber based on the type of analytical instrument to be used after extraction (GC-MS, LC-MS, direct injection to MS) and the requirements dictated by the system. The second most common geometry is the thin film microextraction (TFME), which employs similar extractive phase materials in the shape of a thin film instead of coated on a fiber or needle. Although the thickness of the extractive phase remains pretty much the same as SPME fiber coatings, by increasing the volume of the extractive phase and the area that the analytes come into contact with, better analytical sensitivity and faster extraction kinetics can be

achieved with TFME compared to fiber coated geometries in SPME [203]. An in-depth review of different coating materials, geometries, areas of application, and coupling of SPME with new technologies has been reviewed extensively in the literature [185–188,190–192,196–201,203–205].

1.5.1 Fundamentals of SPME (and TFME)

Most analytical instruments/devices require the analysis sample to be in a specific form or shape; this requirement may also necessitate the analyte to be removed from any matrix it may exist in. The process of isolating, cleaning, and pre-concentrating an analyte from any type of matrix is the extraction step in which analytes are exchanged between two phases with minimal matrix overlap. Traditionally, extractive techniques employ liquid (LLE), or solid (SPE) phases to use relatively large extraction phase volumes to ensure maximum recovery (exhaustive extraction) of analytes from the sample matrix in order to achieve reproducible results, employing preconcentration methods for high sensitivity as needed. In order to quantify the analyte present in the extract, traditional extraction methods usually employ straightforward calibration methods where stock solutions of analytes with different concentrations are used to determine concentrations of analytes in the extract. However, analytes may behave differently in complex sample matrices, and recovery percentages could vary from matrix to matrix. The modus operandi of SPME is based on a partition equilibrium between the sample matrix and the extractive phase, and a mass balance equation can be written to relate the amount of extracted analyte as follows [193]:

$$n_e^{eq} = \frac{K_{es}V_eV_sC_s^0}{K_{es}V_e + V_s} \quad \text{Equation I}$$

where n_e^{eq} is the mass of the extracted analyte at equilibrium, K_{es} ($= C_e^{eq}/C_s^0$) is the distribution coefficient of the analyte between the sample matrix and extractive phase, V_e is the volume of the extractive phase, V_s is the volume of the sample matrix, and C_s^0 is the initial concentration of the analyte in the sample matrix, and C_e^{eq} is the concentration of the analyte in the extractive phase at equilibrium. In cases where sample matrix volume, V_s , is much larger than extractive phase volume, V_e , the term in the denominator, $K_{es}V_e + V_s$, can be approximated as $K_{es}V_e \ll V_s$ which would simplify the equation to be [193]:

$$n_e^{eq} = K_{es}V_eC_s^0 \quad \text{Equation II}$$

This simplification means that in cases where the assumption $K_{es}V_e \ll V_s$ holds, the amount of extracted, n , is independent of sample volume. This fundamental principle is one of the most vital aspects of SPME and makes extraction from relatively small and large sample matrix volumes possible and reliable. Continuing, another essential description that is fundamental for SPME methods is the recovery (R) and enrichment factor (E). Recovery (R) can be defined by the ratio of the amount of extracted analyte (n_e^{eq}) to the original concentration of analyte (n_s^0) in the sample:

$$R(\%) = \frac{n_e^{eq}}{n_s^0} \times 100 \quad \text{Equation III}$$

Combining equations I and III and defining the phase ratio of the extractive phase volume to the sample volume as $\varphi = V_e/V_s$ gives us:

$$R(\%) = \frac{K_{es}}{K_{es} + \varphi^{-1}} \times 100 \quad \text{Equation IV}$$

Enrichment factor (E), relating the amount of analyte that ends up in the desorption solvent to the amount of analyte in the sample matrix, is defined as:

$$E = \frac{C_e^{eq}}{C_s^0} = \frac{n_e^{eq}}{n_s^0} \times \frac{V_s}{V_e} \quad \text{Equation V}$$

Combining equations IV and V enables us to relate the enrichment factor, E, to the recovery rate over the phase ratio, φ (V_e/V_s):

$$E = \frac{R}{\varphi} \quad \text{Equation VI}$$

Equation IV directly indicates that as long as phase ratio φ is relatively small, which in most cases with SPME, φ^{-1} will be a large number compared to K_{es} , and R(%) will be small. Low recoveries of analytes in SPME should not be a problem as long as instruments with good sensitivity are used for analysis (such as any MS method). In cases where high recovery is necessary, increasing phase ratio, φ , or finding (or modifying) extractive phases to have large K_{es} values can be a solution [206]. Moreover, when the SPME recovery rates are lower than 5%, they can be considered non-depletive, and it can be assumed that the analyte concentrations in the sample will remain almost the same after the extraction. The non-depletive sampling ability of SPME allows it to be employed in biologically active systems without disturbing the existing equilibrium in the system (homeostasis), thus eliminating any possible biological responses due to sampling that could alter analyte concentrations.

One drawback of low recovery rates is that SPME extractive phases, such as PDMS, have low K_{es} values for polar analytes. Instead of coating the extractive phase on a supporting structure as in the case with SPME fibers, preparing thin films with larger extractive phase volumes for microextraction was introduced as a solution to this

issue [206]. As described before, TFME employs a sheet of thin-film as the extractive phase with a high surface-to-volume ratio, meaning that the volume of the extraction phase can be increased while its thickness increases very slowly or even remains the same. Increasing the thickness of the extractive phase could lead to higher equilibrium times, as described in the kinetic theory of extraction as:

$$t_{95\%} = 3 \times \frac{\delta K_{es}(b - a)}{D} \quad \text{Equation VII}$$

where $t_{95\%}$ is the equilibrium time, $b - a$ is the thickness of the extraction phase, δ is the boundary layer, and D is the diffusion coefficient of the analyte. Furthermore, it was experimentally demonstrated that extraction efficiency increases in thin-film extractions with a high surface-to-volume ratio; its relationship is given as [207]:

$$\frac{dn}{dt} = \frac{(DA)}{\delta} C_s \quad \text{Equation VIII}$$

where n is the amount of extracted analyte, and C_s is the analyte concentration in the sample matrix. Equation VIII shows that the extraction rate is initially linearly proportional to the area of the thin film, and it was experimentally shown that as extraction time increased, the extracted analyte amount by thin films with different sizes approached the ratios of the thin film volumes [206]. Thin films also come in different geometries; the extractive phase can be coated on 96 blade format and employed with 96 well-plates for high throughput analysis. Extractive phases can also be coated on magnetic stir bars for kinetically controlled extractions, or just prepared as thin films to be directly placed on top of surfaces. The geometry of the thin film makes TFME a prime candidate for sampling from biological surfaces such as skin, and, as the case in this study, eye.

1.5.2 Applications of SPME (and TFME)

SPME has been employed in a wide range of studies over the years with applications in numerous fields, as shown in Table 1.2 reproduced from a recent review [203] that summarizes significant developments employing SPME sample preparation methods in bioanalytical, food, and environmental studies. An in-depth review of various applications of SPME would be outside of the scope of this thesis. Since *in vivo* applications are of interest, the review of significant and recent studies has been limited to *in vivo* sampling, especially sampling from biological surfaces.

Fundamentals and underlying principles of SPME make it a prime candidate for *in vivo*, indirectly sampling from a biological system, and *ex vivo*, extraction from samples collected from living biological systems. Suitability of SPME for such extractions schemes was realized when biocompatible extractive phases such as polyacrylonitrile (PAN), polyacrylate (PA), polypyrrole (PPY), polyethylene glycol (PEG), and polydimethylsiloxane (PDMS), commercial products have also been developed such as PDMS tips functionalized with C18 suitable for SPME and LC analysis [203,208]. These materials, which were already in use with various medicinal applications, have allowed sampling from living systems without any adverse effects for reasons a) SPME does not disturb the homeostasis since minimal amounts of analytes are extracted and b) materials used as extractive phases are biocompatible by their nature. One of the widely used geometries for *in vivo* SPME applications is biocompatible fiber probes (nitinol wires are commonly used) coated with suitable extractive phases. These fibers allow high-throughput analysis to be performed in 96-well plates can be employed for desorption after sampling [209–211], or can be coupled with an MS instrument for direct ionization without any separation of analytes [208,212,213].

Table 1.2 Applications of SPME. Reproduced with permission from [203] and ACS (continued for next six pages).

Area of study	Application	SPME mode and coating	Extraction and desorption conditions	Instrumentation	Year and Reference
Food analysis	Characterization of human breast milk lipidome	DI, C18/PAN fibers	5 min extraction, 5 min desorption in 2-propanol	LC-MS	2017, [214]
	Screening of apples (<i>Malus × domestica</i> Borkh.) metabolome changes due to fruit maturity	DI, DVB/Car/PDMS and PDMS overcoated-DVB/Car/PDMS fibers	60 min extraction, 25 min desorption at 270 °C	GC × GC-MS	2016, [215]
	Characterization of edible oils components	DI, PDMS/DVB	45 min extraction, 5 min desorption	GC-MS	2017, [216]
	Determination of the volatile metabolites of saprotroph fungi	HS, DVB/Car/PDMS	35 min extraction	GC × GC-MS	2015, [217]
	multi-residue pesticides analysis in grapes	DI, PDMS/DVB/PDMS	30 min extraction, 10 min desorption at 260 °C	GC-MS	2015, [218]
	Development of an extraction method for analysis of avocado samples	DI, PDMS/DVB/PDMS	40 min, 5 min desorption at 270 °C	GC-MS	2017, [219]

Area of study	Application	SPME mode and coating	Extraction and desorption conditions	Instrumentation	Year and Reference
Food analysis	Determination of cannabinoids in human breast milk	HS, PDMS 100 μm	40 min extraction	GC-MS	2017, [220]
	Determination of ochratoxin A in wine	DI, C18 packed in tube SPME	loading 6 min at 0.2 mL min ⁻¹ ; desorption in water/ACN/acetic acid (45.5:45.5:1, v/v/v)	LC-MS/MS	2017, [221]
Environmental analysis	SPME interlaboratory validation of pesticides from surface waters, versus LLE	DI, DVB/PDMS SPME fibers	30 min extractions at 30 °C from 15.5 mL of sample agitated at 500 rpm, pH of 3.0, 4 g NaCl added, desorption at 270 °C for 10 min	GC-MS	2016, [222]
	TF-SPME interlaboratory validation of pesticides from surface waters, versus LLE	DI, DVB/PDMS TF-SPME membranes	30 min extractions at 30 °C from 30 mL of sample agitated at 900 rpm, pH of 2.5, 10% NaCl. TDU desorption at 250 °C for 5 min using 60 mL min ⁻¹ He with cryofocusing at -80°C	TDU/GC-MS	2017, [189]

Area of study	Application	SPME mode and coating	Extraction and desorption conditions	Instrumentation	Year and Reference
	On-site extraction of benzene and naphthalene from city air	Spot air sampling averaged to TWA using DVB/PDMS TF-SPME membranes	1 h equilibrium extractions at measured ambient temperatures with air flow of 3.6 m s^{-1} desorption at $250 \text{ }^{\circ}\text{C}$ for 5 min using 60 mL min^{-1} He with cryofocusing at $-120 \text{ }^{\circ}\text{C}$	TDU/GC-MS	2014, [223]
Environmental analysis	On-site derivatization and determination of free vs aerosol bound formaldehyde from car exhaust	In situ DVB/PDMS SPME fiber and in situ Tenax/Car 1000/Car 1001 NTD	In-excess preloading of PFPH DA, both cold ($16.3 \text{ }^{\circ}\text{C}$) and hot ($45.7 \text{ }^{\circ}\text{C}$) exhaust measured in situ for 60 and 30 s by SPME respectively and 10 mL extraction by NTD. Desorptions at $280 \text{ }^{\circ}\text{C}$ for 1 min	portable GC-MS	2016, [224]
	Extraction of PAHs from certified soil samples	pressure-balanced HS, PDMS CF-SPME	7 mL of air removed from 10 mL vial containing 1 g sand to balance pressure at $200 \text{ }^{\circ}\text{C}$ extraction, Fiber cooled to $30 \text{ }^{\circ}\text{C}$ for 30 min extraction. Desorption at $250 \text{ }^{\circ}\text{C}$	GC-FID, GC/MS	2016, [191]

Area of study	Application	SPME mode and coating	Extraction and desorption conditions	Instrumentation	Year and Reference
	TWA determination of biocides and UV-blocking agents from river water	TWA DI, spot sampling DI. C18/PAN and HLB/PAN TFME blades	TWA extractions performed for 90 days in copper retracted devices. Desorption in 1.8 mL of MeOH/ACN/IPA 50/25/25, v/v/v for 30 min using 1500 rpm vortex agitation.	LC-MS/MS	2017, [225]
Environmental analysis	Rapid screening of select pharmaceuticals from treated wastewater samples	DI, HLB/PAN blade spray device	DI extraction performed for 10 min from 9 mL of sample at 1200 rpm orbital agitation. Quick rinse in DI water. Desorption in 15 μ L 5:95 H ₂ O/MeOH with 12 mMol AA + 0.1% FA. Sprayed at +4 kV	direct-to-MS/MS	2017, [226]
	On-site identification of unknown contaminants from a construction-impacted lake	DI, DVB/PDMS TF-SPME membranes	10 min on-site extractions at 16.5 °C (ambient) using 350 rpm drill agitation. TFME HVD-to-NTD desorption at 250 °C for 5 min using 30 mL min ⁻¹ He, NTD desorption at 280 °C for 1 min	portable HVD-NTD/GC-MS	2016, [227]

Area of study	Application	SPME mode and coating	Extraction and desorption conditions	Instrumentation	Year and Reference
Bioanalysis (biological fluids, animal tissue and cell studies)	Analysis of several doping compounds in urine, plasma, and whole blood	DI, HLB-PAN TFME (on plastic support)	90 min extraction and 20 min desorption in 4:1 methanol/acetonitrile	LC-MS/MS	2015, [228]
	Analysis of VOCs in urine samples as a means to monitor levels of exposure in children living at different environmental conditions	HS, Car/PDMS	15 min extraction (at 30 °C) and 0.2 min desorption at 240 °C (additional 5 min of desorption to avoid carryover)	GC-MS	2016, [229]
	Analysis of repaglinide and two of its main metabolites in human liver microsome media	DI, C18-PAN TFME	60 min extraction and 90 min desorption in 1:1 acetonitrile/water	LC-MS/MS	2015, [230]
	Profiling of <i>E. coli</i> metabolome in response to natural antibacterial agents (cinnamaldehyde, eugenol, and clove oil)	HS, DVB/Car/PDMS fibers and DI, HLB/PS-DVB-PAN TFME	HS: 30 min extraction (at 37 °C) and desorption at 270 °C DI: 120 min extraction and desorption in 1:1 acetonitrile/water	LC-MS/MS and GC × GC-MS	2016, [231,232]

Area of study	Application	SPME mode and coating	Extraction and desorption conditions	Instrumentation	Year and Reference
Bioanalysis (biological fluids, animal tissue and cell studies)	Analysis of the volatilome in breast cancer cell lines and normal human mammary epithelial cells (cells and culture media)	HS, DVB/Car/PDMS fibers	45 min extraction (at 37 °C) and desorption at 250 °C	GC-MS	2017, [233]
	Analysis of the volatilome of urine samples collected from patients with mesangial proliferative glomerulonephritis, IgA nephropathy and normal controls	HS, Car/PDMS fibers	20 min (at 40 °C) and desorption at 200 °C	GC-MS	2015, [234]
	Analysis of the cellular lipidome in human hepatocellular carcinoma cell lines (comparison of SPME and Bligh & Dyer method)	DI, C18-PAN TFME	90 min extraction and 60 min desorption in 1:1 methanol/isopropyl alcohol	LC-MS	2017, [214]
	Profiling of <i>cis</i> -diol containing nucleosides and ribosylated metabolites in urine samples collected from cancer and healthy controls	in-tube SPME using boronate-affinity organic-silica hybrid capillary monolithic column	loading flow rate, 5 µL/min; washing volume, 35 µL; desorption volume, 25 µL	LC-MS/MS	2015, [235]

DI: Direct immersion sampling mode (fiber/probe is directly inserted/makes contact with the sample)

HS: Headspace sampling mode (fiber/probe is immobilized a certain distance above the sample)

PAN: Polyacrylonitrile

DVB: Divinylbenzene

Car: Carboxen

CF-SPME: Cold fiber SPME

TF-SPME: Thin-film SPME (TFME)

HLB: Hydrophilic lipophilic balanced polymeric particles

Similar to SPME, TFME has excellent potential for *in vivo* and *ex vivo* studies, especially from biological surfaces, mainly for skin sampling, with some emerging applications for ocular and oral sampling that have been reviewed recently. [205] Sampling from such biological surfaces has the advantage of providing an easily accessible source for biomolecules that can provide valuable information about the underlying biological systems. Such sampling methods are often less invasive than taking blood or tissue samples and can be designed to be wearable for extended periods. Profiling skin metabolites has been a topic of interest in the last decade [236–239] with applications in fields such as toxicology [240–242], medicinal diagnosis [243,244], and environmental exposomics [245–247]. PDMS thin films have also been used for *in vivo* studies by sampling from the sebum [248] via sorptive tape extraction and analyzed with thermal desorption GC-MS. The oily layer secreted by the body's sebaceous glands that coat the skin, and for sampling volatile compounds from human skin by employing GC-MS analysis [249,250]. In a more recent study, PDMS was used as an extractive phase employing headspace sampling as well as direct sampling methods and analysis by GC-MS [251]. Another *in vivo* study that showcases the potential of TFME for clinical approaches involved PDMS patches placed inside the ears of rabbit test subjects to investigate histological evidence of early-stage ulcer formation by metabolomics screening via GC-MS analysis [252]. Figure 1.5 shows the diagrams of the TFME patches used as extractive phases for skin volatiles [251] and metabolomics screening of sheep subjects [252]. Table 1.3 summarizes some of the recent applications of TFME for skin sampling.

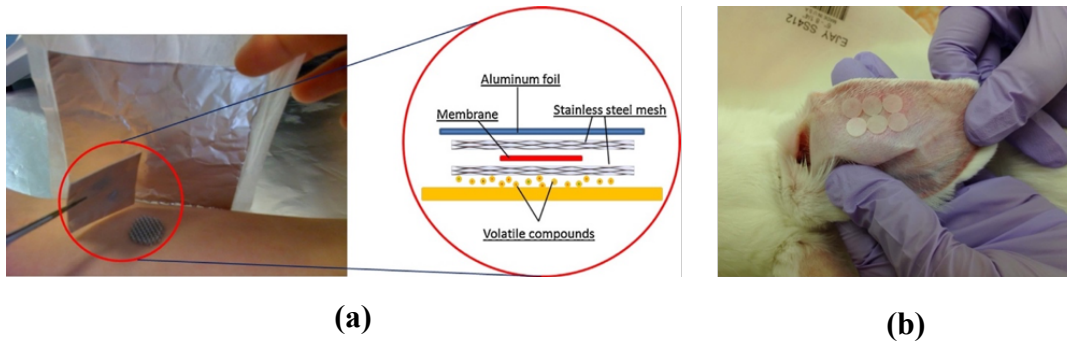


Figure 1.5 (a) Schematic diagram of the “membrane sandwich” headspace sampling for skin volatiles sampling. (b) Polydimethylsiloxane (PDMS) patches placed over the ventral ear surface for direct sampling. These were then covered with PTFE (polytetrafluoroethylene) and Tegaderm ® (not shown). Reproduced from [251,252], with permission from Elsevier and IOP Publishing.

Table 1.3 Summary of skin sampling methods. Reproduced with permission from [205] and MDPI.

Method	Materials	Body part	Analytes	Sampling Time	Instrumentations	Comments
Patch type[251]	PDMS	Upper back, forearms, back thigh	VOCs	1 h	GC-MS	“sandwich membrane”, minimal contamination
Patch type[253]	PDMS	Armpit	Fatty acid metabolites, VOCs	30 min	TD-SESI-MS/TD-GC-MS	suitable for automation
Patch type[254]	PDMS	Forehead	VOCs	30 min	TD-GC-MS	complementary to breath analysis
Patch type[252]	PDMS	Ear	Rabbit skin metabolites, ulcer metabolites	30 min	GC-MS	rabbit model study
Patch type[255]	PDMS	Foot	VOCs	30 min	TD-GC-MS	complementary to bacterial mapping
Patch type[256]	Agarose hydrogel	Lower arm	Skin metabolites	1 min - 3 h	nanoDESI-MS	direct mass spectrometry
Patch type[257]	Agarose hydrogel	Upper and lower limbs, abdomen, back	Psoriatic skin metabolites	20 min	nanoDESI-MS	direct mass spectrometry
Patch type[258]	Agarose hydrogels	Lower arm	Topical drug metabolites, nicotine and scopolamine metabolites	10 min	nanoDESI-MS	direct mass spectrometry
Microneedle[259]	Polylactic acid	Mouse skin	Skin biomarkers	1 h	microplate UV-VIS spectrophotometry, densitometric analysis	limited to biomarkers with known antibodies, can only sample from specific skin depth
Headspace [260]	DVB/carboxen/PDMS (Stableflex)	Volar forearm	VOCs	15 min	GC-MS	glass housing
Headspace [261]	DVB/carboxen/PDMS (Stableflex)	Volar forearm	Skin and fragrance-derived VOCs	5 – 40 min	GC-MS	glass housing
Passive sampling[262]	Silicone	Wrist	PAHs, environmental chemicals	2 – 24 h	GC-MS	low repeatability

1.6 Aim of the study

The aim of this thesis was to develop a contact lens type extractive device suitable for possible *in vivo* applications for sampling small biomolecules from the eye surface, see Figure 1.6. In order for the extractive device to be suitable for future *in vivo* studies, a biocompatible, flexible, (semi-)transparent material with a good affinity towards polar and non-polar analytes was necessary. A suitable material that boasted these properties was found to be polydimethylsiloxane (PDMS). In order to increase the affinity of PDMS towards polar molecules, the functionalization of thin films with amine functional groups was proposed. In order to investigate the success of the proposed methods of synthesis, thin films were characterized using FTIR, TGA, EDX3D printed molds were prepared in order to shape the synthesized thin films in contact lens geometry. Afterward, synthesized thin films were planned to be investigated in order to compare their extractive capabilities with thin films prepared using unmodified PDMS. Extractions were planned to be performed with analytes selected to represent the small biomolecules present on the eye surface to be separated and detected via LC-MS. Phosphate buffered saline solutions buffered to pH 7.4 and from *in vitro* eye models prepared with agarose hydrogels in 3D printed molds that were designed to be similar to the anatomical structure of the human eye spiked with chosen analytes were planned to be used for extractions. After investigating the extractive capability of the synthesized thin films, extraction parameters were planned to be investigated in order to optimize the extraction process, and figures of merit were proposed for the optimized extraction with the best performing extractive contact lens device.

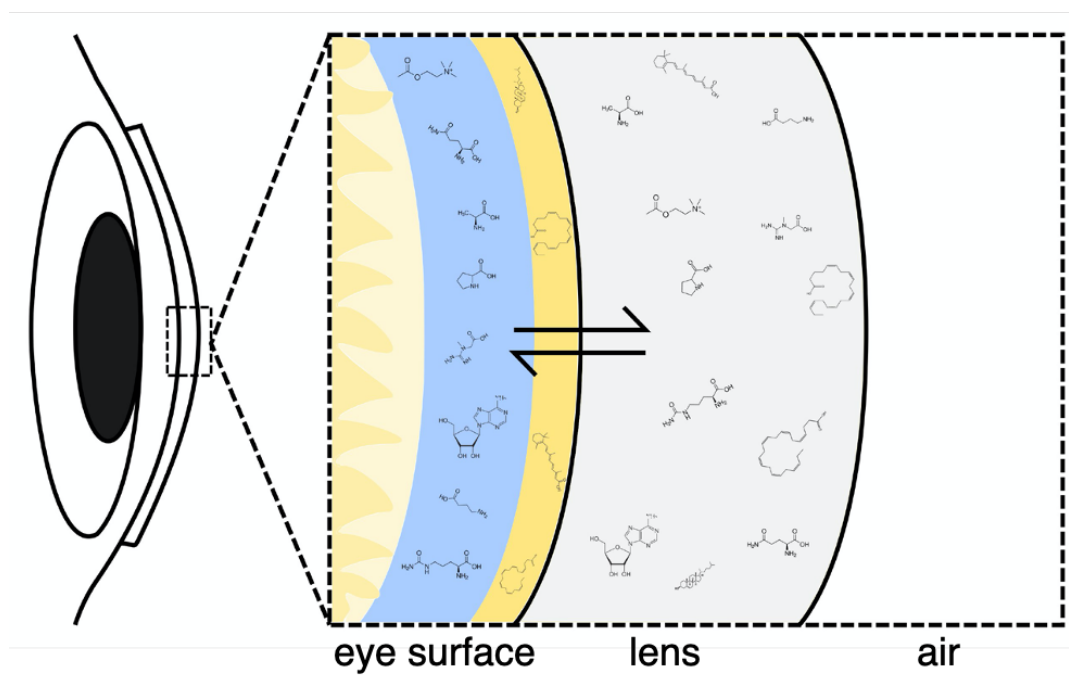


Figure 1.6 Schematic representation of the proposed extraction of analytes with the contact lens type devices from the eye surface

EXPERIMENTAL

2.1 Reagents and Materials

Reagents used in the preparation of contact lens type thin films: polydimethylsiloxane (Dowsil 184 elastomer kit), hydroxyl-terminated PDMS (18,000-22,000 cSt), polymethylhydrosiloxane (PMHS, 15-40 mPa·s), aminopropyltriethoxysilane (APTES), acetic acid (reagent grade), toluene (HPLC grade) and triethoxy-3-(2-imidazolin-1-yl)propylsilane (IZPES) were bought from Sigma-Aldrich. Trifluoroacetic acid (TFA, HPLC grade) was bought from Merck.

Reagents used in *in vitro* eye model: agarose (Type II) was bought from Sigma-Aldrich.

Analytical standards: phenylalanine, proline, citrulline, docosahexaenoic acid, acetylcholine, creatine, γ -aminobutyric acid, acetylcarnitine, and adenosine were purchased from Sigma-Aldrich. Glutamine and tryptophan were purchased from BioChemika. Retinoic acid was purchased from Acros Organics.

LC mobile phases: acetonitrile (HPLC grade), methanol (HPLC grade), and ammonium formate (HPLC grade) were purchased from Merck.

Isopropyl alcohol (IPA) (HPLC grade) and ethanol (both HPLC and reagent grades) were purchased from Sigma Aldrich. Only ultrapure (18.2 M Ω .cm, MilliPore) water was used in all experiments.

Solvents: reagent grade dichloromethane (DCM) Sigma-Aldrich, reagent grade dimethylformamide (DMF) Sigma-Aldrich, reagent grade methanol Merck, reagent grade ethanol Sigma-Aldrich were used for clean-up purposes.

2.2 Instruments

Molds for *in vitro* eye model and contact lens type thin films were designed using CAD software and printed with an SLA (resin printing) 3D printer using FormLabs Form 2 White and Black resins.

Infrared (IR) spectroscopic characterization of contact lens type thin films were done using Thermo Fisher Smart iTR ATR-FTIR instrument, and contact angle measurements were performed with Biolin Scientific Attention Theta Goniometer instrument. Thermogravimetric analysis was performed on Hi-Res TGA 2050 Thermogravimetric Analyzer. SEM and EDX analysis were performed on QUANTA 400F Field Emission SEM.

LC-MS instruments used in the experiments were located in Hacettepe University Chemistry Department in the Mass Spectrometry Laboratory of Prof. Dr. Bekir Salih. Instruments used were Agilent 1200 HPLC system equipped with Merck SeQuant ZIC-HILIC (column dimensions: 100 x 2.1 mm, 3.5 μm , 200 \AA) for polar analytes, and Supelco Ascentis Express F5 (column dimensions: 50 x 2.1 mm, 2.7 μm) for non-polar analytes, coupled to Agilent 6530 Q-TOF mass spectrometer.

2.3 Design of extractive thin film molds

In order for the extractive thin films to be as non-invasive as possible, their thickness and geometry were modeled after commercial contact lenses. Thickness and radius of contact lenses range between 0.050 – 0.260 mm in the central region and 0.080 – 0.240 mm in the peripheral region with a radius between 8.0 – 10.0 mm [263], and the thickness and radius of contact lens type thin films for chosen as 0.150 mm and 10 mm, respectively. Dimensions of the contact lenses were chosen with the limitations of the 3D printer in mind, as details smaller than 0.010 mm could not be printed with the instruments available.

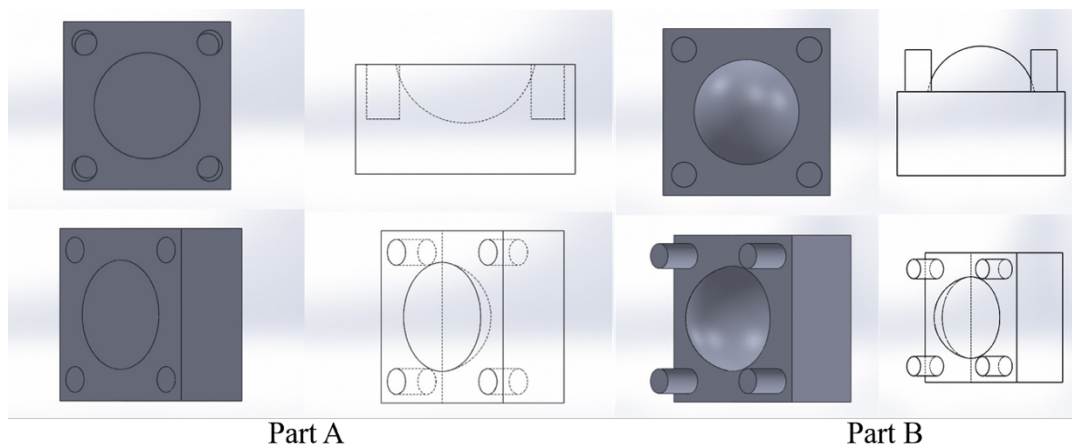


Figure 2.1 3D printed mold for contact lens type extractive thin films, part A (on the left) is made up of a convex half-sphere, and part B (on the right) is made up of a concave half-sphere

The design is relatively straightforward; the mold is made up of two separate parts, part A (on the left) has a convex half-sphere with a radius of 10.0 mm, while the concave half-sphere on part B (on the right) has a radius of 9.85 mm, as can be seen in Figure 2.1 above. When the two parts are connected, as shown in Figure 2.2, using four guidance rods located in part B, the radius difference between spheres in different parts creates a gap of 0.15 mm. A hole located at the center of part A allows the sol-gel mixture to be injected into the mold directly and also serves as an exhaust from which gases produced during the polymerization reaction can escape. The injected sol-gel mixture takes the shape of the gap, and after polymerization, a thin film with contact lens geometry with a thickness of 0.15 mm and a radius of 10.0 mm is produced.

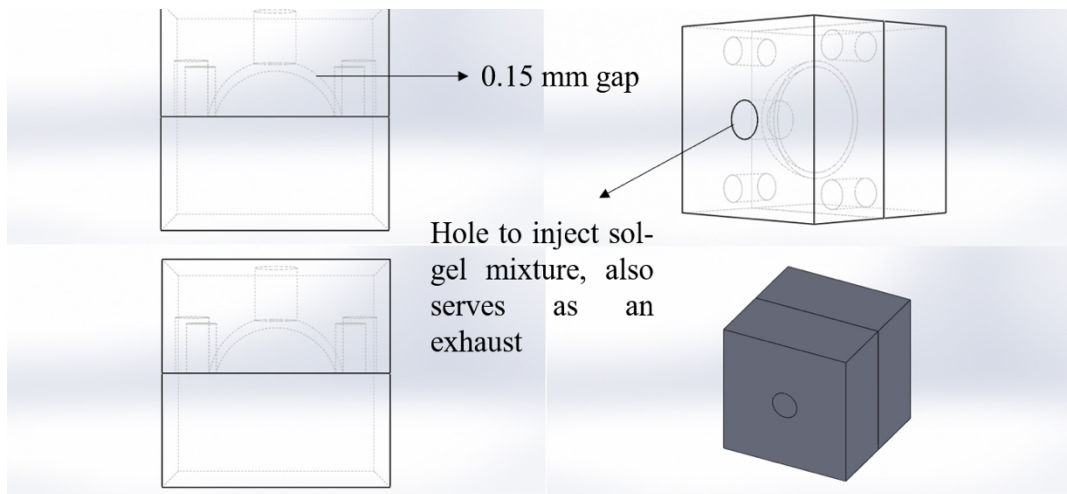


Figure 2.2 The conjoined form of the mold for contact lens type thin films, the hole on the top of part B allows the sol-gel mixture to be directly injected into the mold and also serves as a gas exhaust

2.4 Design of the *in vitro* eye model mold

In order to evaluate the potential of thin films for *in vivo* applications, an *in vitro* model of the human eye had to be developed for conducting static extraction experiments. The dimensions and geometry of the human eye vary from person to person, and its radius is considered to be 24.4 ± 3.0 mm on average [264]. A realistic model of the human eye was designed using CAD software, and molds were prepared using a 3D printing technique.



Figure 2.3 Molds of the eye model designed for *in vitro* extraction experiments, part A (upper part of the figure) features a hole to inject the agarose mixture (similar to the contact lens type thin film mold), two parts of the mold combined via an interlocking mechanism

The *in vitro* eye model consists of two parts, see Figure 2.3, part A features a small hole in which the agarose mixture can be injected into and also serves as a gas/cooling exhaust. Part B is designed to have a rectangular base to provide a level foundation for the mold to rest on safely. Two parts can be conjoined by interlocking the grooves on parts A and B.

2.5 Synthesis of contact lens type thin films

Traditionally, the earliest materials for contact lenses was poly(2-hydroxyethyl)methacrylate (pHEMA) for “soft” lenses and polymethyl methacrylate (PMMA) for “hard” lenses [265]. Since the 1960s and 1970s, silicone-based hydrogels have been used increasingly, and more recently, copolymers of siloxymethacrylates and fluoromethacrylates with silicone monomers alongside more hydrophilic hydrogels such as polyvinyl alcohol (PVA) [265]. Since the ultimate goal of this thesis is *in vivo* applicability, the most important criteria for

material selection was biocompatibility. One of the most commonly used silicone-based hydrogels routinely used in implants is polydimethylsiloxane (PDMS). PDMS is an optically transparent, non-toxic, biocompatible, inert, and flexible biocompatible material [266]. PDMS is a relatively hydrophobic polymer and widely used for the extraction of relatively non-polar analytes [207,267] but does not show similar sensitivity for the extraction of polar analytes [268]. Therefore, a modification either to the surface or bulk properties of PDMS is necessary to cover a wide range of analytes in terms of polarity. Surface and bulk functionalization of PDMS is an active research field with many different reaction schemes and methods documented in the literature [269–275]. These properties of PDMS make it the best candidate material for the contact lens type thin films as it satisfies the requirements to develop *in vivo* extractive thin film for sampling from the eye surface.

Two most commonly used PDMS functionalization techniques are the so-called “post-modification” method and *in situ* modification. In the post-modification technique, PDMS is modified after polymerization reactions take place, and the thin film is given its final shape. On the other hand, *in situ* modification technique directly modifies the siloxane backbone of PDMS before polymerization.

2.5.1 Post-modification method

In the post-modification technique as reported in the literature by Boyaci and Liu as a surface modification technique for silica particles [270,276], siloxane groups on a 0.50 g thin-film PDMS surface were converted to silanol via treatment with 2.0 mL 0.010 M acetic acid for one hour and rinsed with ultrapure water until the acidic medium is washed away. Afterward, activated PDMS was dried for 24 hours at 120 °C and placed in a pre-dried two-neck 25 mL flask with 0.30 mL APTES and 0.90 mL toluene. The reaction flask was connected to a condenser equipped with a drying tube filled with anhydrous CaCl₂ and flushed with N₂ gas continually through its sidearm. The flask was heated in an oil bath at 110 °C for 24 hours and stirred at 200 rpm under constant reflux. After the modification reaction was completed, amine-

modified PDMS is washed with acetone and toluene and dried overnight. Figure 2.4 shows the proposed surface functionalization of the PDMS surface with APTES functional groups[277].

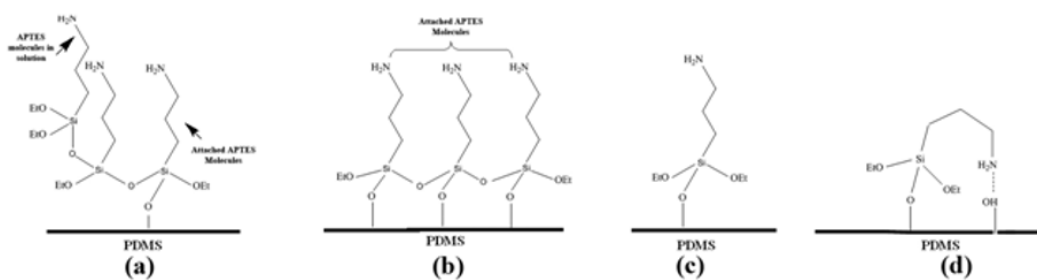


Figure 2.4 Proposed schematic representation of PDMS surface functionalization (a) vertical (b) horizontal (c) upright (d) tilted. Reproduced with permission from [277] and SBAOI.

2.5.2 *In situ* modification method

In situ modification of PDMS thin films were thoroughly investigated by conducting modification experiments with different ratios and with different starting materials. In the initial experiments, APTES precursor was hydrolyzed under acidic conditions (95% TFA) and coupled with -OH terminated PDMS and finally polymerized by employing a PDMS backbone (DOWSIL 194 Elastomer Kit).

A typical *in situ* modification reaction would start with the hydrolysis of 0.050 g of APTES precursor and 1.00 g of OH terminated PDMS in 0.050 g of 95% TFA for 6 hours at room temperature and constant stirring at 800 rpm. Afterward, 2.50 g of DOWSIL 184 Elastomer Kit A, containing PDMS base, was added to the sol-gel mixture and stirred at 800 rpm for 1 hour at room temperature, when homogeneous mixing was achieved 0.25 g of DOWSIL 184 Elastomer Kit B, containing polymerization catalyzer, was added and the mixture was stirred at 800 rpm for 30

minutes. The mixture was then transferred to the 3D printed mold via an injector for polymerization at room temperature and left overnight. After polymerization was completed, the mold was carefully parted and the contact lens thin film was removed to be washed with 5.0 mL portions of DMF, DCM, and methanol consecutively for removal of any excess reagents, afterward thin films were conditioned in 70% ethanol solution overnight. Figure 2.5 outlines the scheme of a typical *in situ* -OH terminated PDMS modification reaction. The extractive thin films prepared with this scheme will be referred to as type I thin films for convenience throughout the thesis.

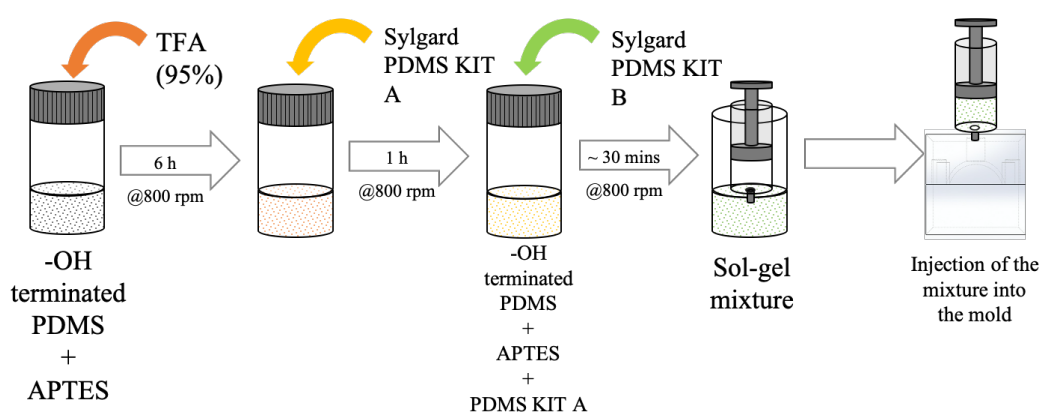


Figure 2.5 Preparation of type I thin films

Figure 2.6 below outlines the hydrolysis of APTES molecule and its coupling reaction to -OH terminated PDMS; after the coupling reaction was completed DOWSIL 184 Elastomer Kit was used for adding the PDMS backbone and for initiating the polymerization reaction. In order to prepare a thin film that satisfies the physical requirements laid out above, i.e., optical transparency, flexibility, different ratios of starting materials and different polymerization schemes were experimented with. Table 2.1 includes the parameters for modification of -OH terminated PDMS with APTES and its consequent polymerization with DOWSIL 184 Elastomer Kit.

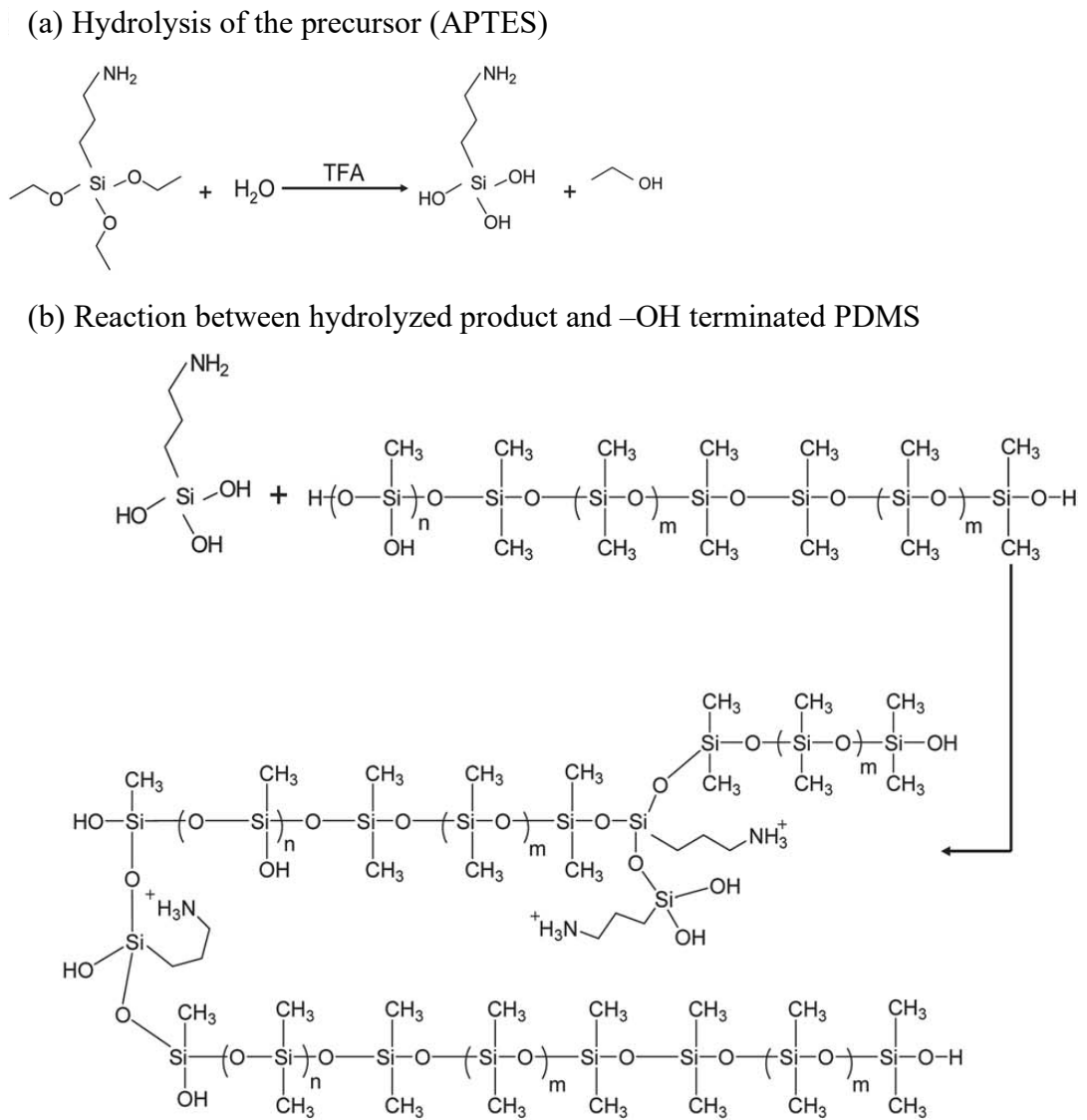


Figure 2.6 Reaction scheme for modification of -OH terminated PDMS with APTES precursor

Table 2.1 Parameters for -OH terminated PDMS modification reactions (continued on the next page).

Sample #	APTES (g)	TFA:H ₂ O (95%) (g)	-OH terminated PDMS (g)	DOWSIL Elastomer Kit A (g)	Reaction temperature and time
1	0	0	0	2.50	80 °C, 2 h
2	0.90	0	0	2.50	
3	0.50	0	0	2.50	
4	0.25	0	0	2.50	
5	0.50	0.50	0	2.50	
6	0.50	0	0.50	2.50	
7	0.50	0	0.25	2.50	
8	0.50	0.25	0.50	2.50	
9	0.75	0.25	0.75	2.50	60 °C, 2 h
10	1.00	0.25	1.00	2.50	
11	0.50	0.25	0.50	2.50	
12	0.75	0.25	0.75	2.50	Room temperature, ~6 h
13	1.00	0.25	1.00	2.50	
14	0.50	1.00	0.50	2.50	
15	0.50	1.50	0.50	2.50	
16	0.50	2.00	0.50	2.50	
17	0.50	1.00	1.00	2.50	
18	0.25	1.00	1.00	2.50	
19	0.10	0.10	1.00	2.50	

Sample #	APTES (g)	TFA:H ₂ O (95%) (g)	-OH terminated PDMS (g)	DOWSIL Elastomer Kit A (g)	Reaction temperature and time
20	0.050	0.050	1.00	2.50	Room
21	0.010	0.010	1.00	2.50	temperature, ~6 h

As can be surmised from the reaction scheme shown in

Figure 2.6 -OH terminated PDMS has limited available sites for APTES modification. However, in order to increase the extraction capabilities of the extractive thin films, it was hypothesized that more polar functional groups have to be introduced. Polymethylhydrosiloxane (PMHS) has a similar molecular structure to PDMS, see Figure 2.7, with one distinctive feature, instead of two methyl groups as in PDMS, PMHS has one methyl group attached to the central Si atom and an H atom attached instead of the second methyl group. Another modification scheme was investigated to increase the amount of amine functional groups by attaching more APTES molecules to the PMHS backbone. Figure 2.8 outlines the modification scheme of PMHS with APTES, and it can be seen that it was virtually identical to the modification scheme of -OH terminated PDMS with one crucial exception, which was the amount of APTES that ends up in the final polymer thin film.

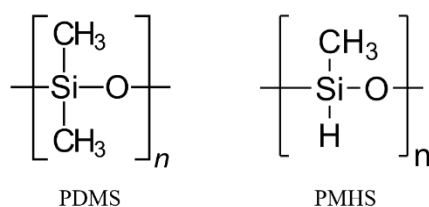


Figure 2.7 Molecular structures of PDMS (on the left) and PMHS (on the right)

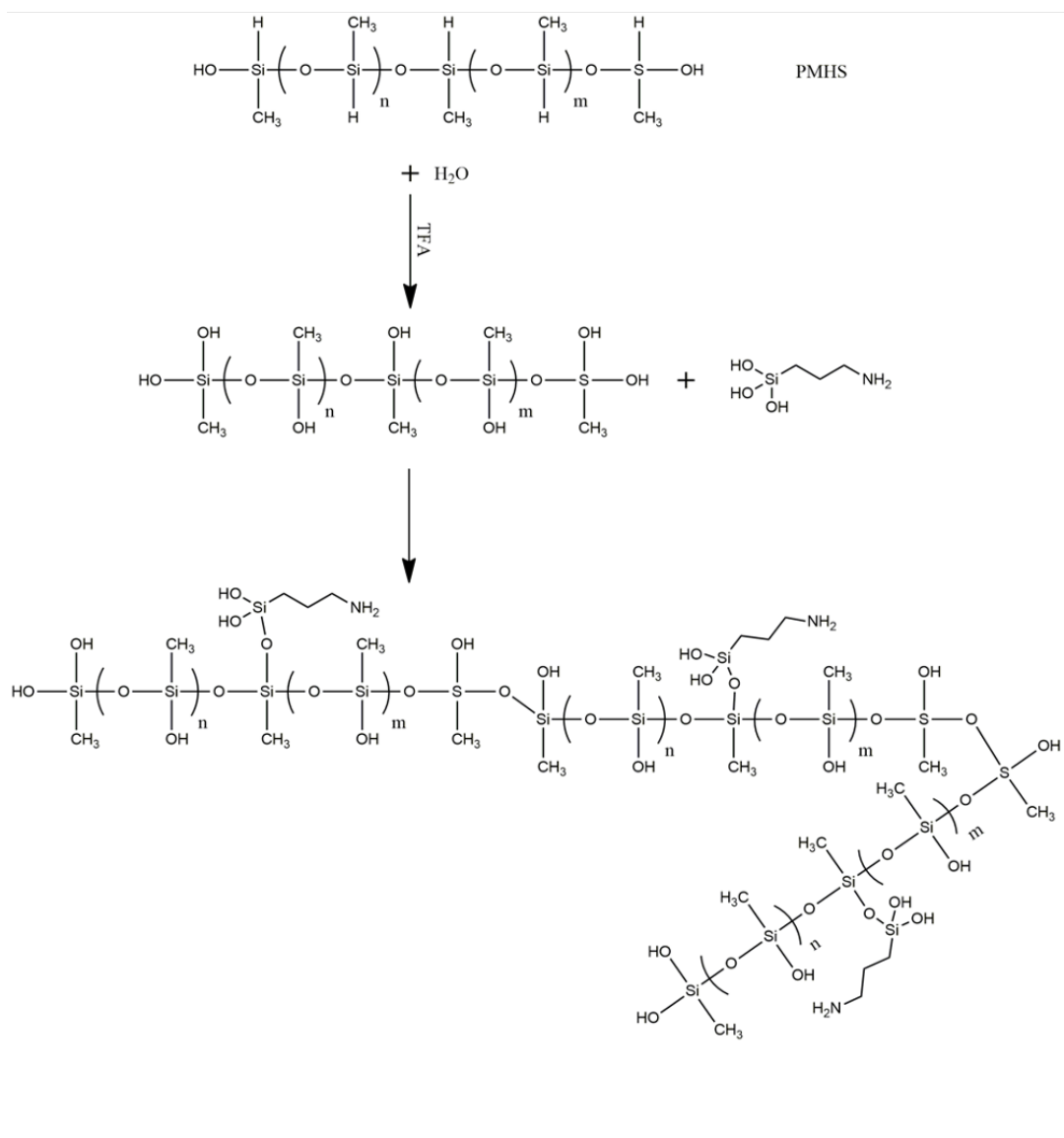


Figure 2.8 Reaction scheme for modification of PMHS with hydrolyzed APTES (hydrolysis of APTES is identical to one shown in

Figure 2.6)

A typical *in situ* modification of PMHS with APTES begins with the hydrolysis of 1.5 g of APTES precursor and 1.0 g of PMHS with 0.10 g of 95% TFA stirred at 800 rpm for 6 hours at room temperature. Afterward, 2.5 g of DOWSIL 184 Elastomer Kit A, containing PDMS base, is added and stirred at 800 rpm for 1-hour room

temperature. When a homogeneous mixture is observed, 0.5 g of DOWSIL 184 Kit B, containing the catalyzer for polymerization reaction, is added and stirred at 800 rpm for 30 minutes at room temperature. Afterward, the mixture is transferred to the 3D printed mold via an injector and left at room temperature for 24 hours. After the polymerization is complete, the mold is carefully parted and the extractive thin film is washed with 5.0 mL portions of DMF, DCM, and methanol consecutively for removal of any leftover from the modification or polymerization reaction. Finally, the thin films are left overnight in 70% ethanol solution for conditioning which also sterilizes the lenses. Figure 2.9 outlines the scheme of a typical *in situ* PMHS modification reaction. The contact lens-type extractive thin films prepared with this scheme will be referred to as type II thin films for convenience throughout the thesis. Table 4 includes the amount of starting material used in type II thin film modification, and all modification reactions were carried on at room temperature.

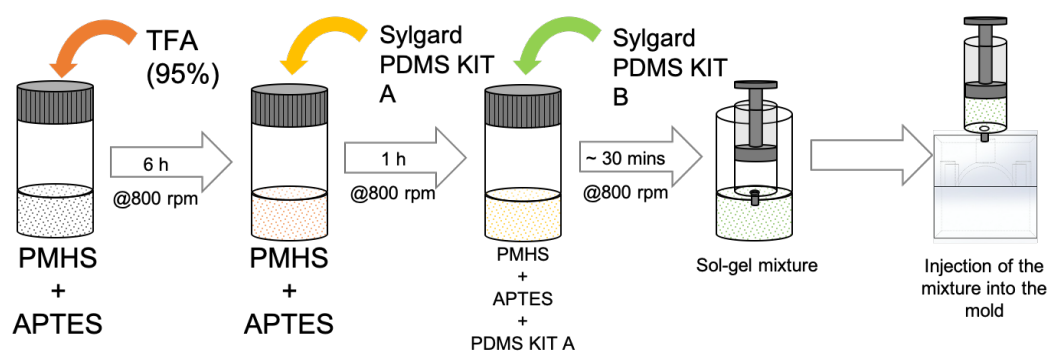


Figure 2.9 Preparation of type II thin films

Table 2.2 Parameters for -OH terminated PMHS (type II thin films) modification reactions

Sample #	APTES (g)	TFA:H ₂ O (95%) (g)	PMHS (g)	DOWSIL Elastomer Kit A (g)	DOWSIL Elastomer Kit B (g)
22	2.00	0.05	1.00	1.75	0.20
23	2.00	0.05	1.00	2.20	0.25
24	1.00	0.05	1.00	2.50	0.25
25	0.50	0.05	1.00	3.00	0.30
26	1.00	0.10	1.00	2.50	0.25
27	2.00	0.25	1.00	2.50	0.25
28	1.50	0.10	1.00	2.50	0.25

As a part of *in situ* modification investigation, PDMS, -OH terminated PDMS and PMHS thin films modified with triethoxy-3-(2-imidazolin-1-yl)propylsilane (IZPES) were also attempted. However, no suitable thin film was able to be synthesized and IZPES modification scheme was eventually abandoned.

2.6 Characterization of extractive thin films

Extractive lenses were characterized using ATR-FTIR spectroscopy, contact angle measurements, and thermogravimetric analysis. ATR-FTIR spectra of thin films were investigated before and after being first submerged in DCM for 3 hours and in 70% ethanol for 24 hours. Since DCM is known to penetrate PDMS and cause swelling [278], the solvents would carry out any reaction leftovers or aggravated molecules. All samples were also cleaned with small portions of reagent grade

ethanol before ATR-FTIR measurements by gentle rinsing and dried at room temperature.

Contact angle measurements were carried out with ultrapure water (18.2 M Ω .cm) before and after thin films were washed with the same procedure laid out above for ATR-FTIR measurements. The principle behind setting contact angle measurements was the same with ATR-FTIR measurements. If any reaction leftovers or aggravated molecules (polymer oligomers) carried out during DCM and ethanol treatment, the surface properties of the thin films would change, affecting their surface hydrophilicity.

TGA was conducted after synthesized thin films were conditioned with 5.0 mL of DCM and left overnight in 70% ethanol solution. In order to drive out any water molecules on the surface or embedded inside the thin films, the samples were parked at 200 °C for 10 minutes and cooled down to RT before analysis.

SEM images and EDX analysis of the thin films were carried out after washing with DCM and 70% ethanol, identically as the procedures laid out above. Thin films were not coated with Au nanoparticles to increase the quality of SEM images as EDX analysis was carried out simultaneously. SEM magnification was set to 500x.

2.7 Preparation of *in vitro* eye model

In order to test the extractive thin films in an environment as similar to the human eye as possible, an eye model was designed with the same anatomical dimensions as the human eye. However, it is a Herculean task to build a model to mimic the complex physiological environment of the human eye closely. Therefore, the aim was for the eye model to represent the type of extraction that would be performed by the lens type thin films, i.e., static extraction, and it was not intended for the eye model to closely replicate the biological environment of the human eye. Agarose was chosen as a promising media for building the eye model as recent literature has

shown its potential as a biomimetic tissue-like material [279,280], and it was even used to build an *in vitro* test platform for contact lenses [281].

Agarose eye model preparation is relatively straightforward, to prepare a 2% gel, 0.1 g of agarose is thoroughly mixed in 5.0 mL of water and heated for 20 seconds at 100 kW power in a commercial microwave. Afterward, the mixture is left to cool down to 40 °C in order to prevent any damage to analyte standards. Then, standards analytes are added while continuously stirring the mixture at 1200 rpm and 40 °C to prevent gelation. After a homogeneous mixture is achieved, agarose is quickly poured in the 3D printed mold to cool down further and given its final shape.

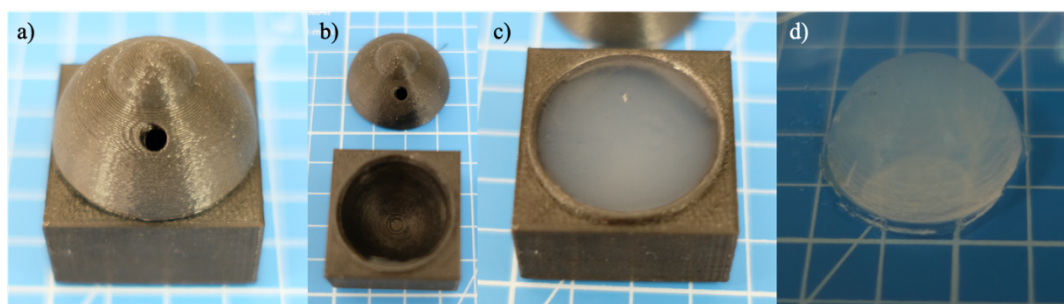


Figure 2.10 a) 3D printed mold (conjoined) b) two separate parts of the mold c) the *in vitro* eye model before being removed from the mold d) *in vitro* eye model after removed from the mold

In vitro eye models were prepared with different agarose contents, i.e., 0.5%, 1%, and 2% agarose, in order to evaluate their physical similarity to the human eye, shown in Figure 2.10. These eye models with different agarose content were also used to determine the water loss of agarose due to evaporation. Five replicate eye models were prepared for each agarose ratio and weighed for every 5 minutes for 2 hours to determine the rate of water loss. Since the concentration of analytes in the agarose eye models would change with water loss, which could also affect the dynamics of extraction, it was crucial to find out whether evaporation would reach equilibrium or at least occur at a predictable rate. Figure 2.11 shows that for all three

gel concentrations, loss of gel mass due to water evaporation stops at around 30 minutes.

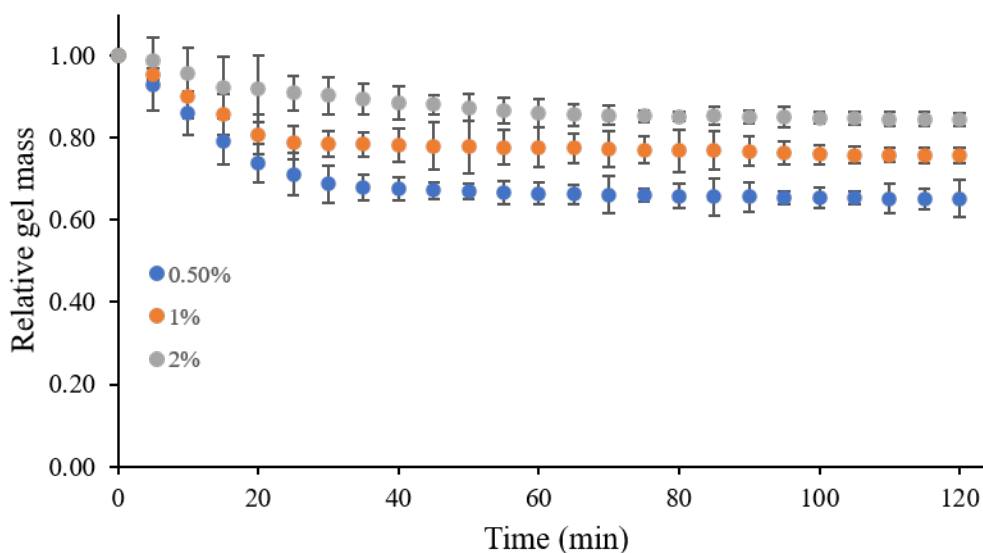


Figure 2.11 Relative mass loss of *in vitro* eye models prepared with agarose hydrogels with different gel concentrations

2.8 Development of LC-MS methods

Two separate LC-MS methods were developed for polar and non-polar analytes. Merck SeQuant ZIC-HILIC (100 x 2.1 mm, 3.5 μm , 200 \AA) HPLC column was used for chromatographic separation of polar analytes. In order to achieve the best sensitivity and lowest LOQ values as possible as well as adequate separation and retention of analytes, various ratios of mobile phases and additives were investigated. After initial experiments where flow rate, additive concentration, the composition of mobile phases, column temperature, injection volume were investigated, it was concluded that the best chromatographic separation was achieved using gradient elution with two mobile phases at 0.40 mL \cdot min $^{-1}$. Solvent A was 0.15% formic acid

and 25 mM ammonium formate buffered to pH 4.5 in ACN:H₂O (80:20, v/v), and Solvent B was 0.15% formic acid and 25 mM ammonium formate buffered to pH 4.5. The gradient started at 100% Solvent A and kept for 5 min at this composition, then changed to 80% A and 20% B in 10 min linearly (2.5% per minute), resulting in final solvent composition of ACN:H₂O (65:35, v/v). Next, the gradient was changed to initial condition 100%A and kept at this composition for 3 min before the next injection. The injection volume of samples was set to 50 µL with a column temperature of 40 °C and the total run time was 15 minutes. Table 2.3 shows LC parameters for the HILIC method.

Table 2.3 LC parameters for HILIC method (polar analytes)

Mobile phase	Mobile phase ratio (A:B, v/v)	Flow rate
A: 25 mM ammonium formate buffered to pH 4.5 in ACN:H ₂ O (80:20, v/v)	0 – 5 min: 100:0	0.20
B: 25 mM ammonium formate in 0.15% formic acid buffered to pH 4.5	5 – 15 min: 80:20 (2%·min ⁻¹) 15 -18 min: 100:0	mL·min ⁻¹

MS parameters for polar analytes were also investigated for best sensitivity and were determined as follows:

Table 2.4 MS parameters used in HILIC LC-MS method for polar analytes

MS parameters	
Ion polarity	Positive
Nebulizer pressure	45 psi
Nebulizer temperature	350 °C
Nozzle voltage	1.50 kV
Capillary potential	3.50 kV

In the case of non-polar analytes, Supelco Ascentis Express F5 HPLC column was used. Various ratios of mobile phases were investigated in order to achieve the best sensitivity, lowest LOQ, and good separation/retention times. After initial experiments, the best chromatographic separation was achieved with 8 min isocratic method with a mobile phase flow velocity of 0.20 mL·min⁻¹. The mobile phase consisted of a mixture of Solvent A (60%) and Solvent B (40%) where Solvent A was MeOH:H₂O (50:50, v/v), and Solvent B was 5.0 mM ammonium formate in ACN:H₂O (90:10, v/v). The injection volume of samples was set to 50 µL with a column temperature of 40 °C. Table 2.5 shows the LC parameters for the reverse phase method.

Table 2.5 LC parameters for reverse phase method (non-polar analytes)

Mobile phase	Mobile phase ratio (A:B, v/v)	Flow rate
A: MeOH:H ₂ O (50:50, v/v)	0 – 6 min: 60:40	0.20 mL · min ⁻¹
B: 5 mM ammonium formate in ACN:H ₂ O (90:10, v/v)	6 – 8 min: 100:0	

MS parameters were investigated to give the best sensitivity for non-polar analytes and were determined as follows:

Table 2.6 MS parameters used in reverse phase LC-MS method for non-polar analytes

MS parameters	
Ion polarity	Negative
Nebulizer pressure	45 psi
Nebulizer temperature	350 °C
Nozzle voltage	1.50 kV
Capillary potential	3.50 kV

2.9 Optimization of extraction parameters

In order to evaluate the extractive capabilities of modified thin films, a series of extraction experiments with unmodified PDMS, type I, and type II thin films were designed. PBS buffered (pH 7.4, 1X) solutions and *in vitro* eye models were spiked with various concentrations of polar and non-polar analytes using stock solutions prepared with analyte standards. Extraction time for *in vitro* eye models, desorption time, and desorption solvents were also investigated to increase the overall sensitivity and reproducibility of the method. All extractions were performed at room temperature with three replicates unless stated otherwise.

2.9.1 Optimization of extractions from PBS buffer solutions

In a typical extraction, outlined in Figure 2.12 below, 4.0 mL of PBS solution was spiked with analyte concentrations ranging from 5.0 ng·mL⁻¹ to 250.0 ng·mL⁻¹ in different 10 mL vials, and circular thin films with 2.0 mm diameter were submerged with a nitinol wire into the solution and continuously stirred at 1200 rpm for 2 hours. In order to quantitatively compare the thin films, each thin film was weighed before extractions, and extracted analyte amounts were corrected using thin films' weight (at no point weight difference exceeded 5%). Afterward, the thin films were gently rinsed with few drops of water to drive away any PBS droplets that may cling to its surface before the desorption step. Desorption was achieved by submerging the thin films with a nitinol wire into 0.40 mL of ACN:MeOH:H₂O (40:40:20, v/v/v) for 30 minutes and continuously stirred at 1200 rpm. The extraction scheme outlined above and shown in Figure 2.12 was used to determine the extraction capabilities of PDMS, type I, and type II thin films. After the best performing lens type thin film was determined with the extraction scheme described above, desorption parameters were optimized as shown in Table 2.7 below.

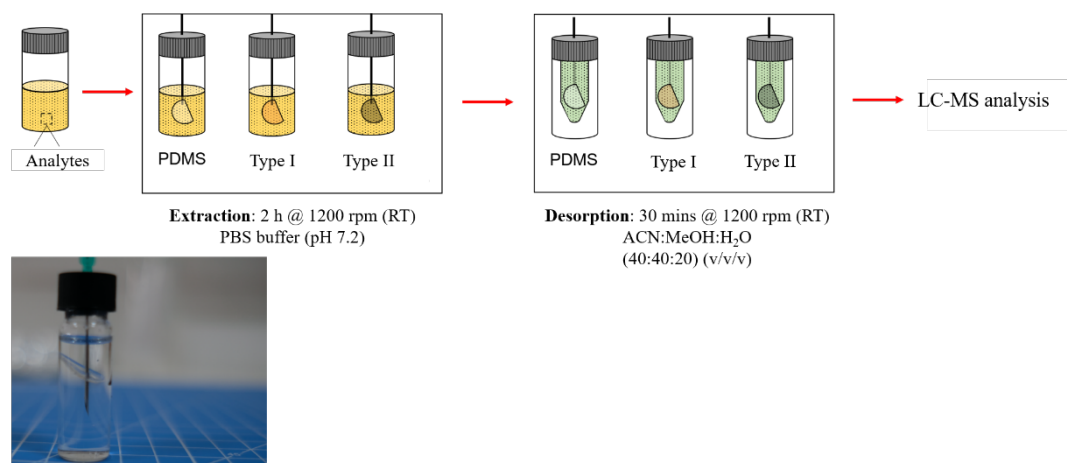


Figure 2.12 A typical extraction from PBS solutions spiked with analytes by extractive thin films

Table 2.7 Optimization of desorption parameters for extractive thin films (Extraction conditions; extraction time: 120 mins, extraction volume: 4.0 mL, extraction agitation: 1200 rpm)

Investigated desorption parameter	Desorption solvent	Analyte concentration	Desorption volume	Desorption agitation	Desorption time
Desorption solvent	ACN:MeOH:H ₂ O (40:40:20, v/v/v)	100.0 ng·mL ⁻¹	0.40 mL	1200 rpm	30 min
	ACN:MeOH (50:50, v/v)				
	ACN:IPA:H ₂ O (40:40:20, v/v/v)				
Desorption time	ACN:MeOH:H ₂ O (40:40:20, v/v/v)	100.0 ng·mL ⁻¹	0.40 mL	1200 rpm	5 min ^a 15 min ^a 30 min ^a 60 min ^a

a) Another round of desorptions was carried out for 30 minutes with constant stirring at 1200 rpm to determine the amount of carryover

Table 2.7 above follows the order of experiments to determine the optimal desorption parameter following extractions with the thin films. First, three different desorption

solvents were investigated to determine which solvent would lead to the most amount of analyte desorbed from the thin films with no carryover. Thin films were submerged into 4.0 mL of PBS solution spiked with $100.0 \text{ ng}\cdot\text{mL}^{-1}$ of analytes and extraction was carried out for 2 hours at 1200 rpm. After the extractions, thin films were rinsed with water and submerged in different desorption solvents for 30 minutes. After the first round of desorptions were completed, the thin films were rinsed with water for a second time, and the second round of desorptions was carried out at 1200 rpm 30 minutes to determine whether all analytes were completely desorbed from the thin films in the first desorption round (a carryover experiment).

The second parameter to be investigated was the desorption time after the best desorption solvent was determined, extractions were performed from 4.0 mL of PBS solutions spiked with $100.0 \text{ ng}\cdot\text{mL}^{-1}$ of analytes for 2 hours at 1200 rpm. Afterward, thin films were rinsed with a few drops of water to drive away any solvent, and desorptions were carried out at 1200 rpm for 5, 15, 30, and 60 minutes in order to determine the least amount of time necessary for complete desorption of analytes from the thin films.

2.9.2 Optimization of extractions from *in vitro* eye model

In order to evaluate the extractive capabilities of lens type thin films from an environment similar to the human eye, extractions from the *in vitro* eye model were carried out, shown in Figure 2.13 below. These extractions were also more similar to *in vivo* conditions as extractions from PBS solutions were carried out under constant stirring. First, in tandem with the PBS solution extractions as laid out above, the best performing thin film was determined with the following extraction experiment. Agarose eye models were prepared and spiked with $250.0 \text{ ng}\cdot\text{mL}^{-1}$ of analytes and unmodified PDMS, type I, and type II thin films with lens shapes were used for extraction. The thin films were placed directly on top of the eye models, ensuring full contact at all times. The extractions were carried out for 2 hours with

no agitation, under static conditions. After extraction, thin films were rinsed with water and desorbed in ACN:MeOH:H₂O (40:40:20, v/v/v) for 30 minutes.

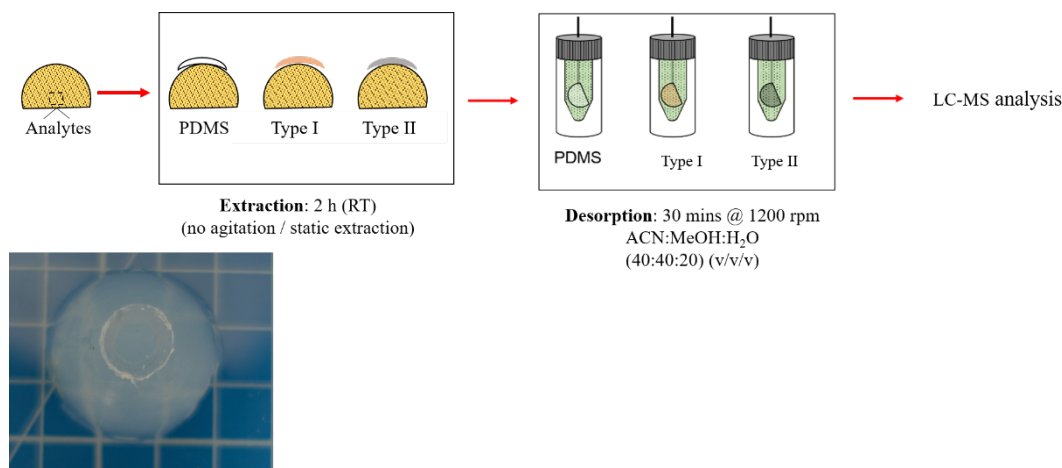


Figure 2.13 A typical extraction and desorption scheme from *in vitro* eye models spiked with analytes by extractive lens type thin films

After the best performing thin film was determined, the extraction time profile for sampling from the *in vitro* eye model was built. Lens type thin films (type II) were placed directly on top of agarose eye models spiked with 250.0 ng·mL⁻¹ of analytes for 15, 30, 60, and 120 minutes in order to determine if an extraction could be carried out with sufficient sensitivity in a lesser amount of time. After extractions were complete, the thin films were rinsed with portions of ethanol and water gently before moving onto the desorption step in 0.40 mL of ACN:MeOH:H₂O (40:40:20, v/v/v) for 30 minutes at 1200 rpm.

After extraction time profiles were built using the most optimal parameters for extraction and desorption, a calibration line for extracted analyte amounts from *in vitro* eye model was built. Agarose eye models were prepared and spiked with 25.0, 50.0, 100.0, 250.0, and 500.0 ng·mL⁻¹ of analytes. Lens type thin films (type II) were placed on top of the eye models, ensuring total contact and extraction was carried out under static conditions for 120 minutes. After the extractions were complete, the

thin films were gently rinsed with portions of ethanol and water before the desorption step was carried out. The thin films were directly submerged with nitinol wires into 0.40 mL of ACN:MeOH:H₂O (40:40:20, v/v/v/) for 30 minutes at 1200 rpm for desorption.

CHAPTER 2

RESULTS AND DISCUSSION

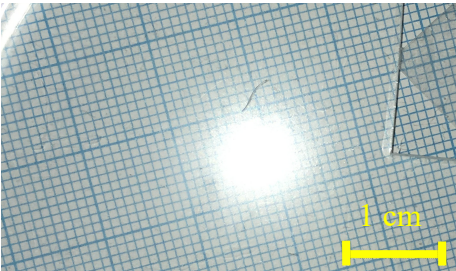
3.1 Evaluation of optimization of synthesis of extractive thin films

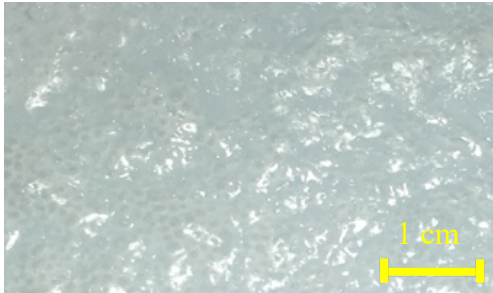

The first step of choosing a suitable thin film for characterization and extraction experiments was its physical attributes. As it was mentioned numerous times throughout the thesis, optical transparency, flexibility, and surface homogeneity were three crucial physical characteristics of any potential extractive thin film. Before any type of characterization, thin films were evaluated by these three properties. Table 3.1 and Table 3.2 lists some of the extractive thin films based on their physical properties. The thin films that had physical properties that satisfy the requirements previously laid out were selected for further characterization and extraction experiments. Evaluation of the physical properties of extractive thin films was based on an out of 10-point system. Unmodified PDMS was selected as to have 10 points out of 10 in flexibility, surface homogeneity, and optical transparency. Modified thin films were evaluated based on the similarity of their physical properties to those of unmodified PDMS thin films.

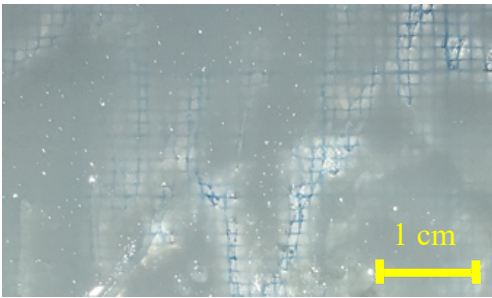
Evaluation of type I (APTES modified -OH terminated PDMS) thin films are given in Table 3.1 below. Modification parameters for the following samples can be found in Table 2.1 (in 2.5.2). Physical evaluation of synthesized thin films was not based on any instrumental analysis but an “eye test” comparing the flexibility, surface homogeneity, and optical transparency of the modified thin films to unmodified PDMS thin film. The most prevalent shortcoming of the modified thin films was the lack of surface homogeneity. It was observed that elevated temperatures cause the coupling reaction to take place too quickly, which traps the gases that evolve during polymerization reactions in bubbles, as can be seen in sample #4. Optical transparency was observed to be directly related to APTES amount, and flexibility

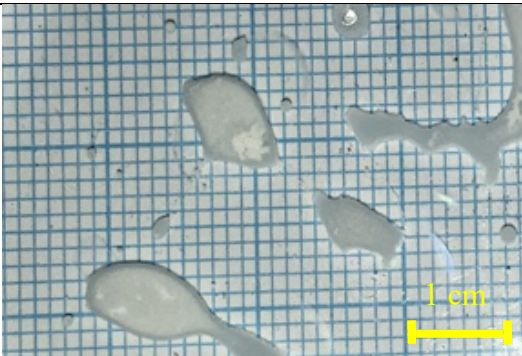
was found to change with controlling the ratio of -OH terminated PDMS to PDMS base (DOWSIL elastomer kit A). Consideration of these parameters showed that sample #21 demonstrated the best overall physical properties and was chosen for further characterization and investigation.

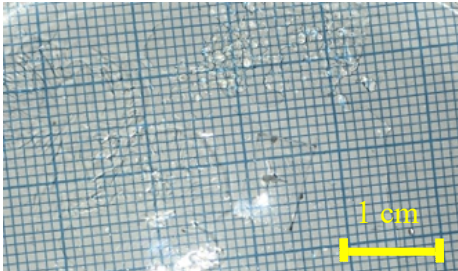
Table 3.1 Physical and visual evaluation of type I thin films

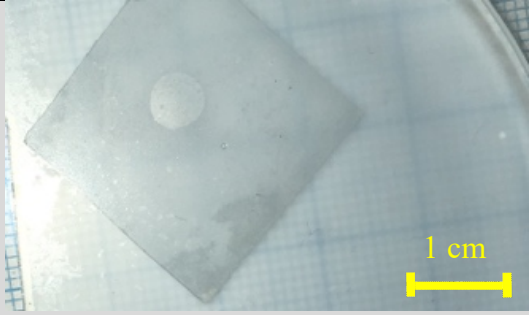
Sample #	Physical properties	Pictures of representative thin films
1 (Unmodified PDMS)	Flexibility: 10/10 Surface homogeneity: 10/10 Optical transparency: 10/10	
2	Flexibility: 2/10 Surface homogeneity: 2/10 Optical transparency: 1/10	No image available
3	Flexibility: 1/10 Surface homogeneity: 2/10 Optical transparency: 2/10	No image available

Sample #	Physical properties	Pictures of representative thin films
4	Flexibility: 1/10 Surface homogeneity: 2/10 Optical transparency: 2/10	
5	Flexibility: 2/10 Surface homogeneity: 2/10 Optical transparency: 2/10	<p style="text-align: center;">No image available</p>
6	Flexibility: 3/10 Surface homogeneity: 3/10 Optical transparency: 2/10	<p style="text-align: center;">No image available</p>
7	Flexibility: 2/10 Surface homogeneity: 3/10 Optical transparency: 3/10:	

Sample #	Physical properties	Pictures of representative thin films
8	Flexibility: 3/10 Surface homogeneity: 3/10 Optical transparency: 4/10	No image available
9	Flexibility: 3/10 Surface homogeneity: 3/10 Optical transparency: 3/10	No image available
10	Flexibility: 4/10 Surface homogeneity: 4/10 Optical transparency: 4/10	 <p>The image shows a thin film on a grid substrate. A yellow scale bar in the bottom right corner indicates a length of 1 cm. The film appears as a light-colored, textured layer on a darker grid background.</p>
11	Flexibility: 4/10 Surface homogeneity: 5/10 Optical transparency: 3/10	No image available

Sample #	Physical properties	Pictures of representative thin films
12	Flexibility: 4/10 Surface homogeneity: 5/10 Optical transparency: 4/10	No image available
13	Flexibility: 5/10 Surface homogeneity: 6/10 Optical transparency: 7/10	No image available
14	Flexibility: 5/10 Surface homogeneity: 6/10 Optical transparency: 6/10	
15	Flexibility: 6/10 Surface homogeneity: 7/10 Optical transparency: 6/10	No image available

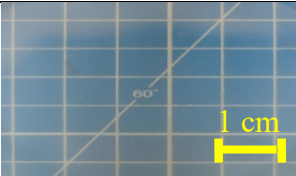
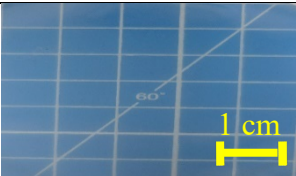

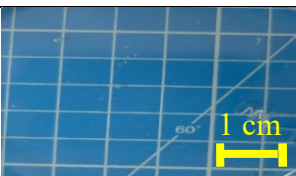
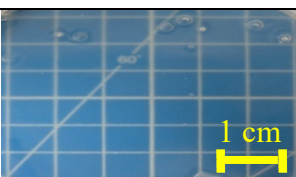

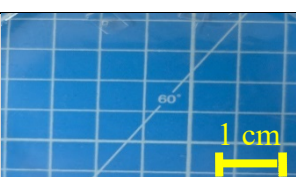
Sample #	Physical properties	Pictures of representative thin films
16	Flexibility: 6/10 Surface homogeneity: 6/10 Optical transparency: 7/10	No image available
17	Flexibility: 6/10 Surface homogeneity: 6/10 Optical transparency: 6/10	No image available
18	Flexibility: 7/10 Surface homogeneity: 7/10 Optical transparency: 9/10	
19	Flexibility: 8/10 Surface homogeneity: 6/10 Optical transparency: 7/10	No image available

Sample #	Physical properties	Pictures of representative thin films
20	Flexibility: 7/10 Surface homogeneity: 8/10 Optical transparency: 6/10	No image available
21	Flexibility: 9/10 Surface homogeneity: 10/10 Optical transparency: 8/10	 <p>(The dark area in the picture is caused by the removal of the square-shaped part of the membrane for ATR-FTIR and contact angle measurements)</p>

Evaluation of type II (APTES modified PMHS thin films) are given in Table 3.2 below. Modification parameters for type II thin films can be found in Table 2.2 (in 2.5.2). Evaluation of type II thin films was based on unmodified PDMS as described for type I thin films above. As it was the case for type I thin films, and type II thin films were also evaluated based on an “eye test”. Optical transparency, flexibility, and surface homogeneity of modified thin films were compared to those of unmodified PDMS thin film. Since reaction temperature and reaction time were optimized for type I films, surface homogeneity of the type II films was very similar to each other. It was observed that starting with PMHS instead of -OH terminated PDMS allowed for more APTES molecules to be incorporated into the final polymer while retaining optical transparency and flexibility to an acceptable degree. Sample

#28 demonstrated the best physical properties, most similar to unmodified PDMS thin film and was chosen for further characterization and investigation.

Table 3.2 Physical and visual evaluation of type II thin films

Sample #	Physical properties	Pictures of representative thin films
22	Flexibility: 6/10 Surface homogeneity: 9/10 Optical transparency: 7/10	
23	Flexibility: 6/10 Surface homogeneity: 9/10 Optical transparency: 7/10	
24	Flexibility: 7/10 Surface homogeneity: 9/10 Optical transparency: 8/10	
25	Flexibility: 6/10 Surface homogeneity: 9/10 Optical transparency: 8/10	
26	Flexibility: 6/10 Surface homogeneity: 3/10 Optical transparency: 7/10	
27	Flexibility: 5/10 Surface homogeneity: 3/10 Optical transparency: 5/10	
28	Flexibility: 8/10 Surface homogeneity: 9/10 Optical transparency: 9.5/10:	

3.2 Characterization of extractive thin films

3.2.1 FTIR characterization of thin films

FTIR spectra of PDMS show characteristic peaks for -CH_3 rocking at 786 cm^{-1} , -CH_3 deformation in Si-CH_3 at 1256 cm^{-1} , asymmetric -CH_3 stretching in Si-CH_3 at 2962 cm^{-1} , asymmetric Si-O-Si stretching at 1010 cm^{-1} [282,283]. Figure 3.1 below clearly shows there is no discernable difference between spectra of unmodified PDMS before and after washing with DCM and 70% ethanol. Both spectra are normalized with respect to wavelengths that show 100% transparency in order to demonstrate that washing does not affect absorbance values of characteristic PDMS peaks, meaning that crosslinking of polymer chains is not affected by washing.

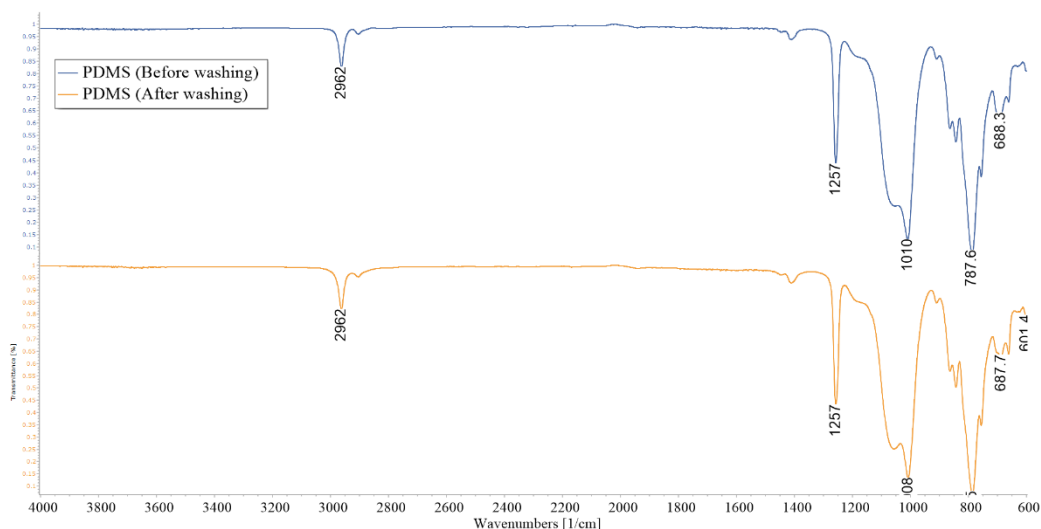


Figure 3.1 FTIR spectra of unmodified PDMS thin films before (upper spectrum) and after (lower spectrum) washing with DCM and 70% ethanol, both spectra are normalized to demonstrate transparency values clearly

ATR-FTIR measurements of type I thin films (APTES modified -OH terminated PDMS), shown in Figure 3.2 below, shows all the characteristic PDMS peaks

described above. Moreover, it can be observed that a distinct peak has appeared at 1674 cm^{-1} characteristic of -N-H bend of primary amines, which the amine group of APTES is. More intricate differences indicating APTES modification is the broadening around 3000 cm^{-1} , assigned to $\nu\text{O-H}$ stretch superimposing with $\nu\text{N-H}$ stretching modes since both -OH terminated PDMS and APTES are present in type I thin films. It can also be observed that -CH₃ rocking at 786 cm^{-1} , -CH₃ deformation in Si-CH₃ at 1256 cm^{-1} , and asymmetric Si-O-Si stretching at 1010 cm^{-1} have decreased absorbance (increased T% values) due to obstruction of APTES-PDMS modification [282]. It can be noticed that APTES related peaks have decreased absorbance, and obstruction caused by APTES modification decreases after washing. This decrease is believed to be an indication that some unreacted starting materials that have been aggravated inside the PDMS polymer are leaching out during washing. However, these are believed to be low in amount since absorbance values only show a 12% decrease at most. Washed thin films continue to show strong APTES related peaks, and obstruction of characteristic PDMS peaks can still be observed.

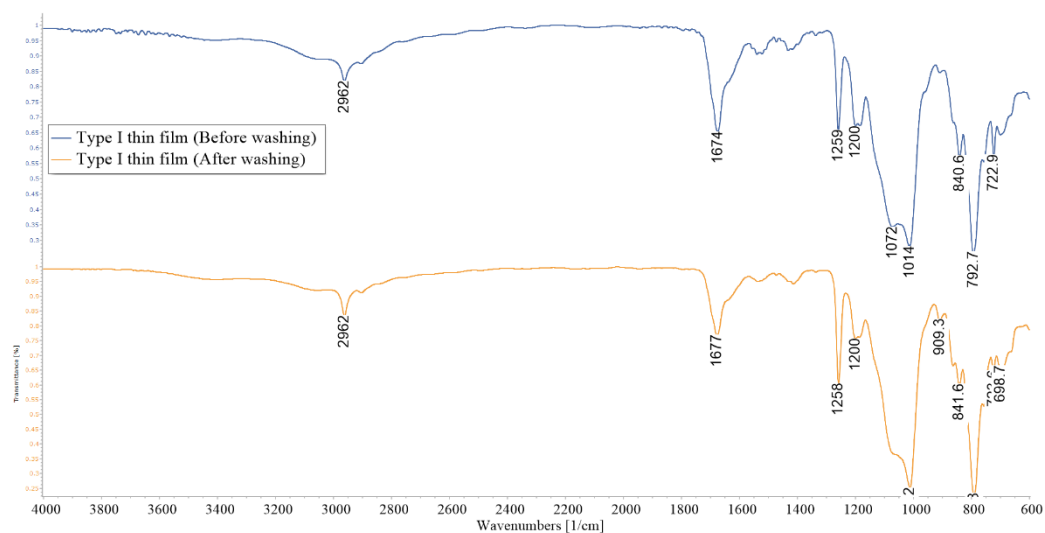


Figure 3.2 FTIR spectra of type I (APTES modified -OH terminated PDMS) thin films before (upper spectrum) and after (lower spectrum) washing with DCM and

70% ethanol, both spectra are normalized to demonstrate transparency values clearly

FTIR spectra of type II (APTES modified PMHS) thin films, given in Figure 3.3 below, also show the characteristic PDMS peaks described in detail above. Spectra for type II thin films also show a drastic increase in peaks attributed to ν O-H stretch and ν N-H stretching modes around 3000 cm^{-1} , causing a broadening effect around -CH₃ stretching in Si-CH₃ at 2962 cm^{-1} . Moreover, it can be observed that the N-H bending indicating the presence of primary amines at 1674 cm^{-1} has an increased absorbance value and is much more pronounced. Peaks that indicate obstruction due to the presence of APTES such as -CH₃ rocking at 786 cm^{-1} , -CH₃ deformation in Si-CH₃ at 1256 cm^{-1} , and asymmetric Si-O-Si stretching at 1010 cm^{-1} also have further decreased absorbance when compared to type I thin films. FTIR spectrum of type II thin films show a decrease in absorbance after washing similar to type I thin film. This trend is again believed to be caused by some starting materials leaching out of the polymer during washing by DCM and 70% ethanol solution. Increased absorbance values for peaks related to APTES molecule also indicate that there is an increase in the amount of APTES molecules that were successfully coupled to the PMHS structure

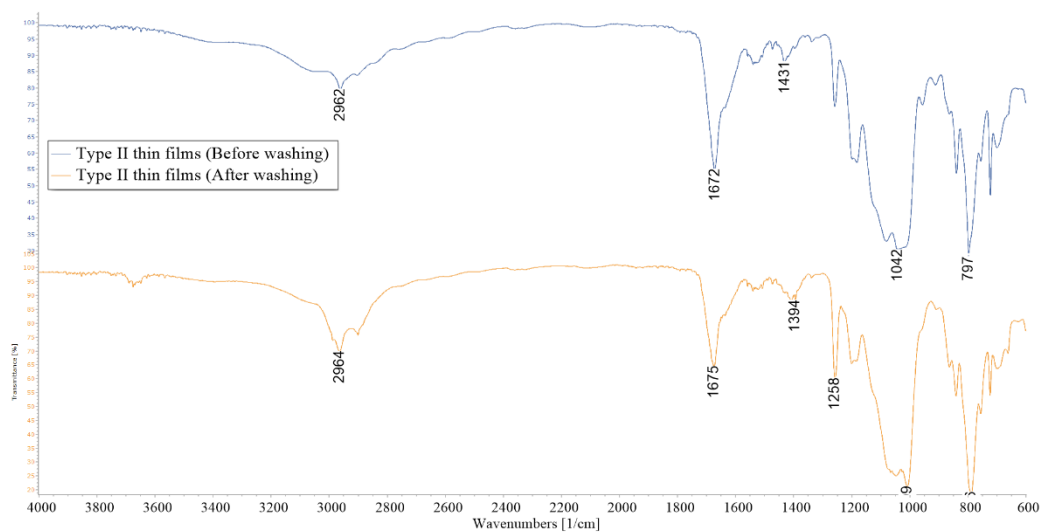


Figure 3.3 FTIR spectra of type II (APTES modified PMHS) thin films before (upper spectrum) and after (lower spectrum) washing with DCM and 70% ethanol, both spectra are normalized to demonstrate transparency values clearly

3.2.2 Contact angle measurements of thin films

After showing that successful coupling was achieved by chemical bonding with FTIR spectra, contact angle measurements with ultrapure (18.2 M Ω .cm) water were taken. As the number of polar groups introduced by the addition of APTES and -OH groups due to oxidation of PMHS backbone increases, the surface hydrophilicity of the thin films is expected to increase.

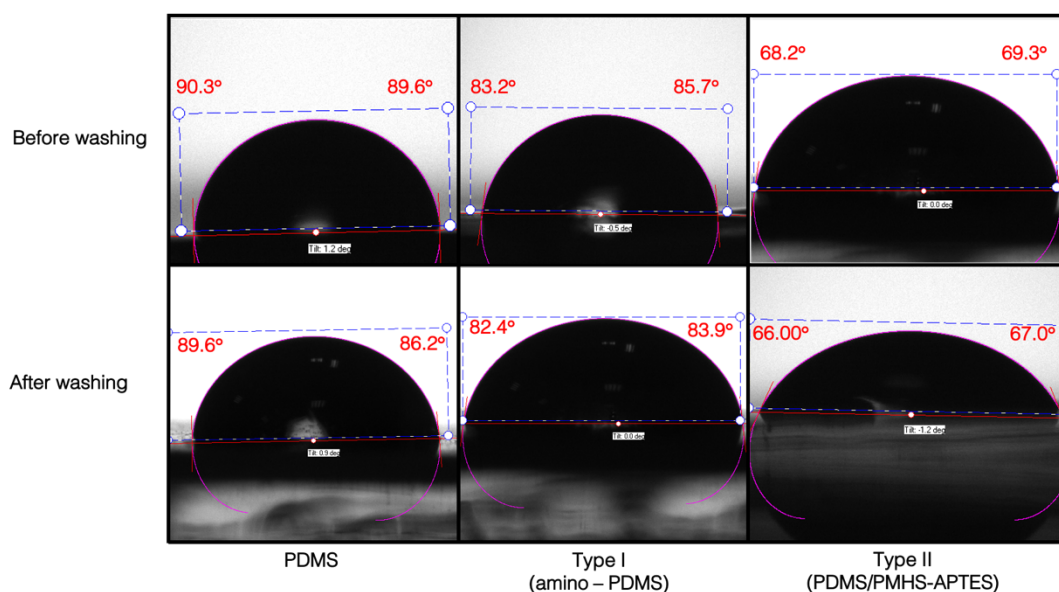


Figure 3.4 Contact angle measurements for unmodified PDMS, type I, and type II thin films. Type II thin films show a surface with drastically increased hydrophilicity.

It can easily be observed from Figure 3.4 that type I and especially type II thin films have a much more polar surface, as evidenced by their increased surface hydrophilicity. Contact angle measurements show that unmodified PDMS thin film has an average contact angle of $87.9^\circ \pm 1.2^\circ$, type I thin film has an average contact angle of $83.2^\circ \pm 0.9^\circ$. In contrast, type II thin film has an average contact angle of $66.5^\circ \pm 1.0^\circ$. The contact angle usually denoted θ , is used to quantitate the wettability of a surface by a liquid. In the case presented above, the surfaces of the thin films are wetted by ultrapure water droplets, and the contact angle θ directly measures the hydrophilicity of the surface. Since hydrophilicity is directly related to polarity, it can be surmised that type I thin film has a more polar surface than unmodified PDMS thin film, and type II thin film has a more polar surface than both type I and PDMS thin films. The high degree of hydrophilicity exhibited by type II thin film is believed to be a direct correlation of its larger number of polar groups, i.e., $-\text{NH}_2$ and $-\text{OH}$, that was shown in the reaction outlined in Figure 2.8 (in Section 2.5.2).

On the other hand, -OH terminated PDMS used in type I films has a drastically lower number of sites where APTES modification takes place, which is why type I films are believed to have a considerably smaller contact angle as its surface is much less hydrophilic. The average contact angle for type II thin films also agrees with the contact angle measurements of APTES modified PDMS surfaces reported in the literature (68.7 °) [284]. However, it is worth mentioning that although similar contact angle results were obtained by the modification strategy used in the reported literature, it would not be appropriate for this study. The approach reported in the literature employs a surface modification in which a large number of silanol groups are created only on the surface of PDMS using an oxygen plasma before its modification. This activation method ensures the binding of a large number of APTES molecules to the surface of PDMS and results in similar surface hydrophilicity to our type II thin films. However, during the extraction from complex biological samples, as intended in this study, amino groups' presence only on the surface may result in the thin films' saturation and erroneous conclusions. On the other hand, modification of the entire PDMS (as performed in this thesis) will eliminate this possibility.

3.2.3 Thermogravimetric analysis of thin films

Thermogravimetric analysis (TGA) of unmodified PDMS, given in Figure 3.5, has shown that there is no discernible weight loss until ~400 °C and can be considered thermally stable, exhibiting very slow and around 5% weight loss starting at 400 °C until 450 °C. Starting at around ~500 °C, unmodified PDMS thin film shows rapid thermal degradation. Modified PDMS thin films, on the other hand, exhibit no discernible weight loss until ~220 °C and can only be considered thermally stable until then. At 460 °C, modified PDMS thin films start very rapid thermal degradation, which agrees with values reported recently in literature with PDMS films modified with similar APTES ratios [285]. Lower thermal stability of the modified extractive films can be explained by the fact that aminopropyl groups overall have much lower

thermal stability and should start decomposing sooner. It should also be considered that the modification of PDMS also lowers its crosslinking to a considerable degree, which further explains the significant weight loss that starts around 500 °C. Although any GC-MS method was not necessary for the analytes chosen in this thesis, the thermal stability of extractive thin films until ~200 °C indicates that they could be suitable for GC analysis can also be used for sampling of volatile biomolecules/metabolites. Further investigations are necessary for testing their final suitability for such methods.

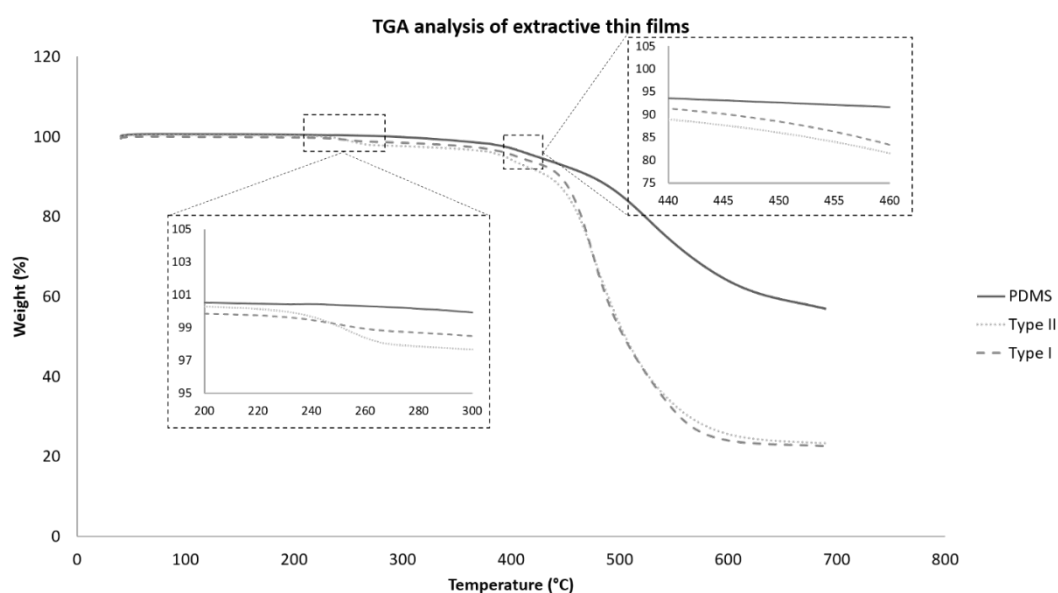


Figure 3.5 TGA curves of extractive thin films

Thermogravimetric analysis (TGA), given in Figure 3.5 above, of extractive thin films, shows that modified PDMS films are stable until around 220 °C. Lower thermal stability of the modified extractive films can be explained by the fact that aminopropyl groups overall have much lower thermal stability and should start decomposing sooner. It should also be considered that the modification of PDMS also lowers its crosslinking to a considerable degree, which further explains the

significant weight loss that starts around 500 °C. Although any GC-MS method was not necessary for the analytes chosen in this thesis, the thermal stability of extractive thin films until ~200 °C indicates that they could be suitable for GC analysis can also be used for sampling of volatile biomolecules/metabolites. Further investigations are necessary for testing their final suitability for such methods.

3.2.4 Scanning electron microscopy and energy dispersive x-ray analysis

Scanning electron microscopy of unmodified PDMS, type I and type II thin films show very few characteristic features. The surface of unmodified PDMS has a very smooth and homogenized appearance, while surfaces of type I and type II films show a less homogenized and porous structure. However, it should be underlined that since the thin film samples were not coated with Au nanoparticles (since it would interfere with EDX measurements), any SEM images shown below should not be taken as conclusive findings regarding the surface morphology of thin films.

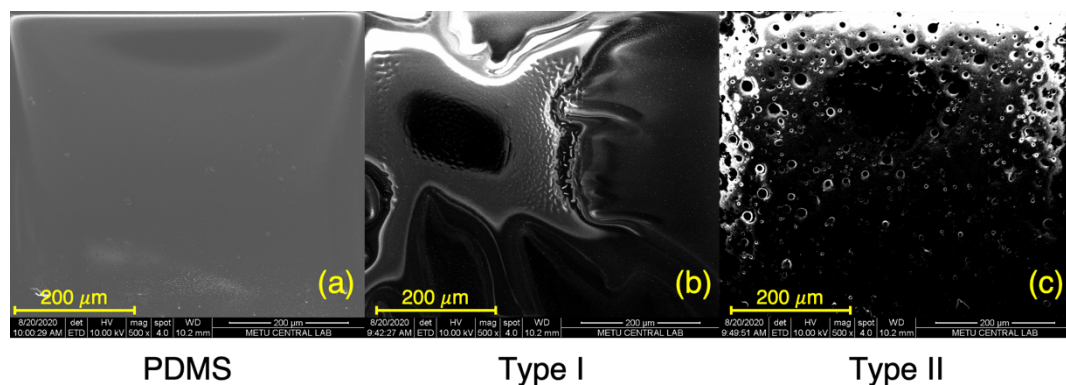


Figure 3.6 SEM images of (a) unmodified PDMS ,(b) type I, and (c) type II thin films, 500x magnification

EDX analysis of all three thin films show increased N at% and O at %for type I and type II films compared to unmodified PDMS (which has no N content). Table 3.3

shows that N at% and O at% for type II thin films are considerably larger than for unmodified PDMS and type I thin films, as was expected since the proposed modification mechanism leads to a large number of APTES and -OH functional groups.

Table 3.3 EDX analysis for unmodified PDMS, type I and type II thin films

Thin film	C at%	O at%	Si at%	N at%
PDMS	69.7 ± 0.5	27.6 ± 0.7	2.7 ± 0.3	
Type I	68.6 ± 1.6	25.4 ± 0.4	5.5 ± 1.4	0.5 ± 0.2
Type II	57.5 ± 4.32	30.9 ± 2.6	5.7 ± 2.8	5.9 ± 2.7

3.3 LC-MS analysis

In order to accurately represent the different classes of biomolecules that exist in the human eye, analytes with a wide range of polarities and functional groups were selected to test the extraction capabilities of the thin films. Before any extraction could be carried out, a suitable chromatographic separation method and examination of analytes with mass spectrometry must be investigated. The physicochemical properties and molecular structures of analytes given in Table 3.4 were used as the basis to develop suitable chromatographic methods.

Table 3.4 Physicochemical properties of analytes

Analyte	Molecular weight (g.mol⁻¹)	log P	pKa
Polar analytes			
Phenylalanine	165.08	-1.38	2.34
Glutamine	146.14	-3.1	2.17
Proline	115.13	-2.54	1.99
Citrulline	175.19	-4.3	2.43
Tryptophan	204.22	-1.05	2.83
Acetylcholine	146.21	-0.2	-7
Creatin	131.13	-1.2	3.4
γ -aminobutyric acid (GABA)	103.12	-3.2	4.03
Acetylcarnitine	203.24	-0.4	4.2
Adenosine	247.24	-1.1	3.6
Non-polar analytes			
Docosahexaenoic acid (DHA)	328.2	6.75	4.89

Analyte	Molecular weight (g.mol ⁻¹)	log P	pKa
Cholesterol	387.6	7.06	-1.4
Retinoic acid	300.4	6.3	4.76

In Table 3.3 above, analytes were grouped in either polar or non-polar categories based on their log P values. In order to achieve a good separation with satisfactory sensitivity, different chromatographic methods were used for polar and non-polar analytes.

3.3.1 HILIC LC-MS method: chromatographic separation of polar analytes

Polar analytes were first investigated with MS methods in a series of concentrations ranging from 5.0 ng·mL⁻¹ to 250.0 ng·mL⁻¹ in order to find the sensitivity of the instruments and to build instrumental calibration curves for all analytes, shown in Figure B.. Based on the instrumental response, the following LOQ values were calculated for polar analytes, given in Table 3.5. LOQ values were determined by finding the signal that gives a value of S/N = 10 for each analyte and inserting the signal to the calibration curve for calculating the LOQ value in terms of concentration. Similarly, LOD values were calculated by finding the signal that gives a value of S/N = 3 for each analyte.

Table 3.5 Observed m/z and calculated LOQ and LOD values for polar analytes

Analyte	log P	pKa	Observed m/z	LOQ (ng mL ⁻¹)	LOD (ng mL ⁻¹)
Tryptophan	-1.05	2.83	205.28 [M+H] ⁺	2.7 ± 1.1	0.9 ± 1.1
Proline	-2.54	1.99	116.07 [M+H] ⁺	7.0 ± 1.0	2.7 ± 1.0
Glutamine	-3.1	2.17	147.12 [M+H] ⁺	2.9 ± 1.6	1.0 ± 1.6
Phenylalanine	-1.38	2.34	183.04 [M+NH ₄] ⁺	3.4 ± 0.9	1.1 ± 0.9
Acetylcarnitine	-0.4	4.2	204.13 [M+H] ⁺	2.6 ± 1.3	0.9 ± 1.3
Citrulline	-4.3	2.43	176.28 [M+H] ⁺	3.4 ± 0.5	1.1 ± 0.5
Creatine	-1.2	3.4	132.08 [M+H] ⁺	9.0 ± 1.1	3.0 ± 1.1
γ-aminobutyric acid (GABA)	-3.2	4.03	104.07 [M+H] ⁺	6.1 ± 1.3	2.0 ± 1.3
Acetylcholine	-0.2	-7	146.21 [M] ⁺	2.0 ± 1.8	0.7 ± 1.8
Adenosine	-1.1	3.6	268.11 [M+H] ⁺	1.8 ± 1.4	0.6 ± 1.4

3.3.2 Reverse phase LC-MS method chromatographic separation of non-polar analytes

Non-polar analytes were first investigated with MS/MS methods in a series of concentrations ranging from 5.0 ng·mL⁻¹ to 250.0 ng·mL⁻¹ to establish an instrumental curve and to determine the instrumental sensitivity, given in Figure B.. Based on the instrumental calibration curves, the following LOQ and LOD values were calculated for non-polar analytes exactly as described above for polar analytes and given in Table 3.6 below.

Table 3.6 Observed m/z and calculated LOQ values for non-polar analytes

Analyte	log P	pKa	Observed m/z	LOQ (ng mL ⁻¹)	LOD (ng mL ⁻¹)
Docosahexaenoic acid	6.75	4.89	327.231 [M-H] ⁻	2.3 ± 1.3	0.8 ± 1.3
Retinoic acid	7.06	-1.4	299.200 [M-H] ⁻	3.0 ± 1.0	1.0 ± 0.8
Cholesterol	6.3	4.76	386.413 [M-H] ⁻	8.2 ± 2.2	2.7 ± 1.1

3.4 Extraction of selected analytes with synthesized thin films

3.4.1 Comparison of extraction performances of thin films

The first extractions were performed to determine the extraction performance of PDMS, type I, and type II thin films. Extraction results, given in Figure 3.8, for each

analyte clearly show the trend that type I and type II thin films had increased extraction capabilities towards polar analytes compared to unmodified PDMS thin film. For non-polar analyte extraction, all three thin films appear to have similar extraction capabilities. PDMS is known to be an excellent extractive phase for non-polar analytes [286]. Although type I and type II thin films are modified to include some polar functional groups into their polymer chains, the bulk of the polymer is still made up of PDMS chains. As laid out in 2.5.2, PDMS is added after modification of -OH terminated PDMS or PMHS by APTES is completed and therefore is unaffected by any coupling reactions. The similar extraction capabilities of all three thin films towards non-polar analytes indicate that these molecules are extracted in PDMS-rich moieties of thin films.

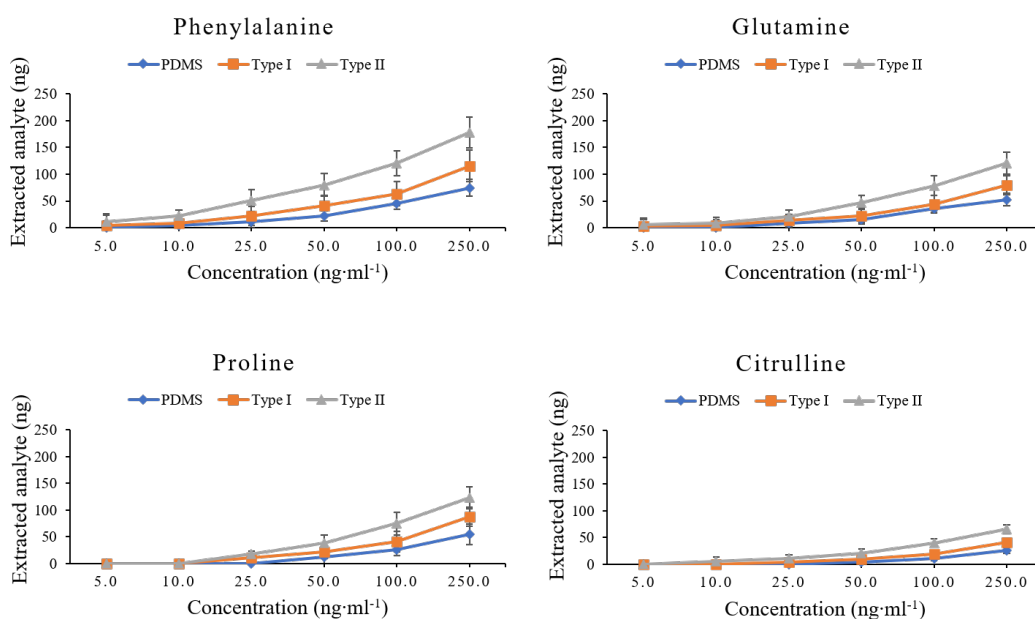


Figure 3.7 Comparison of PDMS, Type I, and Type II thin films from PBS solutions spiked with 5.0, 10.0, 25.0, 50.0, 100.0, and 250.0 ng·mL⁻¹ analytes (Extraction conditions; extraction time: 120 mins, sample volume: 4.0 mL, agitation speed: 1200 rpm, extraction temperature: RT, analyte concentrations: 5.0, 10.0, 25.0, 50.0, 100, 250.0 ng·mL⁻¹. Desorption conditions; desorption solvent: ACN:MeOH:H₂O (40:40:20, v/v/v), desorption volume: 0.40 mL, desorption time: 30 mins, desorption speed: 1200 rpm) (continued)

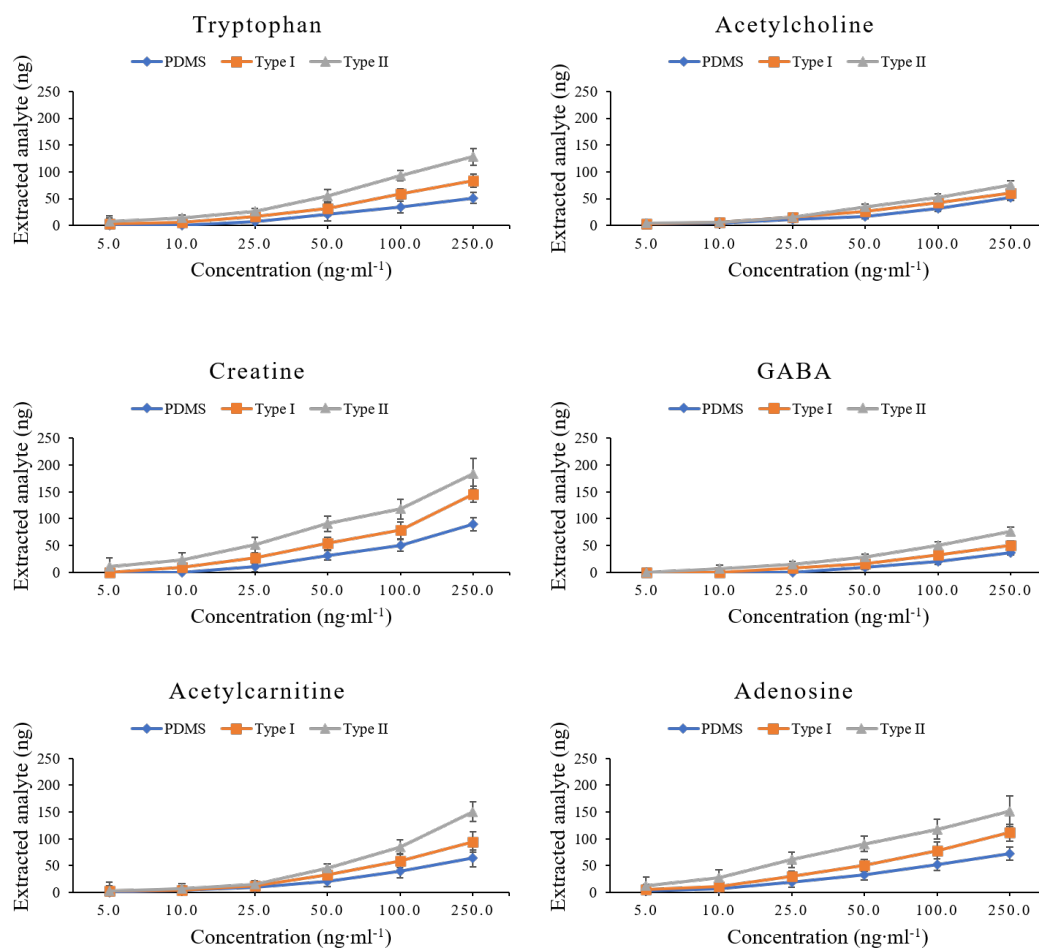


Figure 3.7 Comparison of PDMS, Type I, and Type II thin films from PBS solutions (Extraction conditions; extraction time: 120 mins, sample volume: 4.0 mL, agitation speed: 1200 rpm, extraction temperature: RT, analyte concentrations: 5.0, 10.0, 25.0, 50.0, 100.0, 250.0 ng·mL⁻¹. Desorption conditions; desorption solvent: ACN:MeOH:H₂O (40:40:20, v/v/v), desorption volume: 0.40 mL, desorption time: 30 mins, desorption speed: 1200 rpm) (continued)

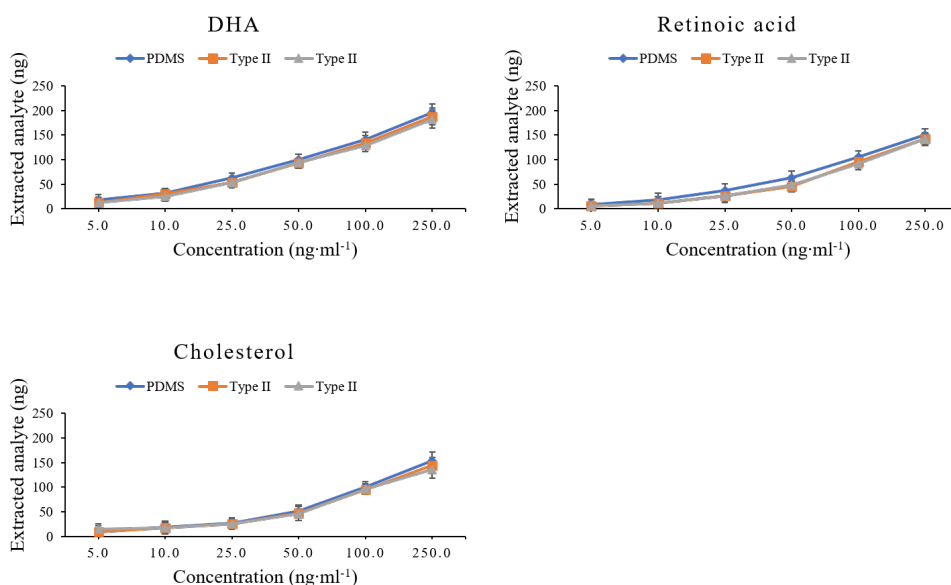


Figure 3.7 Comparison extraction performances of PDMS, type I, and type II thin films from PBS solutions (Extraction conditions; extraction time: 120 mins, sample volume: 4.0 mL, agitation speed: 1200 rpm, extraction temperature: RT, analyte concentrations: 5.0, 10.0, 25.0, 50.0, 100.0, 250.0 ng·mL⁻¹. Desorption conditions; desorption solvent: ACN:MeOH:H₂O (40:40:20, v/v/v), desorption volume: 0.40 mL, desorption time: 30 mins, desorption speed: 1200 rpm)

3.4.2 Optimization of desorption solvent

After the best performing thin film was determined as type II thin films, optimization of extraction parameters was carried out as described in Table 2.7 (in 2.9.1). The first parameter to be optimized was the desorption solvent. Three solvents were investigated: ACN:MeOH:H₂O (40:40:20, v/v/v), ACN:MeOH (50:50, v/v), and ACN:IPA:H₂O (40:40:20, v/v/v). Results obtained for polar analytes (Figure 3.8) indicate that ACN:MeOH:H₂O (40:40:20, v/v/v) has performed better in all concentrations. Increased performance of this mixture of desorption solvents is believed to be a mixture of its polar/non-polar solvent ratio and excellent hydrogen bond breaking ability of MeOH. For non-polar analytes, all three desorption solvents resulted in similar amounts of desorbed analyte, as can be seen in Figure 3.9. In order

to check whether there was a significant difference between desorption solvents for non-polar analytes a simple t-test for comparing two means can be used [287]. In the form of t-test in which two means can be compared to see if they are statistically different or not, \bar{x}_1 and \bar{x}_2 are the means that are being compared, s_{pooled} is the pooled standard deviation of two means, N_1 and N_2 are the number of measurements, which are 3 in our case as three parallel desorptions were conducted.

$$t = \frac{\bar{x}_1 - \bar{x}_2}{s_{pooled} \sqrt{\frac{N_1 + N_2}{N_1 N_2}}} \quad \text{Equation IX}$$

$$s_{pooled} = \sqrt{\frac{(N_1 - 1)s_1^2 + (N_2 - 1)s_2^2}{N_1 + N_2 - 2}} \quad \text{Equation X}$$

Using equations IX and X above, we can apply a t-test for all analytes to determine if desorption solvents statistically differs from each other or not. If the experimentally calculated t value is smaller than $t_{critical}$ (2.78 for 95% confidence level and 4 degrees of freedom), then statistically there is no difference between desorption solvents. Results of the t-test for desorption solvents can be found below in Table 3.7, Table 3.8, and Table 3.9 and show that there is no significant difference in extracted non-polar analyte amounts for different desorption solvents. Therefore, ACN:MeOH:H₂O (40:40:20, v/v/v) was selected as the best desorption solvent for both polar and non-polar analytes.

Table 3.7 Calculated $t_{experimental}$ values for non-polar analyte desorptions with ACN:MeOH:H₂O and ACN:MeOH ($t_{critical} = 2.78$)

Analytes	$t_{experimental}$
DHA	1.95
Retinoic acid	1.86
Cholesterol	1.44

Table 3.8 Calculated $t_{experimental}$ values for non-polar analyte desorptions with ACN:MeOH and ACN:IPA:H₂O ($t_{critical} = 2.78$)

Analytes	$t_{experimental}$
DHA	2.28
Retinoic acid	1.88
Cholesterol	1.63

Table 3.9 Calculated $t_{experimental}$ values for non-polar analyte desorptions with ACN:MeOH:H₂O and ACN:IPA:H₂O ($t_{critical} = 2.78$)

Analytes	$t_{experimental}$
DHA	1.33
Retinoic acid	1.03
Cholesterol	1.20

Overall, ACN:MeOH:H₂O (40:40:20, v/v/v) as a desorption solvent was found to perform best for polar analytes while performing statistically the same for non-polar analytes (with 95% confidence level).

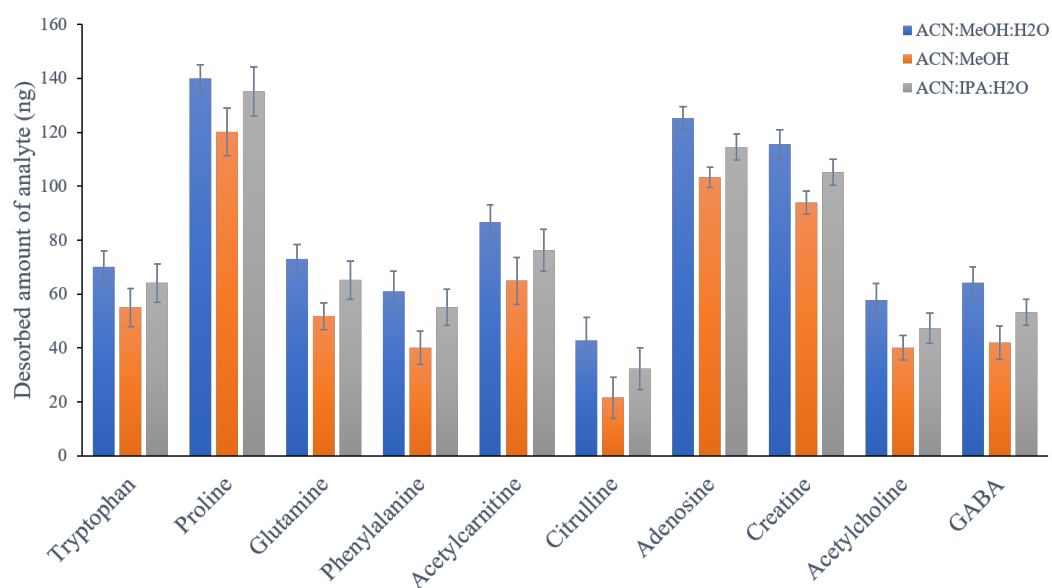


Figure 3.8 Comparison of desorption solvent effectiveness for polar analytes (Extraction conditions; extraction time: 120 mins, sample volume: 4.0 mL, agitation speed: 1200 rpm, extraction temperature: RT, analyte concentrations: 100 ng·mL⁻¹. Desorption conditions; desorption solvent: ACN:MeOH:H₂O (40:40:20, v/v/v), ACN:MeOH (50:50, v/v), ACN:IPA:H₂O (40:40:20, v/v/v), desorption volume: 0.40 mL, desorption time: 30 mins, desorption speed: 1200 rpm)

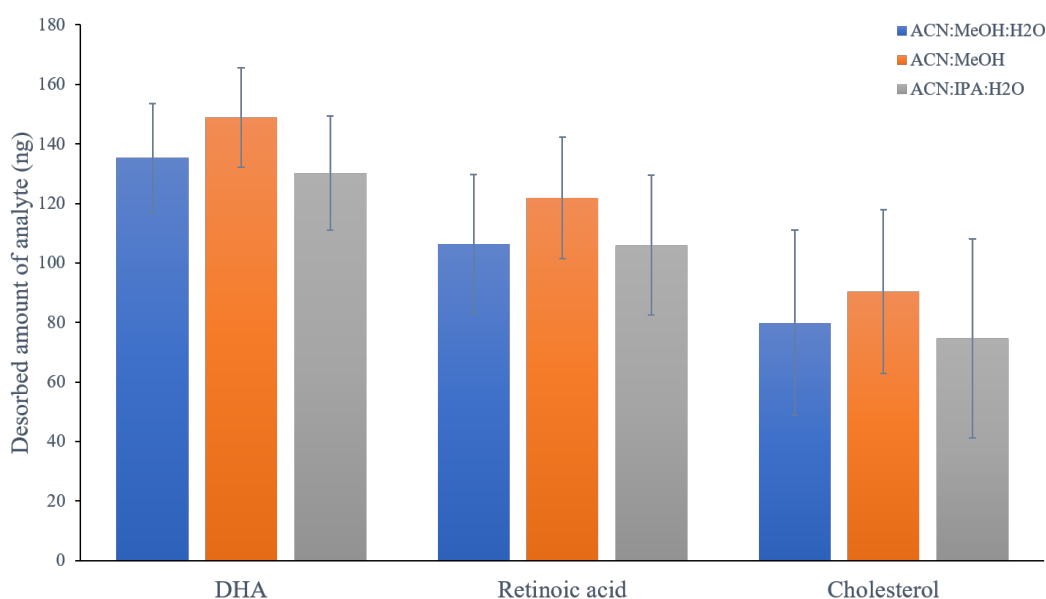


Figure 3.9 Comparison of desorption solvent effectiveness for non-polar analytes (Extraction conditions; extraction time: 120 mins, sample volume: 4.0 mL, agitation speed: 1200 rpm, extraction temperature: RT, analyte concentrations: 100 ng·mL⁻¹. Desorption conditions; desorption solvent: ACN:MeOH:H₂O (40:40:20, v/v/v), ACN:MeOH (50:50, v/v), ACN:IPA:H₂O (40:40:20, v/v/v), desorption volume: 0.40 mL, desorption time: 30 mins, desorption speed: 1200 rpm)

3.4.3 Optimization of desorption time

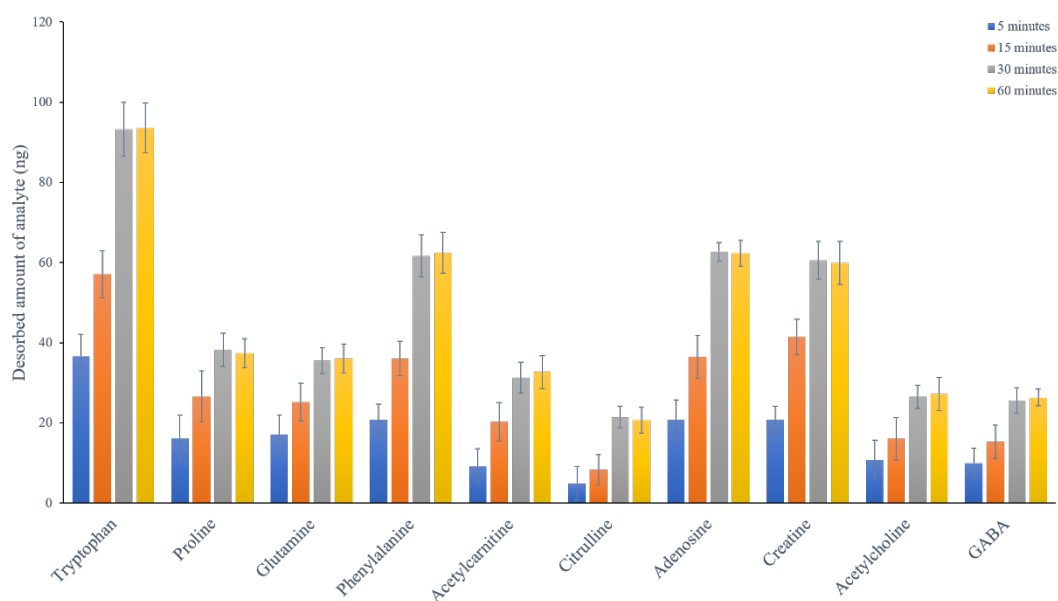
The next optimization parameter was desorption time, in order to ascertain that there were no analytes left on the thin films, all thin films were desorbed a second time with the same solvents for 30 minutes after the first desorption ended. The optimal desorption time that leads to the highest analyte recovery in the least amount of time while causing no carryover of analytes between consecutive desorptions was found to be 30 minutes. Figure 3.10 and Figure 3.11 show that 5 and 15-min desorptions failed to quantitatively desorb both polar and non-polar analytes. As expected, the amount of analyte carryover was found higher for 5 minute desorptions compared to 15 minute desorptions. The amount of carryover from previous desorptions was found to be higher than 120% for some analytes with shorter desorption times.

Furthermore, for the first desorptions, there was no significant difference in desorbed amounts of analytes between desorption times of 30 minutes and 60 minutes, which was again shown using a t-test following the same protocol as laid out above. Results of the t-test comparing desorption times of 30 and 60 minutes can be found below in Table 3.10

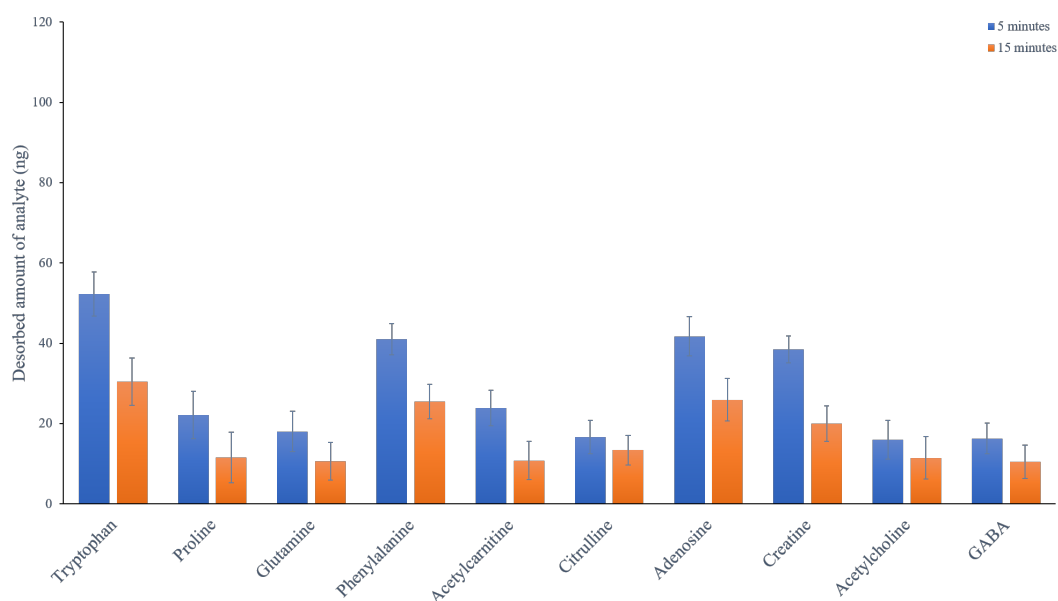
Table 3.10 Calculated $t_{experimental}$ values for amount of extracted analytes from 30 and 60-minute desorptions ($t_{critical} = 2.78$)

Analytes	$t_{experimental}$
Tryptophan	0.97
Proline	1.99
Glutamine	1.40
Phenylalanine	2.28
Acetylcarnitine	2.73
Citrulline	1.36
Adenosine	1.90
Creatine	1.99
Acetylcholine	1.46
GABA	1.84
DHA	2.61
Retinoic acid	2.00
Cholesterol	2.63

Table 3.10 shows that $t_{experimental}$ values of all analytes for 30 minute and 60-minute desorptions fall below the $t_{critical}$ value of 2.78. Therefore, there is no statistically discernible difference between 30 minute and 60-minute desorptions, as 5 and 15-minute desorptions clearly show carryover in subsequent desorption experiments, 30 minutes were chosen as the best performing desorption time.

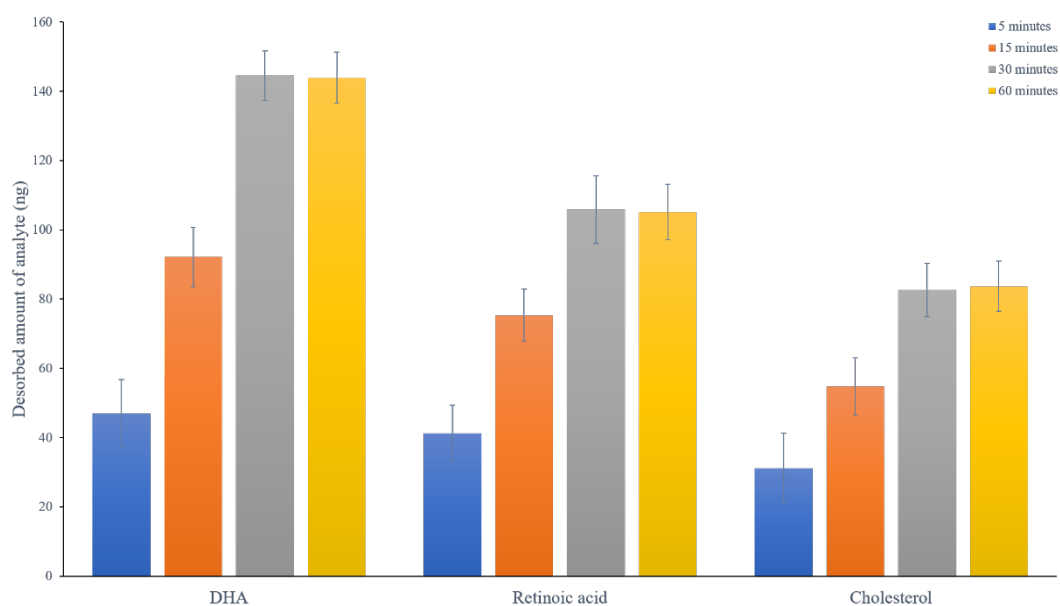


(a)

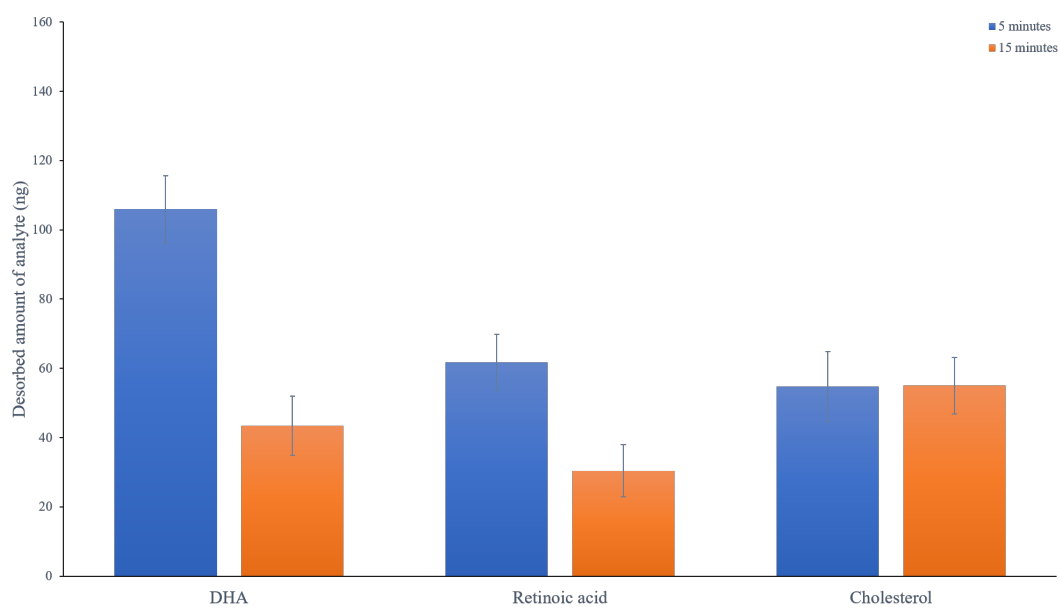


(b)

Figure 3.10 (a) Comparison of the effect of desorption times on extracted amount of polar analytes (Extraction conditions; extraction time: 120 mins, sample volume: 4.0 mL, agitation speed: 1200 rpm, extraction temperature: RT, analyte concentrations: $100 \text{ ng} \cdot \text{mL}^{-1}$. Desorption conditions; desorption solvent: ACN:MeOH:H₂O (40:40:20, v/v/v), desorption volume: 0.40 mL, desorption time: 5, 15, 30, 60 mins, desorption speed: 1200 rpm) (b) Second desorptions for 5 and 15-min desorptions (Desorption conditions; same as above)



(a)



(b)

Figure 3.11 (a) Comparison of the effect of desorption times on extracted amount of non-polar analytes (Extraction conditions; extraction time: 120 mins, sample volume: 4.0 mL, agitation speed: 1200 rpm, extraction temperature: RT, analyte concentrations: 100.0 ng·mL⁻¹. Desorption conditions; desorption solvent: ACN:MeOH:H₂O (40:40:20, v/v/v), desorption volume: 0.40 mL, desorption time: 5, 15, 30, 60 mins, desorption speed: 1200 rpm) (b) Second desorptions for 5 and 15-min desorptions (Desorption conditions; same as above)

To sum up, desorption solvent and desorption time experiments have shown that the best performing solvent was found to be ACN:MeOH:H₂O (40:40:20, v/v/v) and best performing desorption time was concluded as 30 minutes.

3.4.4 Extractions from *in vitro* eye model

3.4.4.1 Comparison of extraction performances of thin films

In order to determine the best performing extractive lens, extractions from agarose eye models were conducted, as described in 2.9.2. Extractions from agarose eye models spiked to contain 250.0 ng·mL⁻¹ of polar analytes have shown that the best performing extractive lens was type II thin films (see Figure 3.12), as was the case in extractions from PBS solutions (see Figure 3.7).

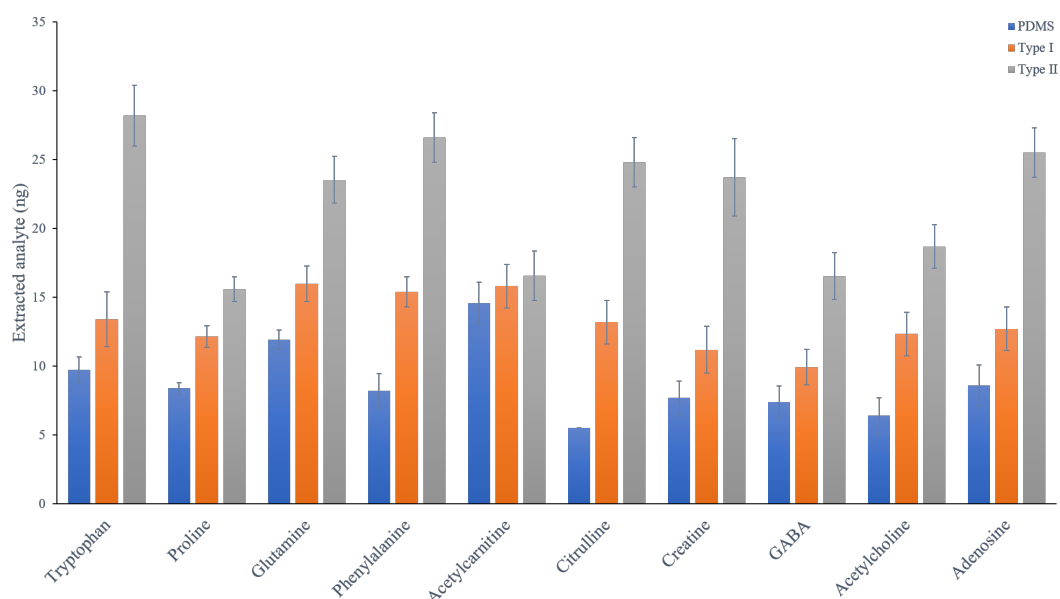


Figure 3.12 Comparison of extractive thin films for polar analytes by extractions from *in vitro* eye model (Extraction conditions; extraction time: 120 mins, sample volume: 4.0 mL, agitation speed: static extraction, extraction temperature: RT, analyte concentrations: 250.0 ng·mL⁻¹. Desorption conditions; desorption solvent: ACN:MeOH:H₂O (40:40:20, v/v/v), desorption volume: 0.40 mL, desorption time: 30 mins desorption speed: 1200 rpm)

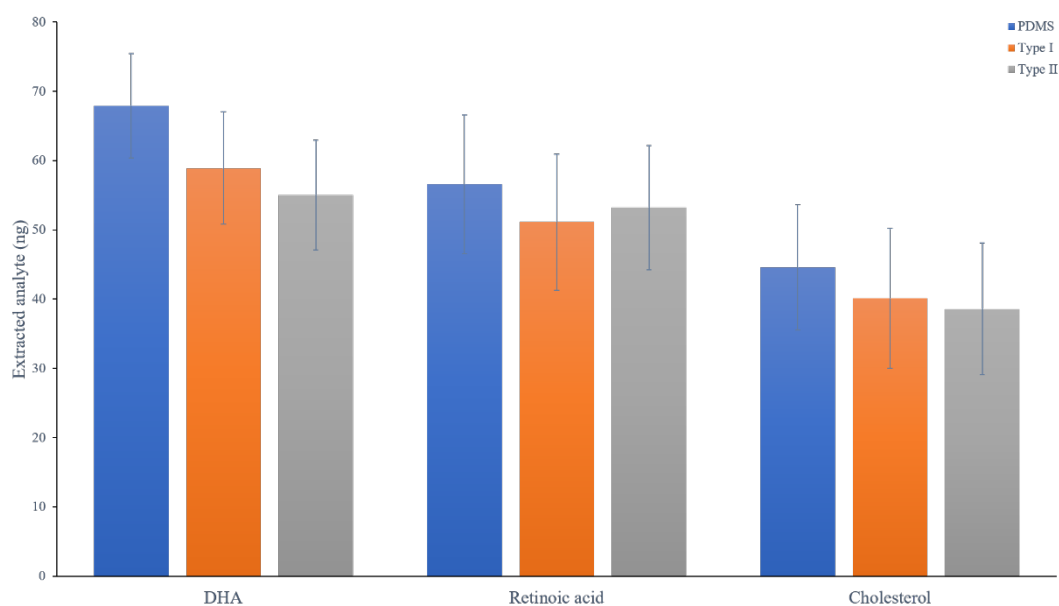


Figure 3.13 Comparison of extractive thin films for non-polar analytes by extractions from *in vitro* eye model (Extraction conditions; extraction time: 120 mins, sample volume: 4.0 mL, agitation speed: static extraction, extraction temperature: RT, analyte concentrations: 250.0 ng·mL⁻¹. Desorption conditions; desorption solvent: ACN:MeOH:H₂O (40:40:20, v/v/v), desorption volume: 0.40 mL, desorption time: 30 mins desorption speed: 1200 rpm)

The extractions used to compare the extractive capabilities of three thin films for both polar and non-polar analytes, given in Figure 3.12 and Figure 3.13, were used to calculate the recovery (R%) of all analytes for all three extractive contact lenses under the experimental conditions. Looking at Table 3.11, it can be seen that type II thin films boast increased recovery rates for polar analytes while showing similar recovery rates for non-polar analytes compared to unmodified PDMS and type I thin films.

Table 3.11 Recovery, (R%), values of all analytes for extractive contact lenses

Analytes	PDMS	Type I	Type II
	Recovery (R%)	Recovery (R%)	Recovery (R%)
Tryptophan	0.97 ± 0.08	1.34 ± 0.11	2.82 ± 0.24
Proline	0.84 ± 0.07	1.22 ± 0.08	3.10 ± 0.21
Glutamine	1.19 ± 0.09	1.60 ± 0.16	2.35 ± 0.14
Phenylalanine	0.82 ± 0.12	1.54 ± 0.10	2.66 ± 0.19
Acetylcarnitine	1.46 ± 0.15	1.58 ± 0.14	1.66 ± 0.15
Citrulline	0.55 ± 0.10	1.31 ± 0.11	2.48 ± 0.17
Adenosine	0.86 ± 0.14	1.27 ± 0.12	2.55 ± 0.20
Creatine	0.77 ± 0.09	1.12 ± 0.08	2.37 ± 0.21
Acetylcholine	0.64 ± 0.08	1.23 ± 0.13	1.87 ± 0.19
GABA	0.74 ± 0.09	1.00 ± 0.12	1.87 ± 0.20
DHA	6.79 ± 0.51	5.89 ± 0.71	5.50 ± 0.52
Retinoic acid	5.66 ± 0.60	5.11 ± 0.48	5.32 ± 0.44
Cholesterol	4.46 ± 0.50	4.01 ± 0.43	3.86 ± 0.39

However, it should be kept in mind that the extractions from the agarose eye model has different mechanics than extraction from PBS solutions, the most important being that there is no agitation. This type of extraction is called static extraction, and longer time for equilibrium is required compared to an extraction where agitation is applied. Therefore, if under the extraction equilibrium is not established under working conditions, the extractive phase makes contact with only a small portion of analytes present in the sample. If the extracted amount of analytes from agarose eye models are compared with those extracted from PBS solutions with the same concentration ($250.0 \text{ ng}\cdot\text{mL}^{-1}$), it can be readily observed that there are around 2 to 5 fold difference for most analytes. Even though both matrices have the same concentration, the amount of extracted analytes are much smaller in static extractions

performed from gel surface as the equilibrium was not reached and the extraction is based on passive diffusion through a large boundary layer. In order to better describe this situation, calculating the longest distance that a molecule can travel to reach the extractive phase in a given time interval. The diffusion path for a molecule can be roughly calculated with a diffusion-based model, employing Fick's law to account for diffusion in agarose eye model. Fick's law states that the mean squared displacement, $\langle x \rangle^2$, is related to the rate of molecular diffusion, D , and time, t , and dimensionality of the system, d , this relationship is expressed as:

$$\langle x \rangle^2 = 2dDt \quad \text{Equation XI}$$

Diffusion rates for small molecules are estimated as $5.8 \times 10^{-6} \text{ cm}^2 \cdot \text{s}^{-1}$, which decreases by 5% in 2% agarose gels [288]. Under the circumstances, in a 3D system, and for an extraction time of 2 hours, only molecules that are located just under 3mm from the agarose eye model's surface will come into contact with the lens surface.

Moving on, after type II thin films were established as the best performing thin films for extraction from agarose eye models as well as PBS solutions, the extraction time profiles were investigated. Extraction times of 15, 30, 60, and 120 minutes were investigated for both polar and non-polar analytes.

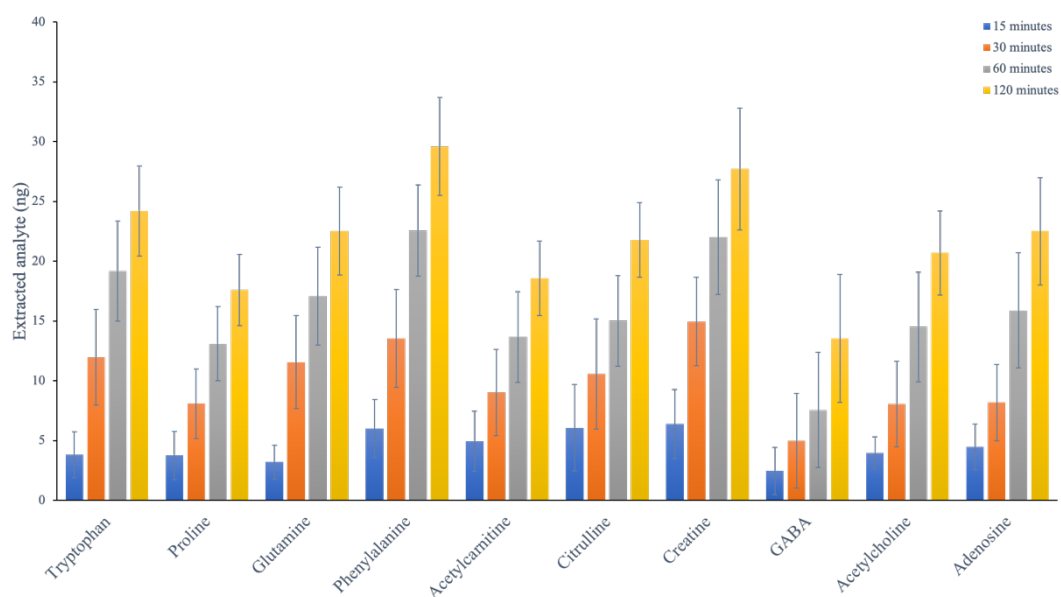


Figure 3.14 Extraction time profile for polar analyte extractions from *in vitro* eye model (Extraction conditions; extraction time: 15, 30, 60, 120 mins, sample volume: 4.0 mL, agitation speed: static extraction, extraction temperature: RT, analyte concentrations: 250.0 ng·mL⁻¹. Desorption conditions; desorption solvent: ACN:MeOH:H₂O (40:40:20, v/v/v), desorption volume: 0.40 mL, desorption time: 30 mins desorption speed: 1200 rpm)

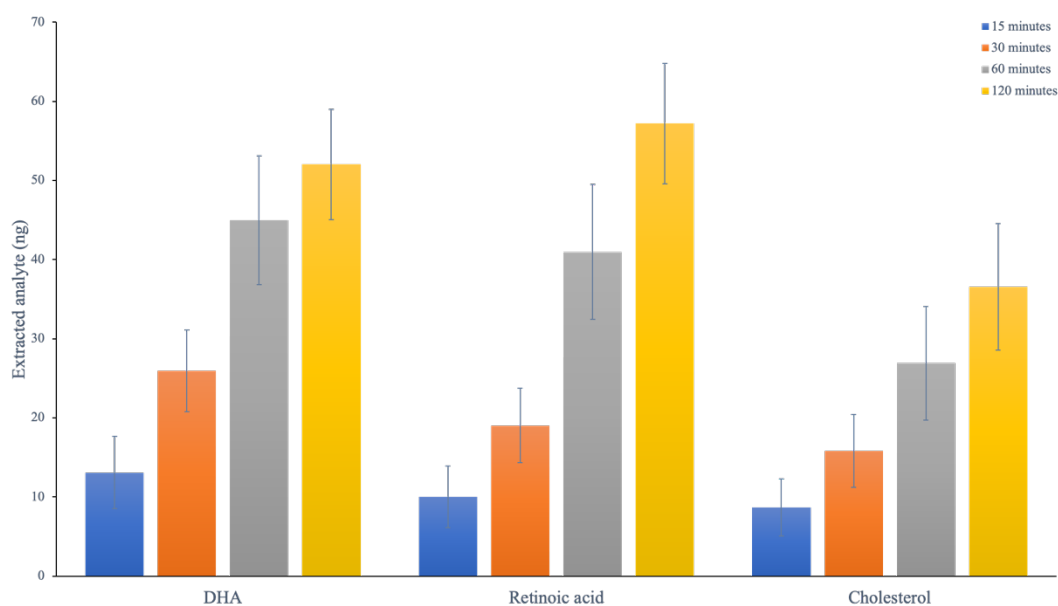


Figure 3.15 Extraction time profile for non-polar analyte extractions from *in vitro* eye model (Extraction conditions; extraction time: 15, 30, 60, 120 mins, sample volume: 4.0 mL, agitation speed: static extraction, extraction temperature: RT, analyte concentrations: 250.0 ng·mL⁻¹. Desorption conditions; desorption solvent: ACN:MeOH:H₂O (40:40:20, v/v/v), desorption volume: 0.40 mL, desorption time: 30 mins desorption speed: 1200 rpm)

Extraction time profiles for both polar and non-polar analytes, see Figure 3.14 and Figure 3.15 above, show that as extraction time is increased, the extracted analyte amount also increases. While 120 minutes of extraction provides the best sensitivity and highest number of extracted analytes, 60 minutes of extraction also provide sufficient information on analyte concentrations. For polar analytes, 15 and 30-minute extractions failed to provide enough extraction for some analytes that had higher LOQ values compared to others such as proline, creatine, and GABA. However, it should be noted that 15 and 30-minute extractions provided sensitive enough results for all other polar and non-polar analytes. With more sensitive analytical methods for proline, creatine, and GABA, shorter extraction times could also have provided sensitive enough extractions.

120-minute extraction was established as the highest sensitive extraction time amongst the investigated extraction times, however it should be noted that equilibrium was not reached at 120 minutes, and reaching equilibrium was not expected for investigated extraction times since the amount of analytes available for extraction were limited by the 3 mm band as mentioned above and there were no agitation conditions to hasten the equilibrium process. After extraction time profiles for both polar and non-polar analytes were constructed, as shown in Figure 3.16 below, extraction calibration plots for every polar and non-polar analyte were built. Extraction parameters for extraction calibration curves were chosen using optimization investigations laid out above. Type II thin films were used for extractions as they have been shown as the best performing extractive lenses, see Figure , extraction was carried out for 120 minutes as it was the extraction time with the highest sensitivity, desorption solvent was chosen as ACN:MeOH:H₂O (40:40:20, v/v/v)since it was the best performing solvent and desorption time was set to 30 minutes to provide quantitative desorption of extracted analytes. For extraction calibration curves, 50.0, 100.0, 250.0, and 500.0 ng·mL⁻¹ concentration range was chosen as extractions from the agarose eye model fall below LOQ levels when spiked with lower analyte concentrations, and some analytes even fall below LOQ levels at 50.0 ng·mL⁻¹ concentration. In order to have better LOQ values, some measures can be taken such as using more sensitive equipment (e.g. MS/MS), desorption to even smaller volume or evaporation of desorption solvent for increasing preconcentration ratios. In order to represent the repeatabilities of extractions performed by type II thin films, RSD (%) of extraction calibrations, given in Table 3.12 below, were calculated as follows:

$$RSD(\%) = \frac{s}{\bar{x}} \times 100 \quad \text{Equation XII}$$

where *s* is the standard deviation of the peak area signal and \bar{x} is the average of the peak area signal of the particular analyte concentration. Extraction calibration curves

were built with 5 extraction replicates instead of 3 as in other experiments. RSD values for type II thin films were found between 9 – 18% for lowest analyte concentration (50.0 ng·mL⁻¹), and between 5- 12% for highest analyte concentration (500.0 ng·mL⁻¹). For type II thin films, recovery rates of polar analytes were found to be between 1.6 and 30.1% and between 3.9 and 5.5% for non-polar analytes. Reported RSD values were found to be within acceptable limits to warrant further investigations using type II thin films for *ex vivo* and ultimately *in vivo* studies.

Table 3.12 Repeatabilities of extraction of selected analytes by type II thin films

<i>(n = 5)</i>	RSD_{50 mg·mL⁻¹} (%)	RSD_{100 mg·mL⁻¹} (%)	RSD_{500 mg·mL⁻¹} (%)
Polar Analytes			
Tryptophan	18.8	13.2	11.7
Proline	13.9	8.5	6.6
Glutamine	10.0	7.9	5.7
Phenylalanine	18.4	15.1	12.4
Acetylcarnitine	16.6	10.4	9.0
Citrulline	12.9	10.0	8.6
Creatine	15.3	12.4	11.9
γ -aminobutyric acid (GABA)	17.1	14.0	12.3
Acetylcholine	16.1	13.7	12.3
Adenosine	16.4	12.5	9.1
Non-polar Analytes			
DHA	9.8	6.2	5.2
Retinoic acid	9.6	9.0	7.4
Cholesterol	12.7	11.2	9.2

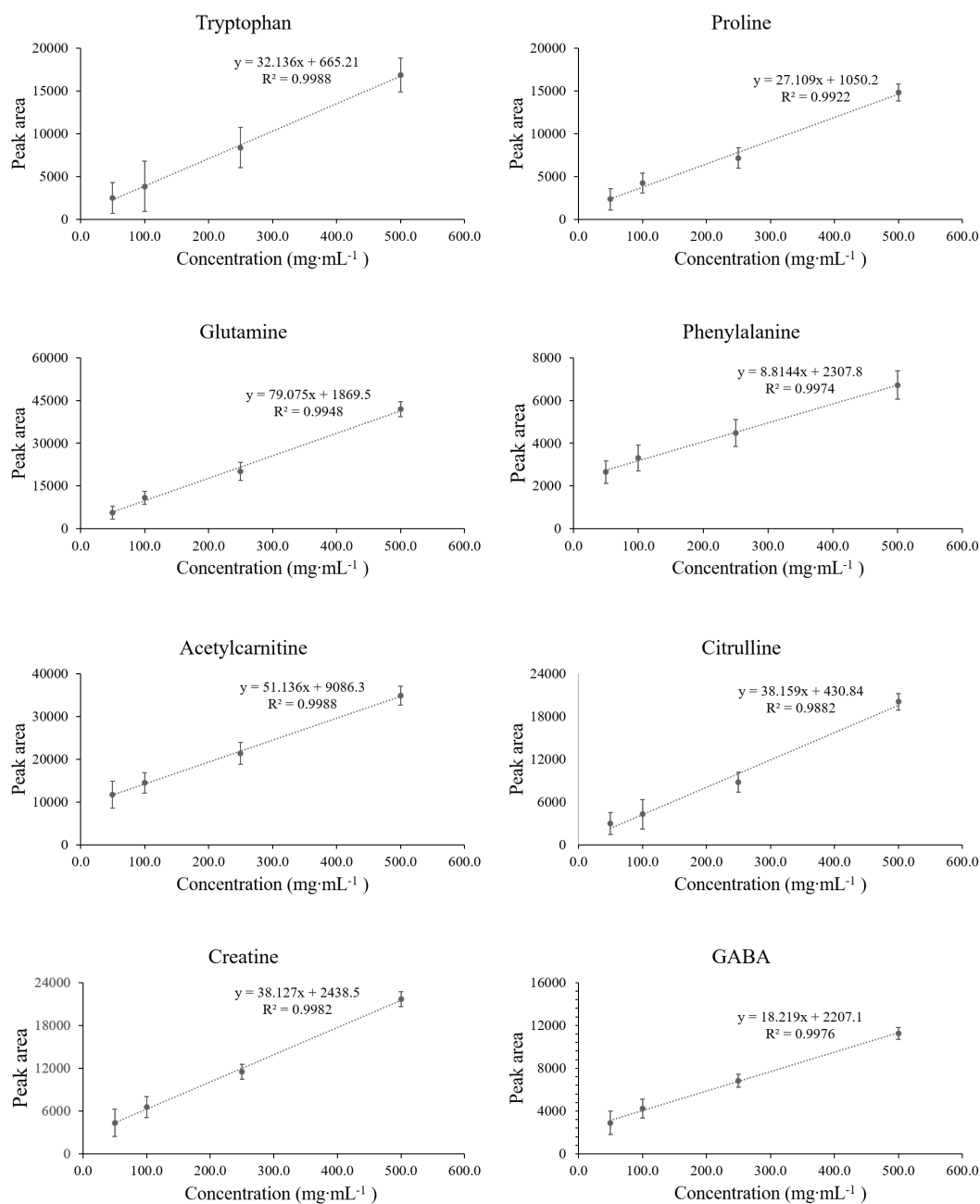


Figure 3.16 Extraction calibration curves for type II lenses (Extraction conditions; extraction time: 120 mins, sample volume: 4.0 mL, agitation speed: static extraction, extraction temperature: RT, analyte concentrations: 50.0, 100.0, 250.0, 500.0 ng·mL⁻¹. Desorption conditions; desorption solvent: ACN:MeOH:H₂O (40:40:20, v/v/v), desorption volume: 0.40 mL, desorption time: 30 mins desorption speed: 1200 rpm) (continued)

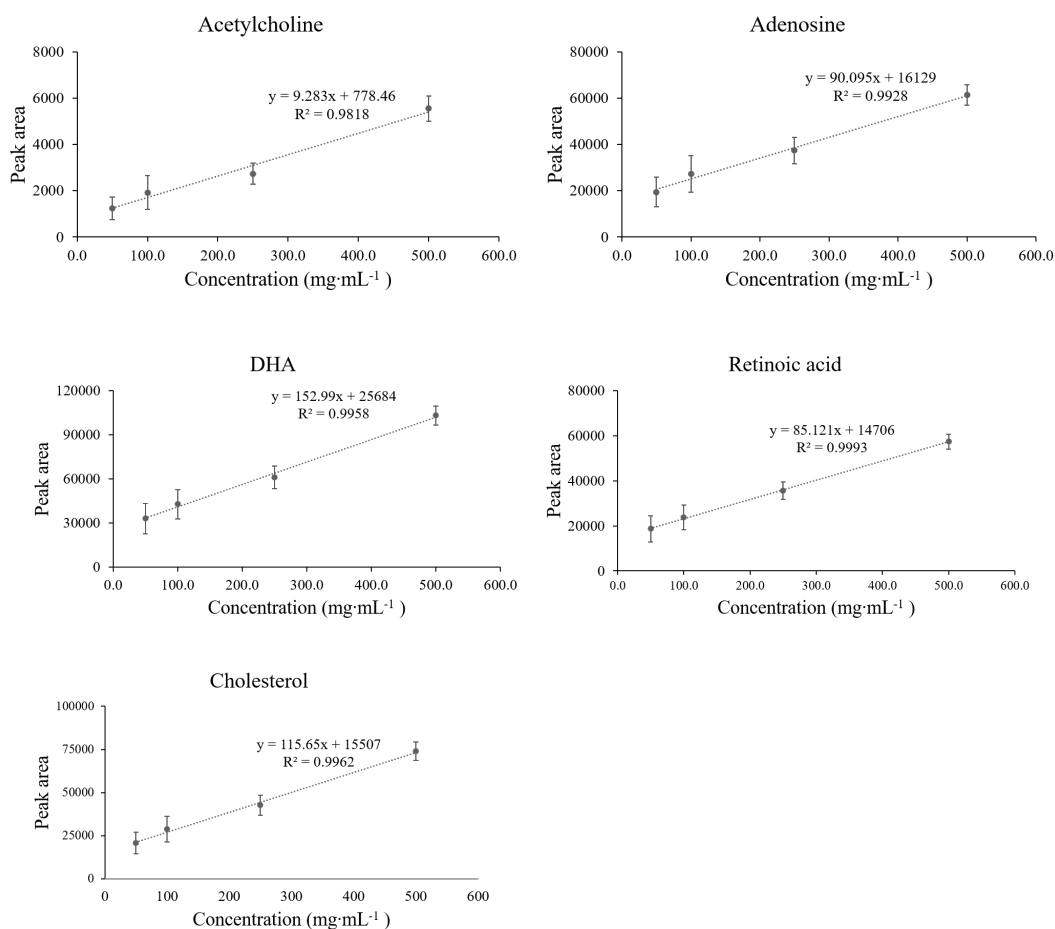


Figure 3.16 Extraction calibration curves for type II lenses (Extraction conditions; extraction time: 120 mins, sample volume: 4.0 mL, agitation speed: static extraction, extraction temperature: RT, analyte concentrations: 50.0, 100.0, 250.0, 500.0 ng·mL⁻¹. Desorption conditions; desorption solvent: ACN:MeOH:H₂O (40:40:20, v/v/v), desorption volume: 0.40 mL, desorption time: 30 mins desorption speed: 1200 rpm)

CHAPTER 3

SUMMARY AND CONCLUSION

The human eye presents a window into the biomolecules that are related to ocular and systemic diseases and disorders. The high number of capillary blood vessels carries biomolecules that are related to systemic diseases via the circulatory system, while the spatial relationship of the eye and the brain provide an easily accessible surface that can be used to investigate biomolecules related to neurodegenerative diseases. Although eye surface has a plethora of biological information and massive potential for diagnostic investigations, only limited studies have been conducted to develop analytical tools applicable for its *in vivo* investigations. In this study, extractive thin films in contact lens geometry that can potentially be used for sampling from the human eye were designed with PDMS as a starting material. The non-polar structure of PDMS is known to perform poorly for the extraction of polar molecules and was modified by APTES, which has amine functional groups to increase the polar extraction capability of thin films.

In order to modify PDMS thin films with amine functional groups, two modification techniques were investigated. Post-modification technique where PDMS thin films are prepared in the desired geometry and its surface is then modified. Thin films prepared with this technique were prepared to be brittle and non-transparent, and this technique was ultimately abandoned. The second modification technique was the *in situ* modification method, where APTES molecules are hydrolyzed and coupled to -OH terminated PDMS oligomers before polymerization. Following this modification technique, starting reagents and modification conditions were optimized, and type I thin films were synthesized as follows: 0.010 g APTES was hydrolyzed using 0.010 g of TFA:H₂O (90:10, v/v) and reacted with 1.00 g of -OH terminated PDMS for 6 h at 800 rpm under room temperature. Afterward, this sol-gel mixture was reacted with 2.50 g of PDMS base (DOWSIL PDMS Kit A) for 1 h at 800 rpm at room

temperature. After the sol-gel mixture was thoroughly mixed, 0.25 g of polymerization catalyst (DOWSIL PDMS Kit B) was added and mixed for 30 mins at 800 rpm at room temperature. The final mixture was directly injected into the 3D printed lens mold, and the contact lens geometry is achieved. After preliminary investigations of type I thin films, a new modification using *in situ* technique was proposed. Type II thin films were prepared with a different starting reagent, PMHS, which was proposed to be modified to have more sites that APTES molecules could potentially bind to. Starting reagents and modification conditions were optimized, and type II thin films were synthesized as follows: 1.50 g of APTES was hydrolyzed using 0.10 g of TFA:H₂O (90:10, v/v) and reacted with 1.00 g PMHS for 6 hours at 800 rpm at room temperature. Afterward, the resulting sol-gel mixture is reacted with 2.50 g of PDMS base (DOWSIL PDMS Kit A) for 1 h at 800 rpm at room temperature. After the mixture is thoroughly mixed, 0.25 g of polymerization catalyst (DOWSIL PDMS Kit B) is reacted for 30 minutes at 800 rpm at room temperature. The final sol-gel mixture was then directly injected into the 3D printed lens mold, and the contact lens geometry was achieved. A third *in situ* modification scheme was also investigated using IZPES instead of APTES as the functional group. However, the resulting mixtures with IZPES could not be polymerized completely, and the contact lens geometry could not be achieved. The modification scheme with IZPES was ultimately abandoned as a result.

After modification, synthesized thin films were characterized with (a) ATR-FTIR spectroscopy, which showed peaks indicating the presence of amine and hydroxyl functional groups in modified thin films, (b) contact angle measurements, which showed increased surface hydrophilicity of modified thin films, (c) TGA, which showed that thermal stability of modified thin films had decreased compared to unmodified PDMS thin films and that modified thin films were thermally stable around 220 °C which indicated modified thin films could be used for extraction of more volatile analytes and detected using thermodesorption GC-MS, (d) SEM imaging and EDX analysis, which showed the presence of nitrogen atom in modified

thin films and an increase in oxygen atom ratio in modified thin films compared to unmodified PDMS thin films.

Using 3D printed molds, prepared thin films were given contact lens geometry, and thin films with different modification schemes were investigated to determine the thin film with the best extraction capability. In order to mimic the extraction conditions of the human eye, *in vitro* agarose eye models were prepared by using 3D printed molds to shape agarose hydrogel to represent the anatomical structure and diffusive properties of the human eye. Analytes were chosen to represent the wide range of small biomolecules present in the human eye.

Two different (HILIC method for polar analytes and reverse-phase method for non-polar analytes) LC-MS methods were developed and optimized for the chosen analytes. PDMS, type I, and type II thin films were compared in terms of their extractive performances for both polar and non-polar analytes with extractions from PBS solutions and *in vitro* agarose eye model. Type II thin films were found to have better extractive capacity towards polar analytes while retaining a similar extractive capacity towards non-polar analytes, compared to PDMS and type I thin films. Type II films were found to perform better than non-modified PDMS thin films in terms of extractive capability towards polar molecules (between 60 – 130%) while retaining their affinity towards non-polar molecules (at 95% CL). This result was a complete fulfillment of the main goal of the study, which was to develop an extractive phase with good extractive performance towards polar and non-polar small biomolecule. A series of extractions from PBS solutions were carried out to optimize desorption parameters such as desorption solvent, desorption time. Out of the three solvents investigated for desorption solvent, ACN:MeOH:H₂O (40:40:20, v/v/v) was found to perform best in terms of quantitative desorption of both polar and non-polar analytes. Out of the four desorption times investigated, 30 minutes was found to be the shortest desorption times without any indication for leftover analytes in the extractive phase. After the desorption parameters were optimized, extraction time profiles were built with extractions from the *in vitro* eye model. Investigations of extraction time showed that equilibrium extraction conditions were

not met after 120 minutes. Constructed extraction time profiles also showed that an extraction time as low as 15 minutes led enough extracted analyte amount for quantitative determination. Lastly, linearity and repeatability of the thin films were investigated with the optimized parameters with 120-minute extractions from the *in vitro* agarose eye model. Developed LC-MS methods were found to show good linearities between the lowest analyte concentration (50.0 ng·mL⁻¹) and the highest analyte concentration (500.0 ng·mL⁻¹). LOQ values were calculated using S/N ratios and found to be between 1.8 ng·mL⁻¹ and 9.0 ng·mL⁻¹. Synthesized type II thin films also showed good repeatability for *in vitro* eye model extractions, between 9 – 18% for lowest analyte concentration (50.0 ng·mL⁻¹), and between 5- 12% for highest analyte concentration (500.0 ng·mL⁻¹). Considering that internal standards could not be used for correction, achieving repeatability values below 20% was considered a significant success. For type II thin films, recovery rates of polar analytes were found to be between 1.6 and 30.1% and between 3.9 and 5.5% for non-polar analytes.

Modified thin films show promising results, but further investigations are necessary to determine their *in vivo* potential. One of the crucial investigations to determine *in vivo* applicability of the contact lens type extractive devices prepared in this study is determining whether the extractive capability remains the same in *ex vivo* samples. *Ex vivo* samples have a much more complex sample matrix, and interfering analytes could potentially reduce the extraction capability of extractive contact lenses towards small molecules. Another essential investigation for *in vivo* applicability is whether the dynamic extraction conditions of the human eye changes the extraction dynamics of the synthesized thin films. Concentrations of analytes in the eye are not constant as the biological processes continue during sampling. It should also be underlined that even though contact lens geometry of the thin films is proposed to be low invasive, their contact with the eye surface could affect the concentration of some biomolecules present in the eye. As stated throughout the text, the synthesized thin films are prepared to be biocompatible. However, the toxicity of the final product has to be investigated before any *in vivo* studies can be carried out.

REFERENCES

- [1] T. Costa, C.R. Scriver, B. Childs, J.M. Opitz, J.F. Reynolds, The effect of Mendelian disease on human health: A measurement, *American Journal of Medical Genetics*. 21 (1985) 231–242. <https://doi.org/10/bwktgz>.
- [2] C. Freund, D.J. Horsford, R.R. McInnes, Transcription factor genes and the developing eye: a genetic perspective, *Human Molecular Genetics*. 5 (1996) 1471–1488. <https://doi.org/10/gg49fk>.
- [3] V. van Heyningen, Developmental eye disease — a genome era paradigm, *Clinical Genetics*. 54 (1998) 272–282. <https://doi.org/10/d4k25n>.
- [4] D.G.I. Chigbu, *Allergic Disorders of the Ocular Surface*, Nova Science Publishers, Incorporated, 2013.
- [5] M. Yanoff, J.W. Sassani, *Ocular Pathology*, Elsevier, 2019.
- [6] A. Rentka, K. Koroskenyi, J. Harsfalvi, Z. Szekanecz, G. Szucs, P. Szodoray, A. Kemeny-Beke, Evaluation of commonly used tear sampling methods and their relevance in subsequent biochemical analysis, *Annals of Clinical Biochemistry*. (2017) 000456321769584. <https://doi.org/10/gg486d>.
- [7] W.D. Stamer, A.M. Williams, S. Pflugfelder, S.E. Coupland, Accessibility to and Quality of Human Eye Tissue for Research: A Cross-Sectional Survey of ARVO Members, *Invest. Ophthalmol. Vis. Sci*. 59 (2018) 4783–4792. <https://doi.org/10/gfd9vz>.
- [8] F.A. Guarnieri, *Corneal Biomechanics*, in: F.A. Guarnieri (Ed.), *Corneal Biomechanics and Refractive Surgery*, Springer New York, New York, NY, 2015: pp. 7–31. https://doi.org/10.1007/978-1-4939-1767-9_2.
- [9] C. Aass, I. Norheim, E.F. Eriksen, P.M. Thorsby, M. Pepaj, Single unit filter-aided method for fast proteomic analysis of tear fluid, *Analytical Biochemistry*. 480 (2015) 1–5. <https://doi.org/10/f7cmj7>.

- [10] B. Redl, Human tear lipocalin, *Biochimica et Biophysica Acta (BBA) - Protein Structure and Molecular Enzymology*. 1482 (2000) 241–248. [https://doi.org/10.1016/S0167-4838\(00\)00142-4](https://doi.org/10.1016/S0167-4838(00)00142-4).
- [11] R.D. Semba, J.J. Enghild, V. Venkatraman, T.F. Dyrland, J.E. Van Eyk, The Human Eye Proteome Project: Perspectives on an emerging proteome, *Proteomics*. 13 (2013) 2500–2511. <https://doi.org/10/f2d4p3>.
- [12] J. Soria, J.A. Durán, J. Etxebarria, J. Merayo, N. González, R. Reigada, I. García, A. Acera, T. Suárez, Tear proteome and protein network analyses reveal a novel pentamarker panel for tear film characterization in dry eye and meibomian gland dysfunction, *Journal of Proteomics*. 78 (2013) 94–112. <https://doi.org/10/f4j6gz>.
- [13] S.H.J. Brown, C.M.E. Kunnen, E. Duchoslav, N.K. Dolla, M.J. Kelso, E.B. Papas, P. Lazon de la Jara, M.D.P. Willcox, S.J. Blanksby, T.W. Mitchell, A Comparison of Patient Matched Meibum and Tear Lipidomes, *Investigative Ophthalmology & Visual Science*. 54 (2013) 7417. <https://doi.org/10/f5jng3>.
- [14] S. Hagan, E. Martin, A. Enríquez-de-Salamanca, Tear fluid biomarkers in ocular and systemic disease: potential use for predictive, preventive and personalised medicine, *EPMA J*. 7 (2016). <https://doi.org/10/ggpq7x>.
- [15] M.D. Willcox, Tear film, contact lenses and tear biomarkers, *Clinical and Experimental Optometry*. (2019). <https://doi.org/10/ggz7zf>.
- [16] K.B. Green-Church, I. Butovich, M. Willcox, D. Borchman, F. Paulsen, S. Barabino, B.J. Glasgow, The International Workshop on Meibomian Gland Dysfunction: Report of the Subcommittee on Tear Film Lipids and Lipid–Protein Interactions in Health and Disease, *Investigative Ophthalmology & Visual Science*. 52 (2011) 1979. <https://doi.org/10/cmdvqj>.
- [17] M.D.P. Willcox, P. Argüeso, G.A. Georgiev, J.M. Holopainen, G.W. Laurie, T.J. Millar, E.B. Papas, J.P. Rolland, T.A. Schmidt, U. Stahl, T. Suarez, L.N. Subbaraman, O.Ö. Uçakhan, L. Jones, TFOS DEWS II Tear Film Report, *The Ocular Surface*. 15 (2017) 366–403. <https://doi.org/10/gbsjc6>.
- [18] J. You, M.D. Willcox, M.C. Madigan, V. Wasinger, B. Schiller, B.J. Walsh, P.H. Graham, J.H. Kearsley, Y. Li, Tear Fluid Protein Biomarkers, in: *Advances in Clinical Chemistry*, Elsevier, 2013: pp. 151–196. <https://doi.org/10.1016/B978-0-12-800096-0.00004-4>.
- [19] D.G. Durham, DISTRIBUTION OF FREE AMINO ACIDS IN HUMAN INTRAOCULAR FLUIDS, (n.d.) 39.

- [20] L.J. Takemoto, P. Azari, Amino acid composition of normal and cataractous human lens proteins, *Experimental Eye Research*. 23 (1976) 1–7. <https://doi.org/10/drz57h>.
- [21] M.-J. Lu, J.S. Pulido, K.H. Baratz, H. Qian, J.C. Erie, S.A. Shippy, Amino Acid Analysis of Human Tears in Dry vs. Normal Eyes by Capillary Electrophoresis, *Invest. Ophthalmol. Vis. Sci*. 49 (2008) 5307–5307.
- [22] M. Kalloniatis, C.S. Loh, M.L. Acosta, G. Tomisich, Y. Zhu, L. Nivison-Smith, E.L. Fletcher, J. Chua, D. Sun, N. Arunthavasothy, Retinal amino acid neurochemistry in health and disease, *Clinical and Experimental Optometry*. 96 (2013) 310–332. <https://doi.org/10/f4w22w>.
- [23] L. ChenZhuo, J. Murube, A. Latorre, R.M. del Río, Different Concentrations of Amino Acids in Tears of Normal and Human Dry Eyes, in: D.A. Sullivan, M.E. Stern, K. Tsubota, D.A. Dartt, R.M. Sullivan, B.B. Bromberg (Eds.), *Lacrimal Gland, Tear Film, and Dry Eye Syndromes 3: Basic Science and Clinical Relevance Part A and B*, Springer US, Boston, MA, 2002: pp. 617–621. https://doi.org/10.1007/978-1-4615-0717-8_87.
- [24] M. Nakatsukasa, C. Sotozono, K. Shimbo, N. Ono, H. Miyano, A. Okano, J. Hamuro, S. Kinoshita, Amino Acid profiles in human tear fluids analyzed by high-performance liquid chromatography and electrospray ionization tandem mass spectrometry, *Am. J. Ophthalmol*. 151 (2011) 799-808.e1. <https://doi.org/10/cw8hcn>.
- [25] Biomarkers and surrogate endpoints: Preferred definitions and conceptual framework, *Clinical Pharmacology & Therapeutics*. 69 (2001) 89–95. <https://doi.org/10/fccg5x>.
- [26] H.W. Forster, ROSE BENGAL TEST IN DIAGNOSIS OF DEFICIENT TEAR FORMATION, *AMA Arch Ophthalmol*. 45 (1951) 419–424. <https://doi.org/10/dkp7zk>.
- [27] J.G. Lewis, P.J. Stephens, TEAR GLUCOSE IN DIABETICS, *British Journal of Ophthalmology*. 42 (1958) 754–758. <https://doi.org/10/b22qk2>.

- [28] M. Azkargorta, J. Soria, A. Acera, I. Iloro, F. Elortza, Human tear proteomics and peptidomics in ophthalmology: Toward the translation of proteomic biomarkers into clinical practice, *J Proteomics*. 150 (2017) 359–367. <https://doi.org/10/ggpq9h>.
- [29] D. Pieragostino, M. D'Alessandro, M. di Ioia, C.D. Ilio, P. Sacchetta, P.D. Boccio, Unraveling the molecular repertoire of tears as a source of biomarkers: Beyond ocular diseases, *PROTEOMICS – Clinical Applications*. 9 (2015) 169–186. <https://doi.org/10/f2x6tm>.
- [30] R. Shetty, A. Ghosh, R.R. Lim, M. Subramani, K. Mihir, R.A. R, A. Ranganath, S. Nagaraj, R.M.M.A. Nuijts, R. Beuerman, R. Shetty, D. Das, S.S. Chaurasia, A. Sinha-Roy, A. Ghosh, Elevated Expression of Matrix Metalloproteinase-9 and Inflammatory Cytokines in Keratoconus Patients Is Inhibited by Cyclosporine A, *Invest. Ophthalmol. Vis. Sci*. 56 (2015) 738–750. <https://doi.org/10/f67n5r>.
- [31] F. Tsuji, Biomarker Identification of Tear Fluid, *Journal of Postgenomics Drug & Biomarker Development*. 2 (2012). <https://doi.org/10/gg783z>.
- [32] N. von Thun und Hohenstein-Blaul, S. Funke, F.H. Grus, Tears as a source of biomarkers for ocular and systemic diseases, *Experimental Eye Research*. 117 (2013) 126–137. <https://doi.org/10/f5j2qq>.
- [33] L. Zhou, R.W. Beuerman, C.M. Chan, S.Z. Zhao, X.R. Li, H. Yang, L. Tong, S. Liu, M.E. Stern, D. Tan, Identification of tear fluid biomarkers in dry eye syndrome using iTRAQ quantitative proteomics, *J. Proteome Res*. 8 (2009) 4889–4905. <https://doi.org/10/d2bpk5>.
- [34] S. Lauwen, E.K. de Jong, D.J. Lefeber, A.I. den Hollander, *Omics Biomarkers in Ophthalmology*, *Investigative Ophthalmology & Visual Science*. 58 (2017) BIO88. <https://doi.org/10/f98f5r>.
- [35] M. Tamhane, S. Cabrera-Ghayouri, G. Abelian, V. Viswanath, Review of Biomarkers in Ocular Matrices: Challenges and Opportunities, *Pharmaceutical Research*. 36 (2019). <https://doi.org/10/ggz9df>.

- [36] R.J. Fullard, D. Tucker, Tear Protein Composition and the Effects of Stimulus, in: D.A. Sullivan (Ed.), *Lacrimal Gland, Tear Film, and Dry Eye Syndromes: Basic Science and Clinical Relevance*, Springer US, Boston, MA, 1994: pp. 309–314. https://doi.org/10.1007/978-1-4615-2417-5_52.
- [37] K.B. Green-Church, K.K. Nichols, N.M. Kleinholz, L. Zhang, J.J. Nichols, Investigation of the human tear film proteome using multiple proteomic approaches, *Mol. Vis.* 14 (2008) 456–470.
- [38] C. McCollum, G. Foulks, B. Bodner, J. Shepard, K. Daniels, V. Gross, L. Kelly, H. Cavanagh, Rapid assay of lactoferrin in keratoconjunctivitis sicca, *Cornea.* 13 (1994) 505–508.
- [39] Y. Ohashi, R. Ishida, T. Kojima, E. Goto, Y. Matsumoto, K. Watanabe, N. Ishida, K. Nakata, T. Takeuchi, K. Tsubota, Abnormal protein profiles in tears with dry eye syndrome, *American Journal of Ophthalmology.* 136 (2003) 291–299. <https://doi.org/10/dj6kp9>.
- [40] S. Srinivasan, M. Thangavelu, L. Zhang, K.B. Green, K.K. Nichols, iTRAQ Quantitative Proteomics in the Analysis of Tears in Dry Eye Patients, *Invest. Ophthalmol. Vis. Sci.* 53 (2012) 5052–5059. <https://doi.org/10/gg79f4>.
- [41] P. Versura, A. Bavelloni, M. Grillini, M. Fresina, E.C. Campos, Diagnostic performance of a tear protein panel in early dry eye, *Mol Vis.* 19 (2013) 1247–1257.
- [42] A. Acera, E. Vecino, J.A. Duran, Tear MMP-9 Levels as a Marker of Ocular Surface Inflammation in Conjunctivochalasis, *Invest. Ophthalmol. Vis. Sci.* 54 (2013) 8285–8291. <https://doi.org/10/f5v5ts>.
- [43] A. Acera, G. Rocha, E. Vecino, I. Lema, J.A. Durán, Inflammatory Markers in the Tears of Patients with Ocular Surface Disease, *ORE.* 40 (2008) 315–321. <https://doi.org/10/bmpqc3>.

- [44] T.C.Y. Chan, C. Ye, K.P. Chan, K.O. Chu, V. Jhanji, Evaluation of point-of-care test for elevated tear matrix metalloproteinase 9 in post-LASIK dry eyes, *British Journal of Ophthalmology*. 100 (2016) 1188–1191. <https://doi.org/10/f84ddq>.
- [45] S. Chotikavanich, C.S. de Paiva, D.Q. Li, J.J. Chen, F. Bian, W.J. Farley, S.C. Pflugfelder, Production and Activity of Matrix Metalloproteinase-9 on the Ocular Surface Increase in Dysfunctional Tear Syndrome, *Investigative Ophthalmology & Visual Science*. 50 (2009) 3203–3209. <https://doi.org/10/b9975s>.
- [46] J.-F. Huang, R. Yafawi, M. Zhang, M. McDowell, K.D. Rittenhouse, F. Sace, S.H. (Melissa) Liew, S.R. Cooper, E.H. Pickering, Immunomodulatory Effect of the Topical Ophthalmic Janus Kinase Inhibitor Tofacitinib (CP-690,550) in Patients with Dry Eye Disease, *Ophthalmology*. 119 (2012) e43–e50. <https://doi.org/10/f2hdrh>.
- [47] C. Lopez, S. Park, S. Edwards, S. Vong, S. Hou, M. Lee, H. Sauerland, J.-J. Lee, K.J. Jeong, Matrix Metalloproteinase-Deactivating Contact Lens for Corneal Melting, *ACS Biomaterials Science & Engineering*. 5 (2019) 1195–1199. <https://doi.org/10/gf4fvh>.
- [48] E.M. Messmer, V. von Lindenfels, A. Garbe, A. Kampik, Matrix Metalloproteinase 9 Testing in Dry Eye Disease Using a Commercially Available Point-of-Care Immunoassay, *Ophthalmology*. 123 (2016) 2300–2308. <https://doi.org/10/f9dszb>.
- [49] J. Pinto-Fraga, A. Enríquez-de-Salamanca, M. Calonge, M.J. González-García, A. López-Miguel, A. López-de la Rosa, C. García-Vázquez, V. Calder, M.E. Stern, I. Fernández, Severity, therapeutic, and activity tear biomarkers in dry eye disease: An analysis from a phase III clinical trial, *The Ocular Surface*. 16 (2018) 368–376. <https://doi.org/10/gdt6pc>.
- [50] R. Sambursky, Presence or absence of ocular surface inflammation directs clinical and therapeutic management of dry eye, *Clin Ophthalmol*. 10 (2016) 2337–2343. <https://doi.org/10/f9rtz8>.

- [51] R. Sambursky, W.F.I. Davitt, M. Friedberg, S. Tauber, Prospective, Multicenter, Clinical Evaluation of Point-of-Care Matrix Metalloproteinase-9 Test for Confirming Dry Eye Disease, *Cornea*. 33 (2014) 812–818. <https://doi.org/10/f583rn>.
- [52] M. Schargus, S. Ivanova, V. Kakkassery, H.B. Dick, S. Joachim, Correlation of Tear Film Osmolarity and 2 Different MMP-9 Tests With Common Dry Eye Tests in a Cohort of Non-Dry Eye Patients, *Cornea*. 34 (2015) 739–744. <https://doi.org/10/f7hd8r>.
- [53] A. Solomon, D. Dursun, Z. Liu, Y. Xie, A. Macri, S.C. Pflugfelder, Pro- and Anti-inflammatory Forms of Interleukin-1 in the Tear Fluid and Conjunctiva of Patients with Dry-Eye Disease, *Invest. Ophthalmol. Vis. Sci*. 42 (2001) 2283–2292.
- [54] L. Tong, R. Beuerman, S. Simonyi, D.A. Hollander, M.E. Stern, Effects of Punctal Occlusion on Clinical Signs and Symptoms and on Tear Cytokine Levels in Patients with Dry Eye, *The Ocular Surface*. 14 (2016) 233–241. <https://doi.org/10/f8kd36>.
- [55] Y. Uchino, J. Mauris, A.M. Woodward, J. Dieckow, F. Amparo, R. Dana, F. Mantelli, P. Argüeso, Alteration of Galectin-3 in Tears of Patients With Dry Eye Disease, *American Journal of Ophthalmology*. 159 (2015) 1027-1035.e3. <https://doi.org/10/f3hcqs>.
- [56] K.R. VanDerMeid, S.P. Su, K.L. Krenzer, K.W. Ward, J.-Z. Zhang, A method to extract cytokines and matrix metalloproteinases from Schirmer strips and analyze using Luminex, *Mol Vis*. 17 (2011) 1056–1063.
- [57] L. Zhang, Z. Su, Z. Zhang, J. Lin, D.-Q. Li, S.C. Pflugfelder, Effects of Azithromycin on Gene Expression Profiles of Proinflammatory and Anti-inflammatory Mediators in the Eyelid Margin and Conjunctiva of Patients With Meibomian Gland Disease, *JAMA Ophthalmol*. 133 (2015) 1117–1123. <https://doi.org/10/gg79hm>.

- [58] F.J. Gil-Bea, M. García-Alloza, J. Domínguez, B. Marcos, M.J. Ramírez, Evaluation of cholinergic markers in Alzheimer's disease and in a model of cholinergic deficit, *Neurosci. Lett.* 375 (2005) 37–41. <https://doi.org/10/dnzvmt>.
- [59] M.G. Lionetto, R. Caricato, A. Calisi, M.E. Giordano, T. Schettino, Acetylcholinesterase as a Biomarker in Environmental and Occupational Medicine: New Insights and Future Perspectives, *Biomed Res Int.* 2013 (2013). <https://doi.org/10/gbdww9>.
- [60] N. Waiskopf, S. Shenhar-Tsarfaty, H. Soreq, Serum Cholinesterase Activities as Biomarkers of Cardiac Malfunctioning, in: V.B. Patel, V.R. Preedy (Eds.), *Biomarkers in Cardiovascular Disease*, Springer Netherlands, Dordrecht, 2016: pp. 197–218. https://doi.org/10.1007/978-94-007-7678-4_10.
- [61] J.R. Delanghe, M.M. Speeckaert, M.L.D. Buyzere, Is creatine kinase an ideal biomarker in rhabdomyolysis? Reply to Lippi et al.: Diagnostic biomarkers of muscle injury and exertional rhabdomyolysis (<https://doi.org/10.1515/cclm-2018-0656>), *Clinical Chemistry and Laboratory Medicine (CCLM)*. 57 (2019) e75–e76. <https://doi.org/10/gg79hw>.
- [62] J. Kim, D.J. Amante, J.P. Moody, C.K. Edgerly, O.L. Bordiuk, K. Smith, S.A. Matson, W.R. Matson, C.R. Scherzer, H.D. Rosas, S.M. Hersch, R.J. Ferrante, Reduced creatine kinase as a central and peripheral biomarker in Huntington's disease, *Biochim Biophys Acta.* 1802 (2010) 673–681. <https://doi.org/10/cx5s47>.
- [63] S. Pajares, A. Arias, J. García-Villoria, P. Briones, A. Ribes, Role of creatine as biomarker of mitochondrial diseases, *Molecular Genetics and Metabolism.* 108 (2012). <https://doi.org/10/f4j69w>.
- [64] N. Cawley, B.S. Solanky, N. Muhlert, C. Tur, R.A.E. Edden, C.A.M. Wheeler-Kingshott, D.H. Miller, A.J. Thompson, O. Ciccarelli, Reduced gamma-aminobutyric acid concentration is associated with physical disability in progressive multiple sclerosis, *Brain.* 138 (2015) 2584–2595. <https://doi.org/10/f7rtvk>.

- [65] M. Trousselard, B. Lefebvre, L. Caillet, Y. Andruetan, F. de Montleau, J. Denis, F. Canini, Is plasma GABA level a biomarker of Post-Traumatic Stress Disorder (PTSD) severity? A preliminary study, *Psychiatry Res.* 241 (2016) 273–279. <https://doi.org/10/f8vz55>.
- [66] Z. Wang, L. Bian, C. Mo, H. Shen, L.J. Zhao, K.-J. Su, M. Kukula, J.T. Lee, D.W. Armstrong, R. Recker, J. Lappe, L.F. Bonewald, H.-W. Deng, M. Brotto, Quantification of aminobutyric acids and their clinical applications as biomarkers for osteoporosis, *Communications Biology.* 3 (2020) 1–14. <https://doi.org/10/gg79h2>.
- [67] R.E. Frye, S. Melnyk, D.F. MacFabe, Unique acyl-carnitine profiles are potential biomarkers for acquired mitochondrial disease in autism spectrum disorder, *Transl Psychiatry.* 3 (2013) e220. <https://doi.org/10/f4jwgw>.
- [68] C. Nasca, B. Bigio, F.S. Lee, S.P. Young, M.M. Kautz, A. Albright, J. Beasley, D.S. Millington, A.A. Mathé, J.H. Kocsis, J.W. Murrough, B.S. McEwen, N. Rasgon, Acetyl-l-carnitine deficiency in patients with major depressive disorder, *Proceedings of the National Academy of Sciences.* 115 (2018) 8627–8632. <https://doi.org/10/gd4zdt>.
- [69] P.Y. Lee, G.S. Schulert, S.W. Canna, Y. Huang, J. Sundel, Y. Li, K.J. Hoyt, R.B. Blaustein, A. Wactor, T. Do, O. Halyabar, M.H. Chang, F. Dedeoglu, S.M. Case, E. Meidan, M.S. Lo, R.P. Sundel, E.T. Richardson, J.W. Newburger, M.S. Hershfield, M.B. Son, L.A. Henderson, P.A. Nigrovic, Adenosine deaminase 2 as a biomarker of macrophage activation syndrome in systemic juvenile idiopathic arthritis, *Annals of the Rheumatic Diseases.* 79 (2020) 225–231. <https://doi.org/10/gg79h6>.
- [70] J.-M. Michot, Y. Madec, S. Bulifon, C. Thorette-Tcherniak, N. Fortineau, N. Noël, O. Lambotte, Y. El Jahiri, H. Delacour, J.-F. Delfraissy, F.-X. Blanc, Adenosine deaminase is a useful biomarker to diagnose pleural tuberculosis in low to medium prevalence settings, *Diagnostic Microbiology and Infectious Disease.* 84 (2016) 215–220. <https://doi.org/10/f8cgwz>.
- [71] A.C. Patterson, A. Chalil, J.J. Aristizabal Henao, I.T. Streit, K.D. Stark, Omega-3 polyunsaturated fatty acid blood biomarkers increase linearly in men and women after tightly controlled intakes of 0.25, 0.5, and 1 g/d of EPA + DHA, *Nutr Res.* 35 (2015) 1040–1051. <https://doi.org/10/f74jqz>.

- [72] Z. Makhoul, A.R. Kristal, R. Gulati, B. Luick, A. Bersamin, B. Boyer, G.V. Mohatt, Associations of very high intakes of eicosapentaenoic and docosahexaenoic acids with biomarkers of chronic disease risk among Yup'ik Eskimos, *Am J Clin Nutr.* 91 (2010) 777–785. <https://doi.org/10/dvpng9>.
- [73] J.A. Cooper, G.J. Miller, S.E. Humphries, A comparison of the PROCAM and Framingham point-scoring systems for estimation of individual risk of coronary heart disease in the Second Northwick Park Heart Study, *Atherosclerosis.* 181 (2005) 93–100. <https://doi.org/10/d9sc59>.
- [74] V. Dobrotkova, P. Chlapek, P. Mazanek, J. Sterba, R. Veselska, Traffic lights for retinoids in oncology: molecular markers of retinoid resistance and sensitivity and their use in the management of cancer differentiation therapy, *BMC Cancer.* 18 (2018). <https://doi.org/10/gfmwpp>.
- [75] R.M. Niles, Biomarker and animal models for assessment of retinoid efficacy in cancer chemoprevention, *Acta Pharmacologica Sinica.* 28 (2007) 1383–1391. <https://doi.org/10/cgk76p>.
- [76] G.B. Steventon, S.C. Mitchell, Phenylalanine hydroxylase: A biomarker of disease susceptibility in Parkinson's disease and Amyotrophic lateral sclerosis, *Medical Hypotheses.* 118 (2018) 29–33. <https://doi.org/10/gd4rt3>.
- [77] C. Madeira, C. Vargas-Lopes, C.O. Brandão, T. Reis, J. Laks, R. Panizzutti, S.T. Ferreira, Elevated Glutamate and Glutamine Levels in the Cerebrospinal Fluid of Patients With Probable Alzheimer's Disease and Depression, *Front. Psychiatry.* 9 (2018). <https://doi.org/10/gg79jd>.
- [78] S.Y. Rhee, E.S. Jung, H.M. Park, S.J. Jeong, K. Kim, S. Chon, S.-Y. Yu, J.-T. Woo, C.H. Lee, Plasma glutamine and glutamic acid are potential biomarkers for predicting diabetic retinopathy, *Metabolomics.* 14 (2018). <https://doi.org/10/gg79jc>.
- [79] A.L. ten Hoeve, M.A. Roda, F. Redegeld, G. Folkerts, J.E. Blalock, A. Gaggar, Proline-Glycine-Proline as a Potential Biomarker in Chronic Obstructive Pulmonary Disease and Cystic Fibrosis, *Tanaffos.* 11 (2012) 12–15.

- [80] S.N. Kaore, N.M. Kaore, Chapter 53 - Citrulline: Pharmacological perspectives and role as a biomarker in diseases and toxicities, in: R.C. Gupta (Ed.), *Biomarkers in Toxicology*, Academic Press, Boston, 2014: pp. 883–905. <https://doi.org/10.1016/B978-0-12-404630-6.00053-1>.
- [81] S. Nikolaus, B. Schulte, N. Al-Massad, F. Thieme, D.M. Schulte, J. Bethge, A. Rehman, F. Tran, K. Aden, R. Häslner, N. Moll, G. Schütze, M.J. Schwarz, G.H. Waetzig, P. Rosenstiel, M. Krawczak, S. Szymczak, S. Schreiber, Increased Tryptophan Metabolism Is Associated With Activity of Inflammatory Bowel Diseases, *Gastroenterology*. 153 (2017) 1504-1516.e2. <https://doi.org/10/cch2>.
- [82] N. Samad, F. Yasmin, N. Manzoor, Biomarkers in Drug Free Subjects with Depression : Correlation with Tryptophan, *Psychiatry Investig*. 16 (2019) 948–953. <https://doi.org/10/gg79jj>.
- [83] K. Santisukwongchote, Y. Amornlertwatana, T. Sastraruji, C. Jaikang, Possible Use of Blood Tryptophan Metabolites as Biomarkers for Coronary Heart Disease in Sudden Unexpected Death, *Metabolites*. 10 (2020) 6. <https://doi.org/10/gg79jh>.
- [84] A. Enríquez-de-Salamanca, E. Castellanos, M.E. Stern, I. Fernández, E. Carreño, C. García-Vázquez, J.M. Herreras, M. Calonge, Tear cytokine and chemokine analysis and clinical correlations in evaporative-type dry eye disease, *Mol Vis*. 16 (2010) 862–873.
- [85] H. Lam, L. Bleiden, C.S. de Paiva, W. Farley, M.E. Stern, S.C. Pflugfelder, Tear Cytokine Profiles in Dysfunctional Tear Syndrome, *American Journal of Ophthalmology*. 147 (2009) 198-205.e1. <https://doi.org/10/fcj4qj>.
- [86] A. López-Miguel, M. Tesón, V. Martín-Montañez, A. Enríquez-de-Salamanca, M.E. Stern, M. Calonge, M.J. González-García, Dry Eye Exacerbation in Patients Exposed to Desiccating Stress under Controlled Environmental Conditions, *American Journal of Ophthalmology*. 157 (2014) 788-798.e2. <https://doi.org/10/f2qh5v>.

- [87] S.C. Pflugfelder, D. Jones, Z. Ji, A. Afonso, D. Monroy, Altered cytokine balance in the tear fluid and conjunctiva of patients with Sjögren's syndrome keratoconjunctivitis sicca, *Current Eye Research*. 19 (1999) 201–211. <https://doi.org/10/bqthwq>.
- [88] N. Boehm, S. Funke, M. Wiegand, N. Wehrwein, N. Pfeiffer, F.H. Grus, Alterations in the Tear Proteome of Dry Eye Patients—A Matter of the Clinical Phenotype, *Invest. Ophthalmol. Vis. Sci*. 54 (2013) 2385–2392. <https://doi.org/10/gg79j3>.
- [89] F.H. Grus, V.N. Podust, K. Bruns, K. Lackner, S. Fu, E.A. Dalmaso, A. Wirthlin, N. Pfeiffer, SELDI-TOF-MS ProteinChip Array Profiling of Tears from Patients with Dry Eye, *Invest. Ophthalmol. Vis. Sci*. 46 (2005) 863–876. <https://doi.org/10/cxf7vg>.
- [90] N. Perumal, S. Funke, N. Pfeiffer, F.H. Grus, Proteomics analysis of human tears from aqueous-deficient and evaporative dry eye patients, *Scientific Reports*. 6 (2016) 29629. <https://doi.org/10/f8v33h>.
- [91] J. Soria, A. Acera, J. Merayo-LLoves, J.A. Durán, N. González, S. Rodriguez, N. Bistolas, S. Schumacher, F.F. Bier, H. Peter, W. Stöcklein, T. Suárez, Tear proteome analysis in ocular surface diseases using label-free LC-MS/MS and multiplexed-microarray biomarker validation, *Scientific Reports*. 7 (2017) 17478. <https://doi.org/10/gcrdggf>.
- [92] N. Boehm, A.I. Riechardt, M. Wiegand, N. Pfeiffer, F.H. Grus, Proinflammatory Cytokine Profiling of Tears from Dry Eye Patients by Means of Antibody Microarrays, *Invest. Ophthalmol. Vis. Sci*. 52 (2011) 7725–7730. <https://doi.org/10/dcsmb4>.
- [93] A. Enríquez-de-Salamanca, S. Bonini, M. Calonge, Molecular and cellular biomarkers in dry eye disease and ocular allergy, *Current Opinion in Allergy and Clinical Immunology*. 12 (2012) 523–533. <https://doi.org/10/gg79j6>.
- [94] L. Sun, C. Guo, J. Cao, J. Burnett, Z. Yang, Y. Ran, D. Sun, Over-Expression of Alpha-Enolase as a Prognostic Biomarker in Patients with Pancreatic Cancer, *Int J Med Sci*. 14 (2017) 655–661. <https://doi.org/10/gbp3z4>.

- [95] A. Alunno, O. Bistoni, F. Pratesi, G.M.C. La Paglia, I. Puxeddu, P. Migliorini, R. Gerli, Anti-citrullinated alpha enolase antibodies, interstitial lung disease and bone erosion in rheumatoid arthritis, *Rheumatology* (Oxford). 57 (2018) 850–855. <https://doi.org/10/gc2ngq>.
- [96] C. López-Pedrerá, J.M. Villalba, E. Siendones, N. Barbarroja, C. Gómez-Díaz, A. Rodríguez-Ariza, P. Buendía, A. Torres, F. Velasco, Proteomic analysis of acute myeloid leukemia: Identification of potential early biomarkers and therapeutic targets, *PROTEOMICS*. 6 (2006) S293–S299. <https://doi.org/10/bgkrms>.
- [97] M. Berry, R.B. Ellingham, A.P. Corfield, Human precocular mucins reflect changes in surface physiology, *British Journal of Ophthalmology*. 88 (2004) 377–383. <https://doi.org/10/c52ztw>.
- [98] D.N. Stephens, N.A. McNamara, Altered Mucin and Glycoprotein Expression in Dry Eye Disease, *Optometry and Vision Science*. 92 (2015) 931–938. <https://doi.org/10/f7qjkm>.
- [99] Y. Uchino, M. Uchino, N. Yokoi, M. Dogru, M. Kawashima, N. Okada, T. Inaba, S. Tamaki, A. Komuro, Y. Sonomura, H. Kato, P. Argüeso, S. Kinoshita, K. Tsubota, Alteration of Tear Mucin 5AC in Office Workers Using Visual Display Terminals: The Osaka Study, *JAMA Ophthalmol*. 132 (2014) 985–992. <https://doi.org/10/gf2p7t>.
- [100] J. Zhang, X. Yan, H. Li, Analysis of the Correlations of Mucins, Inflammatory Markers, and Clinical Tests in Dry Eye, *Cornea*. 32 (2013) 928–932. <https://doi.org/10/f47jkr>.
- [101] H. Zhao, J.E. Jumblatt, T.O. Wood, M.M. Jumblatt, Quantification of MUC5AC Protein in Human Tears, *Cornea*. 20 (2001) 873–877. <https://doi.org/10/cdwm45>.

- [102] M.C. Edman, S.R. Janga, Z. Meng, M. Bechtold, A.F. Chen, C. Kim, L. Naman, A. Sarma, N. Teekappanavar, A.Y. Kim, S. Madrigal, S. Singh, E. Ortiz, S. Christianakis, D.G. Arkfeld, W.J. Mack, M. Heur, W. Stohl, S.F. Hamm-Alvarez, Increased Cathepsin S activity associated with decreased protease inhibitory capacity contributes to altered tear proteins in Sjögren's Syndrome patients, *Scientific Reports*. 8 (2018) 11044. <https://doi.org/10/gdxzc5>.
- [103] S.F. Hamm-Alvarez, S.R. Janga, M.C. Edman, S. Madrigal, M. Shah, S.E. Frousiakis, K. Renduchintala, J. Zhu, S. Bricel, K. Silka, D. Bach, M. Heur, S. Christianakis, D.G. Arkfeld, J. Irvine, W.J. Mack, W. Stohl, Tear cathepsin S as a candidate biomarker for Sjögren's syndrome, *Arthritis & Rheumatology (Hoboken, N.J.)*. 66 (2014) 1872–1881. <https://doi.org/10/f59tjw>.
- [104] B. Golebiowski, C. Chao, F. Stapleton, I. Jalbert, Corneal Nerve Morphology, Sensitivity, and Tear Neuropeptides in Contact Lens Wear, *Optometry and Vision Science*. 94 (2017) 534–542. <https://doi.org/10/gg79ks>.
- [105] A. Lambiase, A. Micera, M. Sacchetti, M. Cortes, F. Mantelli, S. Bonini, Alterations of Tear Neuromediators in Dry Eye Disease, *Arch Ophthalmol*. 129 (2011) 981–986. <https://doi.org/10/dc8nsm>.
- [106] A. Leonardi, Allergy and allergic mediators in tears, *Experimental Eye Research*. 117 (2013) 106–117. <https://doi.org/10/f5kgwg>.
- [107] A. Leonardi, S.J. Curnow, H. Zhan, V.L. Calder, Multiple cytokines in human tear specimens in seasonal and chronic allergic eye disease and in conjunctival fibroblast cultures, *Clinical & Experimental Allergy*. 36 (2006) 777–784. <https://doi.org/10/fh66x2>.
- [108] E. Uchio, S. Ono, Z. Ikezawa, S. Ohno, Tear levels of interferon-gamma, interleukin (IL) -2, IL-4 and IL-5 in patients with vernal keratoconjunctivitis, atopic keratoconjunctivitis and allergic conjunctivitis, *Clinical and Experimental Allergy : Journal of the British Society for Allergy and Clinical Immunology*. 30 (2000) 103–109. <https://doi.org/10/cb3cdc>.

- [109] A.B. Niculescu, H. Le-Niculescu, K. Roseberry, S. Wang, J. Hart, A. Kaur, H. Robertson, T. Jones, A. Strasburger, A. Williams, S.M. Kurian, B. Lamb, A. Shekhar, D.K. Lahiri, A.J. Saykin, Blood biomarkers for memory: toward early detection of risk for Alzheimer disease, pharmacogenomics, and repurposed drugs, *Molecular Psychiatry*. 25 (2020) 1651–1672. <https://doi.org/10/gg79kx>.
- [110] S.F. Hamm-Alvarez, C.T. Okamoto, S.R. Janga, D. Feigenbaum, M.C. Edman, D. Freire, M. Shah, R. Ghanshani, W.J. Mack, M.F. Lew, Oligomeric α -synuclein is increased in basal tears of Parkinson's patients, *Biomarkers in Medicine*. 13 (2019) 941–952. <https://doi.org/10/gg79k3>.
- [111] P.K. Balne, R. Agrawal, V.B. Au, B. Lee, E. Loo, L. Tong, A. Ghosh, S.C. Teoh, J. Connolly, P. Tan, Dataset of tear film cytokine levels in dry eye disease (DED) patients with and without HIV infection, *Data in Brief*. 10 (2017) 14–16. <https://doi.org/10/gg79m4>.
- [112] N. Guyette, L. Williams, M.-T. Tran, T. Than, J. Bradley, L. Kehinde, C. Edwards, M. Beasley, R. Fullard, Comparison of Low-Abundance Biomarker Levels in Capillary-Collected Nonstimulated Tears and Washout Tears of Aqueous-Deficient and Normal Patients, *Invest. Ophthalmol. Vis. Sci*. 54 (2013) 3729–3737. <https://doi.org/10/f44zb8>.
- [113] D. Huang, N. Xu, Y. Song, P. Wang, H. Yang, Inflammatory cytokine profiles in the tears of thyroid-associated ophthalmopathy, *Graefes Arch Clin Exp Ophthalmol*. 250 (2012) 619–625. <https://doi.org/10/ftjjnp>.
- [114] D. Huang, Q. Luo, H. Yang, Y. Mao, Changes of Lacrimal Gland and Tear Inflammatory Cytokines in Thyroid-Associated Ophthalmopathy, *Investigative Ophthalmology & Visual Science*. 55 (2014) 4935–4943. <https://doi.org/10/f6k72v>.
- [115] M.L. Massingale, X. Li, M. Vallabhajosyula, D. Chen, Y. Wei, P.A. Asbell, Analysis of Inflammatory Cytokines in the Tears of Dry Eye Patients, *Cornea*. 28 (2009) 1023–1027. <https://doi.org/10/dpscj3>.

- [116] J.F. Meadows, K. Dionne, K.K. Nichols, Differential Profiling of T-Cell Cytokines as Measured by Protein Microarray Across Dry Eye Subgroups, *Cornea*. 35 (2016) 329–335. <https://doi.org/10/f8c5n9>.
- [117] K.-S. Na, J.-W. Mok, J.Y. Kim, C.R. Rho, C.-K. Joo, Correlations between Tear Cytokines, Chemokines, and Soluble Receptors and Clinical Severity of Dry Eye Disease, *Invest. Ophthalmol. Vis. Sci.* 53 (2012) 5443–5450. <https://doi.org/10/gg79mx>.
- [118] E. Kishazi, M. Dor, S. Eperon, A. Oberic, N. Turck, M. Hamedani, Differential profiling of lacrimal cytokines in patients suffering from thyroid-associated orbitopathy, *Scientific Reports*. 8 (2018) 10792. <https://doi.org/10/gdztd5>.
- [119] K.-C. Yoon, I.-Y. Jeong, Y.-G. Park, S.-Y. Yang, Interleukin-6 and Tumor Necrosis Factor- α Levels in Tears of Patients With Dry Eye Syndrome, *Cornea*. 26 (2007) 431–437. <https://doi.org/10/b643x3>.
- [120] Y. Nakamura, D.C. Sotozono, S. Kinoshita, Inflammatory cytokines in normal human tears, *Current Eye Research*. 17 (1998) 673–676. <https://doi.org/10/d7gtn>.
- [121] J.-F. Huang, Y. Zhang, K.D. Rittenhouse, E.H. Pickering, M.T. McDowell, Evaluations of Tear Protein Markers in Dry Eye Disease: Repeatability of Measurement and Correlation with Disease, *Investigative Ophthalmology & Visual Science*. 53 (2012) 4556–4564. <https://doi.org/10/gg79nt>.
- [122] W. Choi, Z. Li, H.-J. Oh, S.-K. Im, S.-H. Lee, S.-H. Park, I.-C. You, K.-C. Yoon, Expression of CCR5 and Its Ligands CCL3, -4, and -5 in the Tear Film and Ocular Surface of Patients with Dry Eye Disease, *Current Eye Research*. 37 (2012) 12–17. <https://doi.org/10/gg79nw>.
- [123] K.-C. Yoon, C.-S. Park, I.-C. You, H.-J. Choi, K.-H. Lee, S.-K. Im, H.-Y. Park, S.C. Pflugfelder, Expression of CXCL9, -10, -11, and CXCR3 in the Tear Film and Ocular Surface of Patients with Dry Eye Syndrome, *Invest. Ophthalmol. Vis. Sci.* 51 (2010) 643–650. <https://doi.org/10/cbw8fr>.

- [124] G.A. de Souza, L.M. de Godoy, M. Mann, Identification of 491 proteins in the tear fluid proteome reveals a large number of proteases and protease inhibitors, *Genome Biol.* 7 (2006) R72. <https://doi.org/10/drkq6s>.
- [125] S. Funke, D. Azimi, D. Wolters, F.H. Grus, N. Pfeiffer, Longitudinal analysis of taurine induced effects on the tear proteome of contact lens wearers and dry eye patients using a RP-RP-Capillary-HPLC–MALDI TOF/TOF MS approach, *Journal of Proteomics.* 75 (2012) 3177–3190. <https://doi.org/10/f33rj8>.
- [126] F.-H. Grus, A.J. Augustin, High Performance Liquid Chromatography Analysis of Tear Protein Patterns in Diabetic and Non-Diabetic Dry-Eye Patients, *European Journal of Ophthalmology.* 11 (2001) 19–24. <https://doi.org/10/gg785c>.
- [127] S. Herber, F.H. Grus, P. Sabuncuo, A.J. Augustin, Two-dimensional analysis of tear protein patterns of diabetic patients, *ELECTROPHORESIS.* 22 (2001) 1838–1844. <https://doi.org/10/b95f7p>.
- [128] L. Zhou, R.W. Beuerman, Tear analysis in ocular surface diseases, *Progress in Retinal and Eye Research.* 31 (2012) 527–550. <https://doi.org/10/f4fnsg>.
- [129] F.H. Grus, B. Dick, A.J. Augustin, N. Pfeiffer, Analysis of the Antibody Repertoire in Tears of Dry-Eye Patients, *OPH.* 215 (2001) 430–434. <https://doi.org/10/b2kfjc>.
- [130] F.H. Grus, P. Sabuncuo, A.J. Augustin, Analysis of tear protein patterns of dry-eye patients using fluorescent staining dyes and two-dimensional quantification algorithms, *ELECTROPHORESIS.* 22 (2001) 1845–1850. <https://doi.org/10/bb7x83>.
- [131] F.H. Grus, S.C. Joachim, N. Pfeiffer, Proteomics in ocular fluids, *PROTEOMICS – Clinical Applications.* 1 (2007) 876–888. <https://doi.org/10/ckwskk>.

- [132] F.H. Grus, P. Sabuncuo, H.B. Dick, A.J. Augustin, N. Pfeiffer, Changes in the tear proteins of diabetic patients, *BMC Ophthalmol.* 2 (2002) 4. <https://doi.org/10/fqvtpv>.
- [133] S. Herber, F.H. Grus, P. Sabuncuo, A.J. Augustin, Changes in the Tear Protein Patterns of Diabetic Patients Using Two-Dimensional Electrophoresis, in: D.A. Sullivan, M.E. Stern, K. Tsubota, D.A. Dartt, R.M. Sullivan, B.B. Bromberg (Eds.), *Lacrimal Gland, Tear Film, and Dry Eye Syndromes 3: Basic Science and Clinical Relevance Part A and B*, Springer US, Boston, MA, 2002: pp. 623–626. https://doi.org/10.1007/978-1-4615-0717-8_88.
- [134] P.T. Janssen, O.P. Van Bijsterveld, Comparison of electrophoretic techniques for the analysis of human tear fluid proteins, *Clinica Chimica Acta.* 114 (1981) 207–218. <https://doi.org/10/d4m7rk>.
- [135] C. Reitz, W. Breipohl, A. Augustin, J. Bours, Analysis of tear proteins by one- and two-dimensional thin-layer isoelectric focusing, sodium dodecyl sulfate electrophoresis and lectin blotting. Detection of a new component: cystatin C, *Graefe's Arch Clin Exp Ophthalmol.* 236 (1998) 894–899. <https://doi.org/10/dg6643>.
- [136] F.H. Grus, A.J. Augustin, N.G. Evangelou, K. Toth-Sagi, Analysis of Tear-Protein Patterns as a Diagnostic Tool for the Detection of Dry Eyes, *European Journal of Ophthalmology.* 8 (1998) 90–97. <https://doi.org/10/gg786k>.
- [137] F.-H. Grus, A.J. Augustin, Analysis of tear protein patterns by a neural network as a diagnostical tool for the detection of dry eyes, *ELECTROPHORESIS.* 20 (1999) 875–880. <https://doi.org/10/ft8bcm>.
- [138] M.P. Molloy, S. Bolis, B.R. Herbert, K. Ou, M.I. Tyler, D.D. van Dyk, M.D.P. Willcox, A.A. Gooley, K.L. Williams, C.A. Morris, B.J. Walsh, Establishment of the human reflex tear two-dimensional polyacrylamide gel electrophoresis reference map: New proteins of potential diagnostic value, *ELECTROPHORESIS.* 18 (1997) 2811–2815. <https://doi.org/10/dkijnvt>.

- [139] B.-S. Koo, D.-Y. Lee, H.-S. Ha, J.-C. Kim, C.-W. Kim, Comparative Analysis of the Tear Protein Expression in Blepharitis Patients Using Two-Dimensional Electrophoresis, *J. Proteome Res.* 4 (2005) 719–724. <https://doi.org/10/fbn54k>.
- [140] J.Y.M.N. Engwegen, M.-C.W. Gast, J.H.M. Schellens, J.H. Beijnen, Clinical proteomics: searching for better tumour markers with SELDI-TOF mass spectrometry, *Trends in Pharmacological Sciences.* 27 (2006) 251–259. <https://doi.org/10.1016/j.tips.2006.03.003>.
- [141] A. Barmada, S.A. Shippy, Thread-based assay for quantitative small molecule analysis of mice tear fluid by capillary electrophoresis, *Anal Bioanal Chem.* 411 (2019) 329–338. <https://doi.org/10/gg87cj>.
- [142] R.J. Fullard, Identification of proteins in small tear volumes with and without size exclusion HPLC fractionation, *Current Eye Research.* 7 (1988) 163–179. <https://doi.org/10/bjcjmn>.
- [143] G. Baier, G. Wollensak, E. Mur, B. Redl, G. Stöffler, W. Göttinger, Analysis of human tear proteins by different high-performance liquid chromatographic techniques, *Journal of Chromatography B: Biomedical Sciences and Applications.* 525 (1990) 319–328. <https://doi.org/10/cdxx2n>.
- [144] L. Zhou, S.Z. Zhao, S.K. Koh, L. Chen, C. Vaz, V. Tanavde, X.R. Li, R.W. Beuerman, In-depth analysis of the human tear proteome, *Journal of Proteomics.* 75 (2012) 3877–3885. <https://doi.org/10/gg7849>.
- [145] R. Dams, M.A. Huestis, W.E. Lambert, C.M. Murphy, Matrix effect in bioanalysis of illicit drugs with LC-MS/MS: Influence of ionization type, sample preparation, and biofluid, *J Am Soc Mass Spectrom.* 14 (2003) 1290–1294. <https://doi.org/10/fh2rz3>.
- [146] E. Peré-Trepat, S. Lacorte, R. Tauler, Solving liquid chromatography mass spectrometry coelution problems in the analysis of environmental samples by multivariate curve resolution, *Journal of Chromatography A.* 1096 (2005) 111–122. <https://doi.org/10/btpnq7>.

- [147] D. Sviridov, B. Meilinger, S.K. Drake, G.T. Hoehn, G.L. Hortin, Coelution of Other Proteins with Albumin during Size-Exclusion HPLC: Implications for Analysis of Urinary Albumin, *Clin Chem.* 52 (2006) 389–397. <https://doi.org/10/cv6smm>.
- [148] C. Eule, S. Jurk, N. Boehm, F. Grus, Tear Protein Pattern Detected via MALDI-TOF in Healthy Dogs and in Dogs With Keratoconjunctivitis Sicca (KCS), *Invest. Ophthalmol. Vis. Sci.* 50 (2009) 2607–2607.
- [149] F.H. Grus, N. Boehm, S. Berneiser, J. Lamparter, M. Wiegand, N. Wiegel, N. Pfeiffer, Analysis of Tear Protein Profiles in Dry-Eye Patients by Mass Spectrometry, *Investigative Ophthalmology & Visual Science.* 50 (2009) 2546–2546.
- [150] A. Lebrecht, D. Boehm, M. Schmidt, H. Koelbl, F.H. Grus, Surface-enhanced Laser Desorption/Ionisation Time-of-flight Mass Spectrometry to Detect Breast Cancer Markers in Tears and Serum, *Cancer Genomics Proteomics.* 6 (2009) 75–83.
- [151] U.J.E. Thiel, R. Feltens, B. Adryan, R. Gieringer, C. Brochhausen, R. Schuon, T. Fillies, F. Grus, W.J. Mann, J. Brieger, Analysis of differentially expressed proteins in oral squamous cell carcinoma by MALDI-TOF MS, *Journal of Oral Pathology & Medicine.* 40 (2011) 369–379. <https://doi.org/10/dnf6wx>.
- [152] B. Lu, A. Motoyama, C. Ruse, J. Venable, J.R. Yates, Improving Protein Identification Sensitivity by Combining MS and MS/MS Information for Shotgun Proteomics Using LTQ-Orbitrap High Mass Accuracy Data, *Anal. Chem.* 80 (2008) 2018–2025. <https://doi.org/10/chn7pd>.
- [153] A. Makarov, E. Denisov, A. Kholomeev, W. Balschun, O. Lange, K. Strupat, S. Horning, Performance Evaluation of a Hybrid Linear Ion Trap/Orbitrap Mass Spectrometer, *Anal. Chem.* 78 (2006) 2113–2120. <https://doi.org/10/bww2vp>.
- [154] J.R. Yates, D. Cociorva, L. Liao, V. Zabrouskov, Performance of a Linear Ion Trap-Orbitrap Hybrid for Peptide Analysis, *Anal. Chem.* 78 (2006) 493–500. <https://doi.org/10/b9bvmw>.

- [155] S. Hu, J.A. Loo, D.T. Wong, Human body fluid proteome analysis, *PROTEOMICS*. 6 (2006) 6326–6353. <https://doi.org/10/c5x387>.
- [156] J.D. Wulfschle, C.P. Paweletz, P.S. Steeg, E.F. Petricoin, L. Liotta, Proteomic Approaches to the Diagnosis, Treatment, and Monitoring of Cancer, in: A. Llombart-Bosch, V. Felipo (Eds.), *New Trends in Cancer for the 21st Century: Proceedings of the International Symposium on Cancer: New Trends in Cancer for the 21st Century, Held November 10–13, 2002, in Valencia, Spain, Springer US, Boston, MA, 2003*: pp. 59–68. https://doi.org/10.1007/978-1-4615-0081-0_7.
- [157] N. Boehm, D. Wolters, U. Thiel, U. Lossbrand, N. Wiegel, N. Pfeiffer, F.H. Grus, New insights into autoantibody profiles from immune privileged sites in the eye: A glaucoma study, *Brain, Behavior, and Immunity*. 26 (2012) 96–102. <https://doi.org/10/d96nm9>.
- [158] S. Horn, A. Lueking, D. Murphy, A. Staudt, C. Gutjahr, K. Schulte, A. König, M. Landsberger, H. Lehrach, S.B. Felix, D.J. Cahill, Profiling humoral autoimmune repertoire of dilated cardiomyopathy (DCM) patients and development of a disease-associated protein chip, *PROTEOMICS*. 6 (2006) 605–613. <https://doi.org/10.1002/pmic.200401293>.
- [159] W.H. Robinson, C. DiGennaro, W. Hueber, B.B. Haab, M. Kamachi, E.J. Dean, S. Fournel, D. Fong, M.C. Genovese, H.E.N. De Vegvar, K. Skriner, D.L. Hirschberg, R.I. Morris, S. Muller, G.J. Pruijn, W.J. van Venrooij, J.S. Smolen, P.O. Brown, L. Steinman, P.J. Utz, Autoantigen microarrays for multiplex characterization of autoantibody responses, *Nature Medicine*. 8 (2002) 295–301. <https://doi.org/10/ctn2j6>.
- [160] P.K. Coyle, P.A. Sibony, Tear immunoglobulins measured by ELISA., *Invest. Ophthalmol. Vis. Sci*. 27 (1986) 622–625.
- [161] C. Garcher, A. Bron, C. Baudouin, L. Bildstein, J. Bara, CA 19-9 ELISA test: a new method for studying mucus changes in tears, *British Journal of Ophthalmology*. 82 (1998) 88–90. <https://doi.org/10.1136/bjo.82.1.88>.

- [162] N.S. Sharma, S.K. Acharya, A.P. Nair, J. Matalia, R. Shetty, A. Ghosh, S. Sethu, Dopamine levels in human tear fluid, *Indian J Ophthalmol.* 67 (2019) 38–41. <https://doi.org/10/gg869v>.
- [163] P. Chhadva, T. Lee, C.D. Sarantopoulos, A.S. Hackam, A.L. McClellan, E.R. Felix, R.C. Levitt, A. Galor, Human Tear Serotonin Levels Correlate with Symptoms and Signs of Dry Eye, *Ophthalmology.* 122 (2015) 1675–1680. <https://doi.org/10/f3hztf>.
- [164] J. Heikenfeld, A. Jajack, J. Rogers, P. Gutruf, L. Tian, T. Pan, R. Li, M. Khine, J. Kim, J. Wang, J. Kim, Wearable Sensors: Modalities, Challenges, and Prospects, *Lab Chip.* 18 (2018) 217–248. <https://doi.org/10/gg7p44>.
- [165] R.C. Tseng, C.-C. Chen, S.-M. Hsu, H.-S. Chuang, Contact-Lens Biosensors, *Sensors (Basel).* 18 (2018). <https://doi.org/10/gg865m>.
- [166] W. March, D. Lazzaro, S. Rastogi, Fluorescent Measurement in the Non-Invasive Contact Lens Glucose Sensor, *Diabetes Technology & Therapeutics.* 8 (2006) 312–317. <https://doi.org/10/bdzcq4>.
- [167] R. Badugu, B.H. Jeng, E.A. Reece, J.R. Lakowicz, Contact lens to measure individual ion concentrations in tears and applications to dry eye disease, *Analytical Biochemistry.* 542 (2018) 84–94. <https://doi.org/10/gc6rph>.
- [168] R. Badugu, J.R. Lakowicz, C.D. Geddes, A Glucose Sensing Contact Lens: A Non-Invasive Technique for Continuous Physiological Glucose Monitoring, *Journal of Fluorescence.* 13 (2003) 371–374. <https://doi.org/10/ddj4ck>.
- [169] R. Badugu, J.R. Lakowicz, C.D. Geddes, Ophthalmic Glucose Monitoring Using Disposable Contact Lenses—A Review, *Journal of Fluorescence.* 14 (2004) 617–633. <https://doi.org/10/d3tz6n>.
- [170] R. Badugu, J.R. Lakowicz, C.D. Geddes, Noninvasive Continuous Monitoring of Physiological Glucose Using a Monosaccharide-Sensing Contact Lens, *Anal. Chem.* 76 (2004) 610–618. <https://doi.org/10/bz69wd>.

- [171] R. Badugu, J.R. Lakowicz, C.D. Geddes, A glucose-sensing contact lens: from bench top to patient, *Current Opinion in Biotechnology*. 16 (2005) 100–107. <https://doi.org/10/dsttp8>.
- [172] A. Domschke, S. Kabilan, R. Anand, M. Caines, D. Fetter, P. Griffith, K. James, N. Karangu, D. Smith, M. Vargas, J. Zeng, A. Hussain, Xiaoping Yang, J. Blyth, A. Mueller, P. Herbrechtsmeier, C. R. Lowe, Holographic sensors in contact lenses for minimally-invasive glucose measurements, in: *SENSORS, 2004 IEEE, 2004*: pp. 1320–1323 vol.3. <https://doi.org/10/dwbrcj>.
- [173] A. Domschke, S. Kabilan, R. Anand, M. Caines, D. Fetter, P. Griffith, K. James, N. Karangu, D. Smith, M. Vargas, J. Zeng, A. Hussain, Xiaoping Yang, J. Blyth, A. Mueller, P. Herbrechtsmeier, C.R. Lowe, Holographic sensors in contact lenses for minimally-invasive glucose measurements, in: *2004 IEEE SENSORS, 2004*: pp. 1320–1323 vol.3. <https://doi.org/10/dwbrcj>.
- [174] A.M. Horgan, A.J. Marshall, S.J. Kew, K.E.S. Dean, C.D. Creasey, S. Kabilan, Crosslinking of phenylboronic acid receptors as a means of glucose selective holographic detection, *Biosensors and Bioelectronics*. 21 (2006) 1838–1845. <https://doi.org/10/dc4xwd>.
- [175] X. Yang, X. Pan, J. Blyth, C.R. Lowe, Towards the real-time monitoring of glucose in tear fluid: Holographic glucose sensors with reduced interference from lactate and pH, *Biosensors and Bioelectronics*. 23 (2008) 899–905. <https://doi.org/10/bgk2w5>.
- [176] Y. Hu, X. Jiang, L. Zhang, J. Fan, W. Wu, Construction of near-infrared photonic crystal glucose-sensing materials for ratiometric sensing of glucose in tears, *Biosensors and Bioelectronics*. 48 (2013) 94–99. <https://doi.org/10/gg8652>.
- [177] J.-L. Ruan, C. Chen, J.-H. Shen, X.-L. Zhao, S.-H. Qian, Z.-G. Zhu, A Gelated Colloidal Crystal Attached Lens for Noninvasive Continuous Monitoring of Tear Glucose, *Polymers*. 9 (2017) 125. <https://doi.org/10/f99ckh>.

- [178] C. Zhang, G.G. Cano, P.V. Braun, Linear and Fast Hydrogel Glucose Sensor Materials Enabled by Volume Resetting Agents, *Advanced Materials*. 26 (2014) 5678–5683. <https://doi.org/10/f2s4p7>.
- [179] M. Ben-Moshe, V.L. Alexeev, S.A. Asher, Fast Responsive Crystalline Colloidal Array Photonic Crystal Glucose Sensors, *Anal. Chem.* 78 (2006) 5149–5157. <https://doi.org/10/dz5vqn>.
- [180] S. Kabilan, A.J. Marshall, F.K. Sartain, M.-C. Lee, A. Hussain, X. Yang, J. Blyth, N. Karangu, K. James, J. Zeng, D. Smith, A. Domschke, C.R. Lowe, Holographic glucose sensors, *Biosensors and Bioelectronics*. 20 (2005) 1602–1610. <https://doi.org/10/fqh6s6>.
- [181] J. Kim, M. Kim, M.-S. Lee, K. Kim, S. Ji, Y.-T. Kim, J. Park, K. Na, K.-H. Bae, H. Kyun Kim, F. Bien, C. Young Lee, J.-U. Park, Wearable smart sensor systems integrated on soft contact lenses for wireless ocular diagnostics, *Nature Communications*. 8 (2017) 14997. <https://doi.org/10/f94xhv>.
- [182] H. Yao, Y. Liao, A.R. Lingley, A. Afanasiev, I. Lähdesmäki, B.P. Otis, B.A. Parviz, A contact lens with integrated telecommunication circuit and sensors for wireless and continuous tear glucose monitoring, *J. Micromech. Microeng.* 22 (2012) 075007. <https://doi.org/10/gg8655>.
- [183] K. Mitsubayashi, T. Arakawa, Cavitas Sensors: Contact Lens Type Sensors & Mouthguard Sensors, *Electroanalysis*. 28 (2016) 1170–1187. <https://doi.org/10/f3mtwr>.
- [184] N. Thomas, I. Lähdesmäki, B.A. Parviz, A contact lens with an integrated lactate sensor, *Sensors and Actuators B: Chemical*. 162 (2012) 128–134. <https://doi.org/10.1016/j.snb.2011.12.049>.
- [185] S. Azzi-Achkouty, N. Estephan, N. Ouaini, D.N. Rutledge, Headspace solid-phase microextraction for wine volatile analysis, *Critical Reviews in Food Science and Nutrition*. 57 (2017) 2009–2020. <https://doi.org/10/gdk2n7>.

- [186] B. Bojko, N. Reyes-Garcés, V. Bessonneau, K. Goryński, F. Mousavi, E.A. Souza Silva, J. Pawliszyn, Solid-phase microextraction in metabolomics, *TrAC Trends in Analytical Chemistry*. 61 (2014) 168–180. <https://doi.org/10/f6mmv2>.
- [187] H. Kataoka, A. Ishizaki, K. Saito, Recent progress in solid-phase microextraction and its pharmaceutical and biomedical applications, *Analytical Methods*. 8 (2016) 5773–5788. <https://doi.org/10.1039/C6AY00380J>.
- [188] B. Kenessov, J.A. Koziel, N.V. Bakaikina, D. Orazbayeva, Perspectives and challenges of on-site quantification of organic pollutants in soils using solid-phase microextraction, *TrAC Trends in Analytical Chemistry*. 85 (2016) 111–122. <https://doi.org/10/f9jgb6>.
- [189] H. Piri-Moghadam, F. Ahmadi, J. Pawliszyn, A critical review of solid phase microextraction for analysis of water samples, *TrAC Trends in Analytical Chemistry*. 85 (2016) 133–143. <https://doi.org/10/f9jdsu>.
- [190] C.-H. Xu, G.-S. Chen, Z.-H. Xiong, Y.-X. Fan, X.-C. Wang, Y. Liu, Applications of solid-phase microextraction in food analysis, *TrAC Trends in Analytical Chemistry*. 80 (2016) 12–29. <https://doi.org/10/gg79n7>.
- [191] J. Xu, G. Chen, S. Huang, J. Qiu, R. Jiang, F. Zhu, G. Ouyang, Application of in vivo solid-phase microextraction in environmental analysis, *TrAC Trends in Analytical Chemistry*. 85 (2016) 26–35. <https://doi.org/10/f9jgkg>.
- [192] Q. Zhang, L. Zhou, H. Chen, C.-Z. Wang, Z. Xia, C.-S. Yuan, Solid-phase microextraction technology for in vitro and in vivo metabolite analysis, *Trends Analyt Chem*. 80 (2016) 57–65. <https://doi.org/10.1016/j.trac.2016.02.017>.
- [193] J. Pawliszyn, *Handbook of solid phase microextraction*, Elsevier, Chennai; Oxford, 2012.

- [194] R.P. Belardi, J.B. Pawliszyn, The Application of Chemically Modified Fused Silica Fibers in the Extraction of Organics from Water Matrix Samples and their Rapid Transfer to Capillary Columns, *Water Quality Research Journal*. 24 (1989) 179–191. <https://doi.org/10/gg87j9>.
- [195] E. Boyacı, Á. Rodríguez-Lafuente, K. Gorynski, F. Mirnaghi, É.A. Souza-Silva, D. Hein, J. Pawliszyn, Sample preparation with solid phase microextraction and exhaustive extraction approaches: Comparison for challenging cases, *Analytica Chimica Acta*. 873 (2015) 14–30. <https://doi.org/10/f7hsm9>.
- [196] A. Amiri, Solid-phase microextraction-based sol–gel technique, *TrAC Trends in Analytical Chemistry*. 75 (2016) 57–74. <https://doi.org/10/gg79pg>.
- [197] M. Fernández-Amado, M.C. Prieto-Blanco, P. López-Mahía, S. Muniategui-Lorenzo, D. Prada-Rodríguez, Strengths and weaknesses of in-tube solid-phase microextraction: A scoping review, *Analytica Chimica Acta*. 906 (2016) 41–57. <https://doi.org/10/f76npm>.
- [198] F. Ghaemi, A. Amiri, R. Yunus, Methods for coating solid-phase microextraction fibers with carbon nanotubes, *TrAC Trends in Analytical Chemistry*. 59 (2014) 133–143. <https://doi.org/10/gg79pt>.
- [199] A. Mehdinia, M.O. Aziz-Zanjani, Advances for sensitive, rapid and selective extraction in different configurations of solid-phase microextraction, *TrAC Trends in Analytical Chemistry*. 51 (2013) 13–22. <https://doi.org/10/f5mbrg>.
- [200] H. Piri-Moghadam, Md.N. Alam, J. Pawliszyn, Review of geometries and coating materials in solid phase microextraction: Opportunities, limitations, and future perspectives, *Analytica Chimica Acta*. 984 (2017) 42–65. <https://doi.org/10/ggnrh6>.
- [201] P. Rocío-Bautista, I. Pacheco-Fernández, J. Pasán, V. Pino, Are metal-organic frameworks able to provide a new generation of solid-phase microextraction coatings? – A review, *Analytica Chimica Acta*. 939 (2016) 26–41. <https://doi.org/10/f87f75>.

- [202] P. Suwannakot, F. Lisi, E. Ahmed, K. Liang, R. Babarao, J.J. Gooding, W.A. Donald, Metal–Organic Framework-Enhanced Solid-Phase Microextraction Mass Spectrometry for the Direct and Rapid Detection of Perfluorooctanoic Acid in Environmental Water Samples, *Anal. Chem.* 92 (2020) 6900–6908. <https://doi.org/10/gg79pm>.
- [203] N. Reyes-Garcés, E. Gionfriddo, G.A. Gómez-Ríos, Md.N. Alam, E. Boyacı, B. Bojko, V. Singh, J. Grandy, J. Pawliszyn, Advances in Solid Phase Microextraction and Perspective on Future Directions, *Analytical Chemistry*. 90 (2018) 302–360. <https://doi.org/10.1021/acs.analchem.7b04502>.
- [204] V. Bessonneau, E. Boyacı, M. Maciazek-Jurczyk, J. Pawliszyn, In vivo solid phase microextraction sampling of human saliva for non-invasive and on-site monitoring, *Analytica Chimica Acta*. 856 (2015) 35–45. <https://doi.org/10.1016/j.aca.2014.11.029>.
- [205] A.A. Nalbant, E. Boyacı, Advancements in Non-Invasive Biological Surface Sampling and Emerging Applications, *Separations*. 6 (2019) 52. <https://doi.org/10/ggcdr4>.
- [206] R. Jiang, J. Pawliszyn, Thin-film microextraction offers another geometry for solid-phase microextraction, *TrAC Trends in Analytical Chemistry*. 39 (2012) 245–253. <https://doi.org/10.1016/j.trac.2012.07.005>.
- [207] I. Bruheim, X. Liu, J. Pawliszyn, Thin-Film Microextraction, *Anal. Chem.* 75 (2003) 1002–1010. <https://doi.org/10/brsd6j>.
- [208] M.L. Musteata, F.M. Musteata, J. Pawliszyn, Biocompatible Solid-Phase Microextraction Coatings Based on Polyacrylonitrile and Solid-Phase Extraction Phases, *Anal. Chem.* 79 (2007) 6903–6911. <https://doi.org/10/d8p2s9>.
- [209] F.S. Mirnaghi, Y. Chen, L.M. Sidisky, J. Pawliszyn, Optimization of the Coating Procedure for a High-Throughput 96-Blade Solid Phase Microextraction System Coupled with LC–MS/MS for Analysis of Complex Samples, *Anal. Chem.* 83 (2011) 6018–6025. <https://doi.org/10/cd6d8w>.

- [210] G.A. Gómez-Ríos, C. Liu, M. Tascon, N. Reyes-Garcés, D.W. Arnold, T.R. Covey, J. Pawliszyn, Open Port Probe Sampling Interface for the Direct Coupling of Biocompatible Solid-Phase Microextraction to Atmospheric Pressure Ionization Mass Spectrometry, *Anal. Chem.* 89 (2017) 3805–3809. <https://doi.org/10/f9qxhh>.
- [211] M. Tascon, G.A. Gómez-Ríos, N. Reyes-Garcés, J. Poole, E. Boyacı, J. Pawliszyn, High-Throughput Screening and Quantitation of Target Compounds in Biofluids by Coated Blade Spray-Mass Spectrometry, *Analytical Chemistry*. 89 (2017) 8421–8428. <https://doi.org/10.1021/acs.analchem.7b01877>.
- [212] S. Ahmad, M. Tucker, N. Spooner, D. Murnane, U. Gerhard, Direct Ionization of Solid-Phase Microextraction Fibers for Quantitative Drug Bioanalysis: From Peripheral Circulation to Mass Spectrometry Detection, *Anal. Chem.* 87 (2015) 754–759. <https://doi.org/10/f6xx9j>.
- [213] G.A. Gómez-Ríos, N. Reyes-Garcés, B. Bojko, J. Pawliszyn, Biocompatible Solid-Phase Microextraction Nanoelectrospray Ionization: An Unexploited Tool in Bioanalysis, *Anal. Chem.* 88 (2016) 1259–1265. <https://doi.org/10/f86fqr>.
- [214] D. Garwolińska, W. Hewelt-Belka, J. Namieśnik, A. Kot-Wasik, Rapid Characterization of the Human Breast Milk Lipidome Using a Solid-Phase Microextraction and Liquid Chromatography–Mass Spectrometry-Based Approach, *J. Proteome Res.* 16 (2017) 3200–3208. <https://doi.org/10/gbqvqx>.
- [215] S. Risticevic, E.A. Souza-Silva, J.R. DeEll, J. Cochran, J. Pawliszyn, Capturing Plant Metabolome with Direct-Immersion in Vivo Solid Phase Microextraction of Plant Tissues, *Anal. Chem.* 88 (2016) 1266–1274. <https://doi.org/10/f86gzs>.
- [216] J. Alberdi-Cedeño, M.L. Ibargoitia, G. Cristillo, P. Sopolana, M.D. Guillén, A new methodology capable of characterizing most volatile and less volatile minor edible oils components in a single chromatographic run without solvents or reagents. Detection of new components, *Food Chemistry*. 221 (2017) 1135–1144. <https://doi.org/10/gg7vw4>.

- [217] P.F. de Lima, M.F. Furlan, F.A. de L. Ribeiro, S.F. Pascholati, F. Augusto, In vivo determination of the volatile metabolites of saprotroph fungi by comprehensive two-dimensional gas chromatography, *Journal of Separation Science*. 38 (2015) 1924–1932. <https://doi.org/10/f27pnq>.
- [218] É.A. Souza-Silva, J. Pawliszyn, Direct Immersion Solid-Phase Microextraction with Matrix-Compatible Fiber Coating for Multiresidue Pesticide Analysis of Grapes by Gas Chromatography–Time-of-Flight Mass Spectrometry (DI-SPME-GC-ToFMS), *J. Agric. Food Chem.* 63 (2015) 4464–4477. <https://doi.org/10/f7c92k>.
- [219] S. De Grazia, E. Gionfriddo, J. Pawliszyn, A new and efficient Solid Phase Microextraction approach for analysis of high fat content food samples using a matrix-compatible coating, *Talanta*. 167 (2017) 754–760. <https://doi.org/10.1016/j.talanta.2017.01.064>.
- [220] G. de O. Silveira, S. Loddi, C.D.R. de Oliveira, A.D. Zucoloto, L.V.G. Fruchtengarten, M. Yonamine, Headspace solid-phase microextraction and gas chromatography–mass spectrometry for determination of cannabinoids in human breast milk, *Forensic Toxicol.* 35 (2017) 125–132. <https://doi.org/10.1007/s11419-016-0346-5>.
- [221] M.A. Andrade, F.M. Lanças, Determination of Ochratoxin A in wine by packed in-tube solid phase microextraction followed by high performance liquid chromatography coupled to tandem mass spectrometry, *Journal of Chromatography A*. 1493 (2017) 41–48. <https://doi.org/10/f9599s>.
- [222] A. Rodriguez-Lafuente, H. Piri-Moghadam, H.L. Lord, T. Obal, J. Pawliszyn, Inter-laboratory validation of automated SPME-GC/MS for determination of pesticides in surface and ground water samples: sensitive and green alternative to liquid–liquid extraction, *Water Quality Research Journal*. 51 (2016) 331–343. <https://doi.org/10/f9bqr6>.
- [223] R. Jiang, J. Pawliszyn, Preparation of a Particle-Loaded Membrane for Trace Gas Sampling, *Anal. Chem.* 86 (2014) 403–410. <https://doi.org/10/f5pxtr>.

- [224] J.J. Poole, J.J. Grandy, G.A. Gómez-Ríos, E. Gionfriddo, J. Pawliszyn, Solid Phase Microextraction On-Fiber Derivatization Using a Stable, Portable, and Reusable Pentafluorophenyl Hydrazine Standard Gas Generating Vial, *Anal. Chem.* 88 (2016) 6859–6866. <https://doi.org/10/f8v8bp>.
- [225] F. Ahmadi, C. Sparham, E. Boyacı, J. Pawliszyn, Time Weighted Average Concentration Monitoring Based on Thin Film Solid Phase Microextraction, *Environ. Sci. Technol.* 51 (2017) 3929–3937. <https://doi.org/10/f9vbk9>.
- [226] J.J. Poole, G.A. Gómez-Ríos, E. Boyacı, N. Reyes-Garcés, J. Pawliszyn, Rapid and Concomitant Analysis of Pharmaceuticals in Treated Wastewater by Coated Blade Spray Mass Spectrometry, *Environ. Sci. Technol.* 51 (2017) 12566–12572. <https://doi.org/10/gck29h>.
- [227] J.J. Grandy, E. Boyacı, J. Pawliszyn, Development of a Carbon Mesh Supported Thin Film Microextraction Membrane As a Means to Lower the Detection Limits of Benchtop and Portable GC/MS Instrumentation, *Anal. Chem.* 88 (2016) 1760–1767. <https://doi.org/10/f78zhf>.
- [228] G. Gómez-Ríos, N. Reyes-Garcés, B. Bojko, J. Pawliszyn, Biocompatible-Solid Phase Microextraction (Bio-SPME)-nano-electrospray ionization (nano-ESI): an unexploited tool in bioanalysis, *Analytical Chemistry*. 88 (2015). <https://doi.org/10/f86fqr>.
- [229] A. Antonucci, M. Vitali, P. Avino, M. Manigrasso, C. Protano, Sensitive multiresidue method by HS-SPME/GC-MS for 10 volatile organic compounds in urine matrix: a new tool for biomonitoring studies on children, *Anal Bioanal Chem.* 408 (2016) 5789–5800. <https://doi.org/10/gg7vw2>.
- [230] R.A. Simões, P.S. Bonato, F.S. Mirnaghi, B. Bojko, J. Pawliszyn, Bioanalytical method for in vitro metabolism study of repaglinide using 96-blade thin-film solid-phase microextraction and LC-MS/MS, *Bioanalysis*. 7 (2015) 65–77. <https://doi.org/10/gg7vww>.

- [231] F. Mousavi, E. Gionfriddo, E. Carasek, E.A. Souza-Silva, J. Pawliszyn, Coupling solid phase microextraction to complementary separation platforms for metabotyping of *E. coli* metabolome in response to natural antibacterial agents, *Metabolomics*. 12 (2016) 169. <https://doi.org/10/gg7vwz>.
- [232] F. Mousavi, B. Bojko, V. Bessonneau, J. Pawliszyn, Cinnamaldehyde Characterization as an Antibacterial Agent toward *E. coli* Metabolic Profile Using 96-Blade Solid-Phase Microextraction Coupled to Liquid Chromatography–Mass Spectrometry, *J. Proteome Res.* 15 (2016) 963–975. <https://doi.org/10/f8c47w>.
- [233] C.L. Silva, R. Perestrelo, P. Silva, H. Tomás, J.S. Câmara, Volatile metabolomic signature of human breast cancer cell lines, *Scientific Reports*. 7 (2017) 43969. <https://doi.org/10/f9s4q3>.
- [234] C. Wang, Y. Feng, M. Wang, X. Pi, H. Tong, Y. Wang, L. Zhu, E. Li, Volatile Organic Metabolites Identify Patients with Mesangial Proliferative Glomerulonephritis, IgA Nephropathy and Normal Controls, *Scientific Reports*. 5 (2015) 14744. <https://doi.org/10/f7tc6w>.
- [235] H.-P. Jiang, C.-B. Qi, J.-M. Chu, B.-F. Yuan, Y.-Q. Feng, Profiling of cis - Diol-containing Nucleosides and Ribosylated Metabolites by Boronate-affinity Organic-silica Hybrid Monolithic Capillary Liquid Chromatography/Mass Spectrometry, *Scientific Reports*. 5 (2015) 7785. <https://doi.org/10/f62stj>.
- [236] Penn Dustin J, Oberzaucher Elisabeth, Grammer Karl, Fischer Gottfried, Soini Helena A, Wiesler Donald, Novotny Milos V, Dixon Sarah J, Xu Yun, Brereton Richard G, Individual and gender fingerprints in human body odour, *Journal of The Royal Society Interface*. 4 (2007) 331–340. <https://doi.org/10/c9hmx4>.
- [237] P. Nemes, A. Vertes, Ambient mass spectrometry for in vivo local analysis and in situ molecular tissue imaging, *Trac-Trends Anal. Chem.* 34 (2012) 22–34. <https://doi.org/10/gf4n8x>.

- [238] L. Dormont, J.-M. Bessi re, A. Cohuet, Human Skin Volatiles: A Review, *Journal of Chemical Ecology*. 39 (2013) 569–578.
<https://doi.org/10.1007/s10886-013-0286-z>.
- [239] L. Andrisic, D. Dudzik, C. Barbas, L. Milkovic, T. Grune, N. Zarkovic, Short overview on metabolomics approach to study pathophysiology of oxidative stress in cancer, *Redox Biol*. 14 (2017) 47–58.
<https://doi.org/10/gf4n8z>.
- [240] A. Prada, K.G. Furton, 3.43 - Recent Advances in Solid-Phase Microextraction for Forensic Applications, in: J. Pawliszyn (Ed.), *Comprehensive Sampling and Sample Preparation*, Academic Press, Oxford, 2012: pp. 877–891. <https://doi.org/10.1016/B978-0-12-381373-2.00117-4>.
- [241] A.M. Curran, P.A. Prada, K.G. Furton, Canine human scent identifications with post-blast debris collected from improvised explosive devices, *Forensic Sci. Int*. 199 (2010) 103–108. <https://doi.org/10/fjpb4>.
- [242] L.E. DeGreeff, K.G. Furton, Collection and identification of human remains volatiles by non-contact, dynamic airflow sampling and SPME-GC/MS using various sorbent materials, *Anal Bioanal Chem*. 401 (2011) 1295–1307.
<https://doi.org/10/d3f884>.
- [243] C. Saudan, N. Baume, N. Robinson, L. Avois, P. Mangin, M. Saugy, Testosterone and doping control, *Br J Sports Med*. 40 (2006) i21–i24.
<https://doi.org/10/ff4t6c>.
- [244] H. Geyer, W. Sch nzer, M. Thevis, Anabolic agents: recent strategies for their detection and protection from inadvertent doping, *Br J Sports Med*. 48 (2014) 820–826. <https://doi.org/10/f5276s>.
- [245] X. Xu, C.P. Weisel, Dermal uptake of chloroform and haloketones during bathing, *J Expo Anal Environ Epidemiol*. 15 (2005) 289–296.
<https://doi.org/10/d533v8>.

- [246] V. Jiřík, O. Machaczka, H. Miturová, I. Tomášek, H. Šlachtová, J. Janoutová, H. Velická, V. Janout, Air Pollution and Potential Health Risk in Ostrava Region - a Review, *Cent. Eur. J. Public Health*. 24 Suppl (2016) S4–S17. <https://doi.org/10/gf4n9h>.
- [247] P. Vineis, M. Chadeau-Hyam, H. Gmuender, J. Gulliver, Z. Herceg, J. Kleinjans, M. Kogevinas, S. Kyrtopoulos, M. Nieuwenhuijsen, D.H. Phillips, N. Probst-Hensch, A. Scalbert, R. Vermeulen, C.P. Wild, The exposome in practice: Design of the EXPOsOMICS project, *Int J Hyg Environ Health*. 220 (2017) 142–151. <https://doi.org/10/f98fhg>.
- [248] S. Sisalli, A. Adao, M. Lebel, I. Fur, P. Sandra, Sorptive Tape Extraction – A Novel Sampling Method for the In Vivo Study of Skin, *LC GC Europe*. 19 (2006) 33–39.
- [249] S. Riazanskaia, G. Blackburn, M. Harker, D. Taylor, C.L.P. Thomas, The analytical utility of thermally desorbed polydimethylsilicone membranes for in-vivo sampling of volatile organic compounds in and on human skin, *Analyst*. 133 (2008) 1020–1027. <https://doi.org/10/dbmckj>.
- [250] A.N. Thomas, S. Riazanskaia, W. Cheung, Y. Xu, R. Goodacre, C.L.P. Thomas, M.S. Baguneid, A. Bayat, Novel noninvasive identification of biomarkers by analytical profiling of chronic wounds using volatile organic compounds, *Wound Repair Regen*. 18 (2010) 391–400. <https://doi.org/10/ck7ghq>.
- [251] R. Jiang, E. Cudjoe, B. Bojko, T. Abaffy, J. Pawliszyn, A non-invasive method for in vivo skin volatile compounds sampling, *Analytica Chimica Acta*. 804 (2013) 111–119. <https://doi.org/10.1016/j.aca.2013.09.056>.
- [252] M. Schivo, A.A. Aksenov, A. Pasamontes, R. Cumeras, S. Weisker, A.M. Oberbauer, C.E. Davis, A rabbit model for assessment of volatile metabolite changes observed from skin: a pressure ulcer case study, *Journal of Breath Research*. 11 (2017) 016007. <https://doi.org/10.1088/1752-7163/aa51d7>.

- [253] H.J. Martin, J.C. Reynolds, S. Riazanskaia, C.L.P. Thomas, High throughput volatile fatty acid skin metabolite profiling by thermal desorption secondary electrospray ionisation mass spectrometry, *The Analyst*. 139 (2014) 4279–4286. <https://doi.org/10.1039/C4AN00134F>.
- [254] H.J. Martin, M.A. Turner, S. Bandelow, L. Edwards, S. Riazanskaia, C.L.P. Thomas, Volatile organic compound markers of psychological stress in skin: a pilot study, *Journal of Breath Research*. 10 (2016) 046012. <https://doi.org/10.1088/1752-7155/10/4/046012>.
- [255] D. Stevens, R. Cornmell, D. Taylor, S.G. Grimshaw, S. Riazanskaia, D.S. Arnold, S.J. Fernstad, A.M. Smith, L.M. Heaney, J.C. Reynolds, C.L.P. Thomas, M. Harker, Spatial variations in the microbial community structure and diversity of the human foot is associated with the production of odorous volatiles, *FEMS Microbiol Ecol*. 91 (2015) 1–11. <https://doi.org/10/f68bsr>.
- [256] E.P. Dutkiewicz, J.-D. Lin, T.-W. Tseng, Y.-S. Wang, P.L. Urban, Hydrogel Micropatches for Sampling and Profiling Skin Metabolites, *Analytical Chemistry*. 86 (2014) 2337–2344. <https://doi.org/10.1021/ac4039338>.
- [257] E.P. Dutkiewicz, K.-T. Hsieh, Y.-S. Wang, H.-Y. Chiu, P.L. Urban, Hydrogel Micropatch and Mass Spectrometry-Assisted Screening for Psoriasis-Related Skin Metabolites, *Clinical Chemistry*. 62 (2016) 1120–1128. <https://doi.org/10.1373/clinchem.2016.256396>.
- [258] E.P. Dutkiewicz, H.-Y. Chiu, P.L. Urban, Micropatch-arrayed pads for non-invasive spatial and temporal profiling of topical drugs on skin surface: Skin analysis, *Journal of Mass Spectrometry*. 50 (2015) 1321–1325. <https://doi.org/10.1002/jms.3702>.
- [259] K.W. Ng, W.M. Lau, A.C. Williams, Towards pain-free diagnosis of skin diseases through multiplexed microneedles: biomarker extraction and detection using a highly sensitive blotting method, *Drug Delivery and Translational Research*. 5 (2015) 387–396. <https://doi.org/10/gf4hjd>.

- [260] E. Duffy, M.R. Jacobs, B. Kirby, A. Morrin, Probing skin physiology through the volatile footprint: Discriminating volatile emissions before and after acute barrier disruption, *Experimental Dermatology*. 26 (2017) 919–925. <https://doi.org/10.1111/exd.13344>.
- [261] E. Duffy, G. Albero, A. Morrin, Headspace Solid-Phase Microextraction Gas Chromatography-Mass Spectrometry Analysis of Scent Profiles from Human Skin, *Cosmetics*. 5 (2018) 62. <https://doi.org/10.3390/cosmetics5040062>.
- [262] S.G. O’Connell, L.D. Kincl, K.A. Anderson, Silicone Wristbands as Personal Passive Samplers, *Environ. Sci. Technol.* 48 (2014) 3327–3335. <https://doi.org/10/f5wv6h>.
- [263] M. Lira, C. Pereira, M.E.C.D.R. Oliveira, E.M.S. Castanheira, Importance of contact lens power and thickness in oxygen transmissibility, *Contact Lens and Anterior Eye*. 38 (2015) 120–126. <https://doi.org/10/f65pt8>.
- [264] H. Gross, F. Blechinger, B. Aichtner, H. Gross, *Survey of optical instruments*, Wiley-VCH, Weinheim, 2008.
- [265] C.S.A. Musgrave, F. Fang, Contact Lens Materials: A Materials Science Perspective, *Materials*. 12 (2019) 261. <https://doi.org/10.3390/ma12020261>.
- [266] P.-J. Wipff, H. Majd, C. Acharya, L. Buscemi, J.-J. Meister, B. Hinz, The covalent attachment of adhesion molecules to silicone membranes for cell stretching applications, *Biomaterials*. 30 (2009) 1781–1789. <https://doi.org/10.1016/j.biomaterials.2008.12.022>.
- [267] M.Y. Bee-DiGregorio, H. Feng, B.S. Pan, N.K. Dokoozlian, G.L. Sacks, Polymeric Sorbent Sheets Coupled to Direct Analysis in Real Time Mass Spectrometry for Trace-Level Volatile Analysis—A Multi-Vineyard Evaluation Study, *Foods*. 9 (2020) 409. <https://doi.org/10/gg6ztj>.
- [268] P. Serra-Mora, C. Rodríguez-Palma, J. Verdú-Andrés, R. Herráez-Hernández, P. Campíns-Falcó, Improving the On-Line Extraction of Polar Compounds by IT-SPME with Silica Nanoparticles Modified Phases, *Separations*. 5 (2018) 10. <https://doi.org/10/gg6ztq>.

- [269] E. Boyacı, N. Horzum, A. Çağır, M.M. Demir, A.E. Eroğlu, Electrospun amino-functionalized PDMS as a novel SPME sorbent for the speciation of inorganic and organometallic arsenic species, *RSC Advances*. 3 (2013) 22261. <https://doi.org/10.1039/c3ra43622e>.
- [270] E. Boyacı, A. Çağır, T. Shahwan, A.E. Eroğlu, Synthesis, characterization and application of a novel mercapto- and amine-bifunctionalized silica for speciation/sorption of inorganic arsenic prior to inductively coupled plasma mass spectrometric determination, *Talanta*. 85 (2011) 1517–1525. <https://doi.org/10.1016/j.talanta.2011.06.021>.
- [271] M. Bračić, T. Mohan, T. Griesser, K. Stana-Kleinschek, S. Strnad, L. Fras-Zemljič, One-Step Noncovalent Surface Functionalization of PDMS with Chitosan-Based Bioparticles and Their Protein-Repellent Properties, *Adv. Mater. Interfaces*. 4 (2017) 1700416. <https://doi.org/10.1002/admi.201700416>.
- [272] Y.J. Chuah, Y.T. Koh, K. Lim, N.V. Menon, Y. Wu, Y. Kang, Simple surface engineering of polydimethylsiloxane with polydopamine for stabilized mesenchymal stem cell adhesion and multipotency, *Sci Rep*. 5 (2016) 18162. <https://doi.org/10.1038/srep18162>.
- [273] P. Ferreira, Á. Carvalho, T.R. Correia, B.P. Antunes, I.J. Correia, P. Alves, Functionalization of polydimethylsiloxane membranes to be used in the production of voice prostheses, *Science and Technology of Advanced Materials*. 14 (2013) 055006. <https://doi.org/10.1088/1468-6996/14/5/055006>.
- [274] A. Kreider, K. Richter, S. Sell, M. Fenske, C. Tornow, V. Stenzel, I. Grunwald, Functionalization of PDMS modified and plasma activated two-component polyurethane coatings by surface attachment of enzymes, *Applied Surface Science*. 273 (2013) 562–569. <https://doi.org/10.1016/j.apsusc.2013.02.080>.
- [275] W. Liu, L. Zhang, S. Chen, H. Duan, X. Chen, Z. Wei, G. Chen, A method by homemade OH/TSO-PMHS fibre solid-phase microextraction coupling with gas chromatography–mass spectrometry for analysis of antiestrogens in biological matrices, *Analytica Chimica Acta*. 631 (2009) 47–53. <https://doi.org/10/c8jf7q>.

- [276] X.D. Liu, S. Tokura, M. Haruki, N. Nishi, N. Sakairi, Surface modification of nonporous glass beads with chitosan and their adsorption property for transition metal ions, *Carbohydrate Polymers*. (2002) 6.
- [277] J. Nourmohammadi, T. Hajibabaei, G. Amoabediny, S.H. Jafari, N. Salehi, Aminosilane Layer Formation Inside the PDMS Tubes Improves Wettability and Cytocompatibility of Human Endothelial Cells, (n.d.) 10.
- [278] M. Cesaria, V. Arima, S. Rella, C. Malitesta, M.G. Manera, R. Rella, PDMS treated with dichloromethane: swollen weight without underestimation due to the solvent volatility and thermal aging to reduce swelling and morphology damage, in: 19th Italian National Conference on Photonic Technologies (Fotonica 2017), Institution of Engineering and Technology, Padua, Italy, 2017: p. 46 (4 .)-46 (4 .). <https://doi.org/10/gg7j2x>.
- [279] M. Ahmed, H.A. Basheer, J.M. Ayuso, D. Ahmet, M. Mazzini, R. Patel, S.D. Shnyder, V. Vinader, K. Afarinkia, Agarose Spot as a Comparative Method for in situ Analysis of Simultaneous Chemotactic Responses to Multiple Chemokines, *Scientific Reports*. 7 (2017) 1075. <https://doi.org/10/f96gj9>.
- [280] F. Campos, A.B. Bonhome-Espinosa, J. Chato-Astrain, D. Sánchez-Porras, Ó.D. García-García, R. Carmona, M.T. López-López, M. Alaminos, V. Carriel, I.A. Rodriguez, Evaluation of Fibrin-Agarose Tissue-Like Hydrogels Biocompatibility for Tissue Engineering Applications, *Front. Bioeng. Biotechnol.* 8 (2020). <https://doi.org/10.3389/fbioe.2020.00596>.
- [281] C.-M. Phan, H. Walther, H. Gao, J. Rossy, L.N. Subbaraman, L. Jones, Development of an In Vitro Ocular Platform to Test Contact Lenses, *J Vis Exp*. (2016). <https://doi.org/10/gg68p2>.
- [282] J.H.L. Beal, A. Bubendorfer, T. Kemmitt, I. Hoek, W. Mike Arnold, A rapid, inexpensive surface treatment for enhanced functionality of polydimethylsiloxane microfluidic channels, *Biomicrofluidics*. 6 (2012). <https://doi.org/10/ggs7qd>.

- [283] L.M. Johnson, L. Gao, C. Shields IV, M. Smith, K. Efimenko, K. Cushing, J. Genzer, G.P. López, Elastomeric microparticles for acoustic mediated bioseparations, *J Nanobiotechnol.* 11 (2013) 22. <https://doi.org/10/f478kd>.
- [284] K.T.L. Trinh, H. Zhang, D.-J. Kang, S.-H. Kahng, B.D. Tall, N.Y. Lee, Fabrication of Polymerase Chain Reaction Plastic Lab-on-a-Chip Device for Rapid Molecular Diagnoses, *Int Neurourol J.* 20 (2016) S38-48. <https://doi.org/10/gg87p9>.
- [285] R.P.C.L. Sousa, B. Ferreira, M. Azenha, S.P.G. Costa, C.J.R. Silva, R.B. Figueira, PDMS Based Hybrid Sol-Gel Materials for Sensing Applications in Alkaline Environments: Synthesis and Characterization, *Polymers.* 12 (2020) 371. <https://doi.org/10/gg87qf>.
- [286] Y. Wen, L. Chen, J. Li, D. Liu, L. Chen, Recent advances in solid-phase sorbents for sample preparation prior to chromatographic analysis, *TrAC Trends in Analytical Chemistry.* 59 (2014) 26–41. <https://doi.org/10/f6dvhc>.
- [287] D.A. Skoog, D.M. West, S.R. Crouch, F.J. Holler, *Fundamentals of Analytical Chemistry*, Thomson-Brooks/Cole, 2013.
- [288] S. Lendor, G.A. Gómez-Ríos, E. Boyacı, H. Vander Heide, J. Pawliszyn, Space-Resolved Tissue Analysis by Solid-Phase Microextraction Coupled to High-Resolution Mass Spectrometry via Desorption Electrospray Ionization, *Anal. Chem.* 91 (2019) 10141–10148. <https://doi.org/10/gg8fsg>.

APPENDICES

A. Mass spectra of analytes

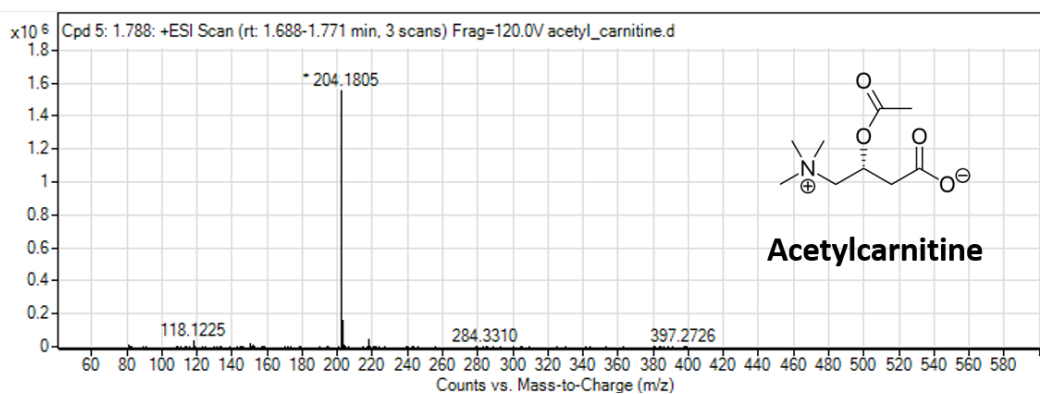


Figure A.1 Mass spectrum of acetylcarnitine

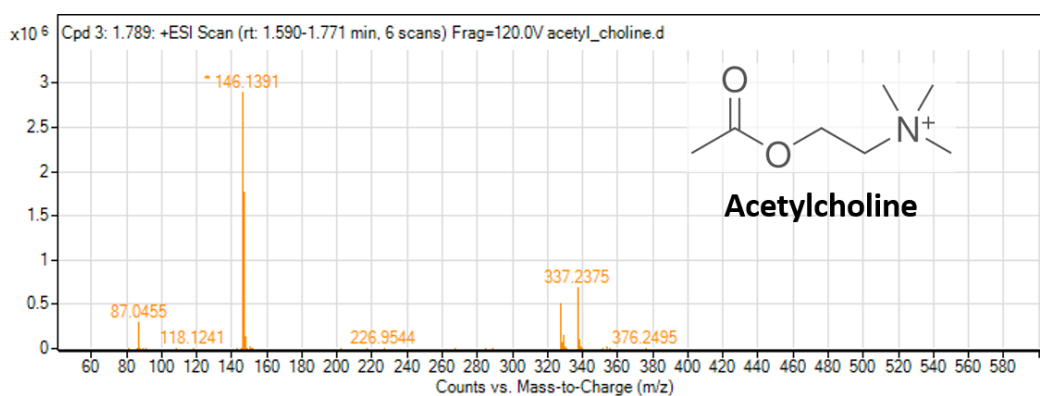


Figure A.2 Mass spectrum of acetylcholine

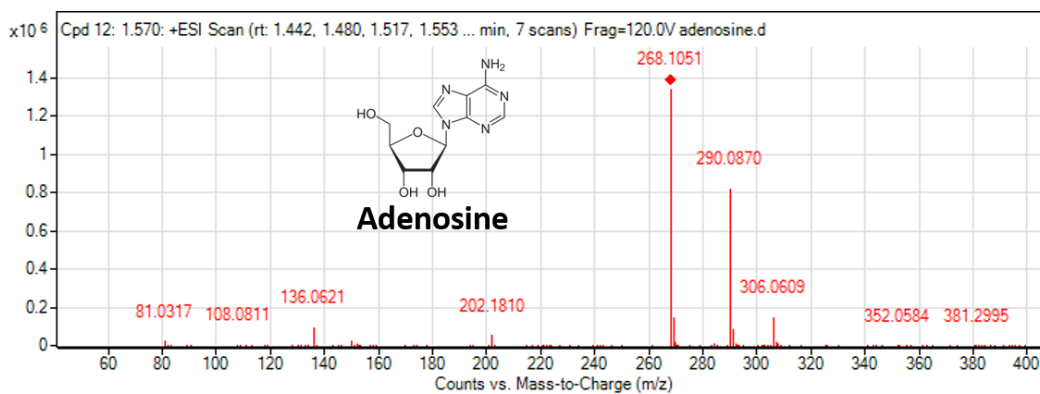


Figure A.3 Mass spectrum of adenosine

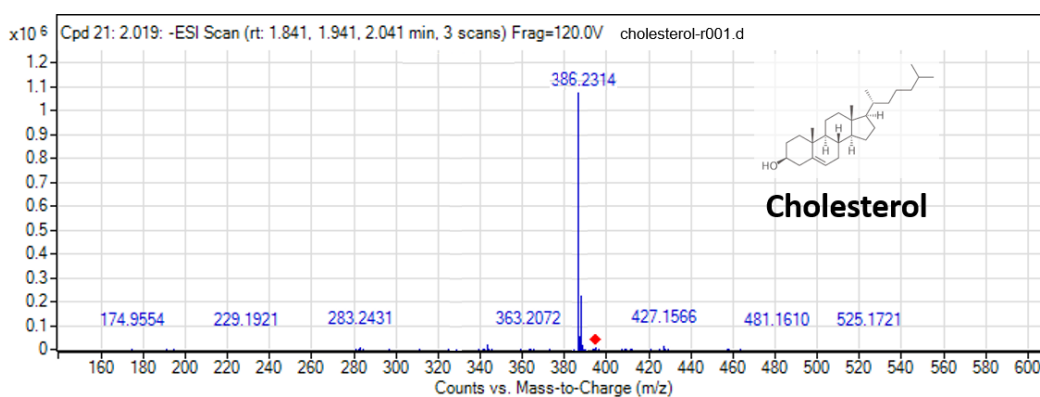


Figure A.4 Mass spectrum of cholesterol

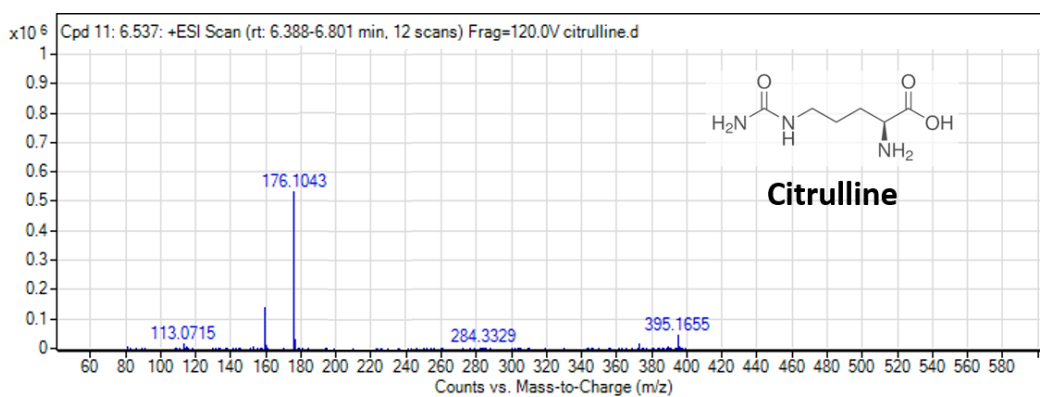


Figure A.5 Mass spectrum of citrulline

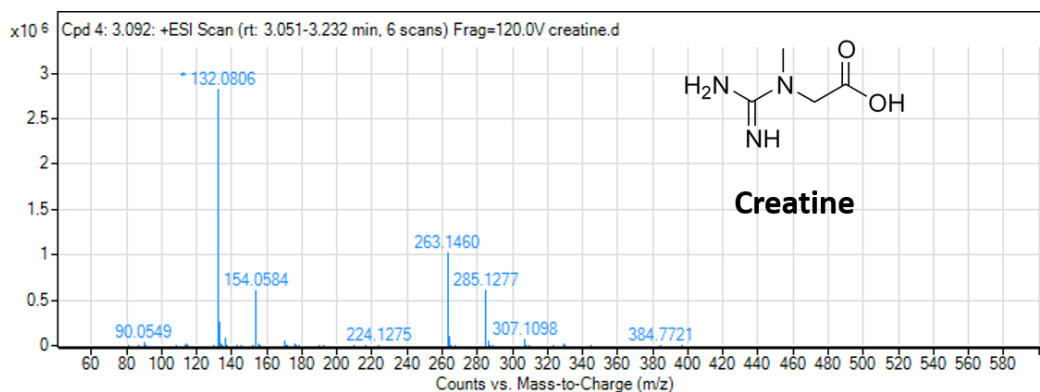


Figure A.6 Mass spectrum of creatine

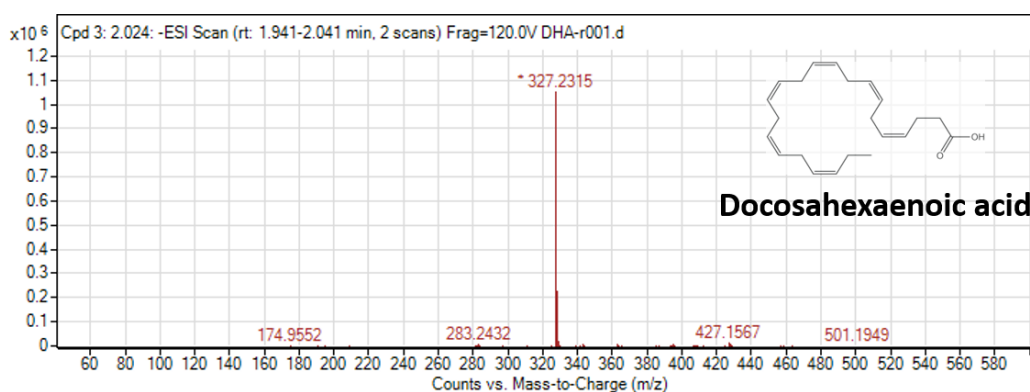


Figure A.7 Mass spectrum of DHA

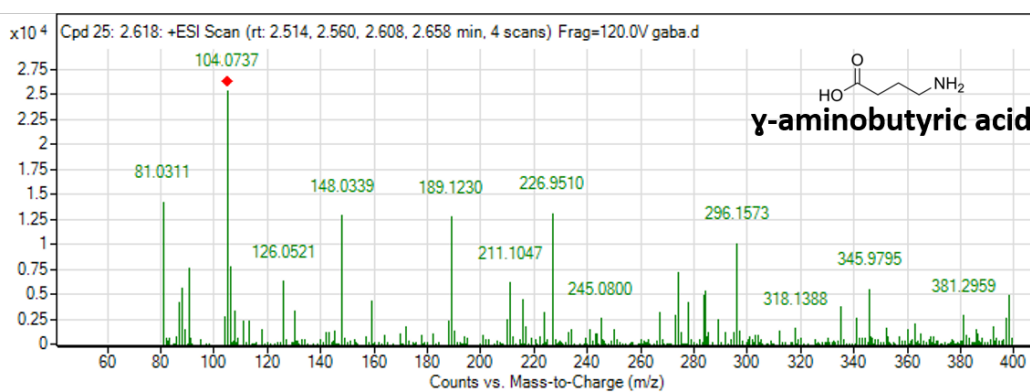


Figure A.8 Mass spectrum of GABA

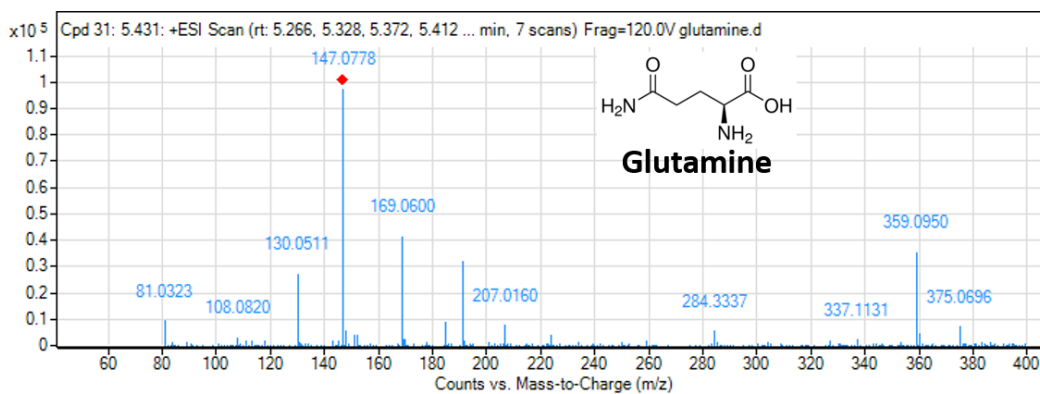


Figure A.9 Mass spectrum of glutamine

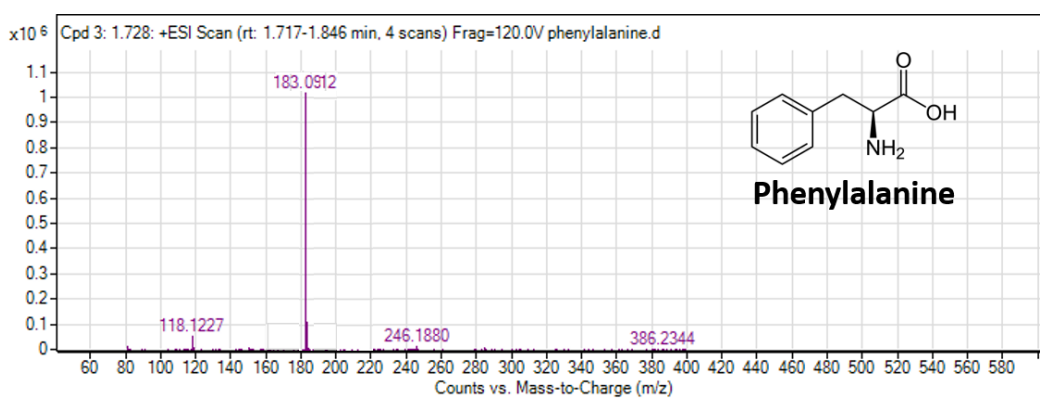


Figure A.10 Mass spectrum of phenylalanine

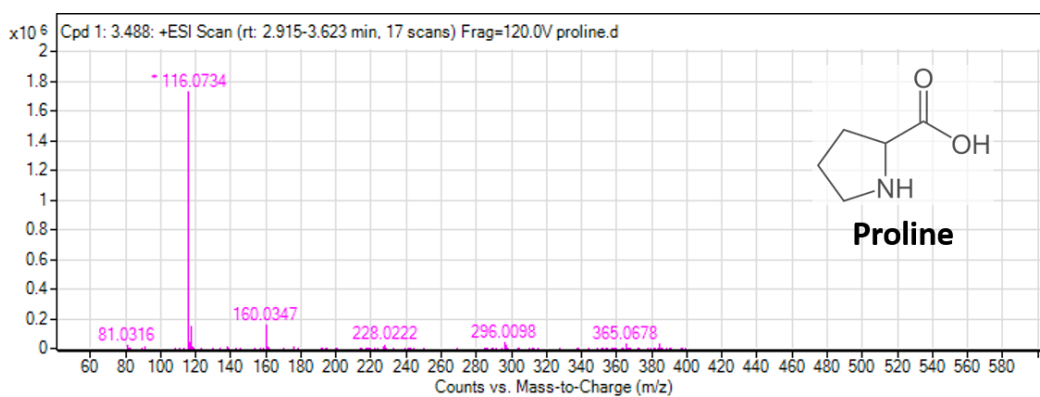


Figure A.11 Mass spectrum of proline

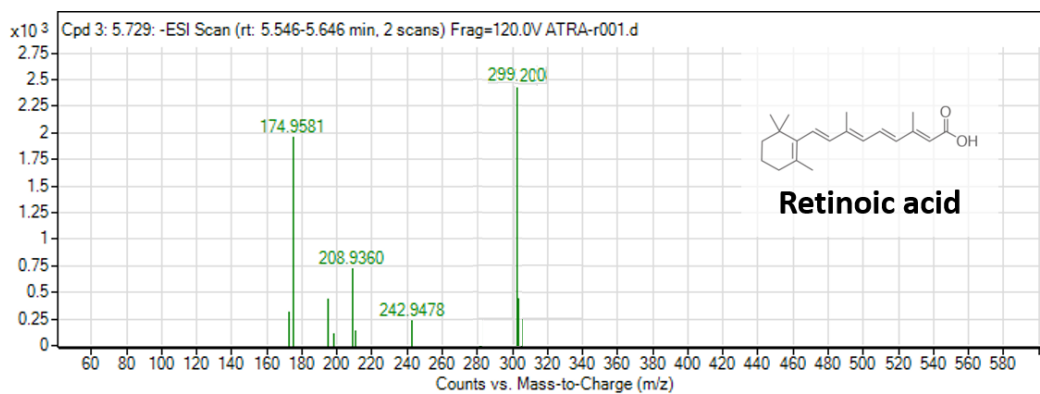


Figure A.12 Mass spectrum of retinoic acid

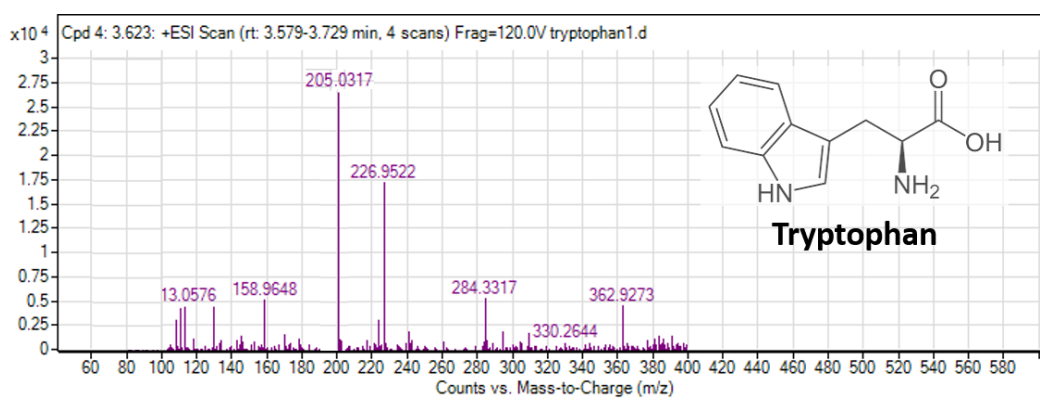


Figure A.13 Mass spectrum of tryptophan

B. Instrumental calibration curves for analytes

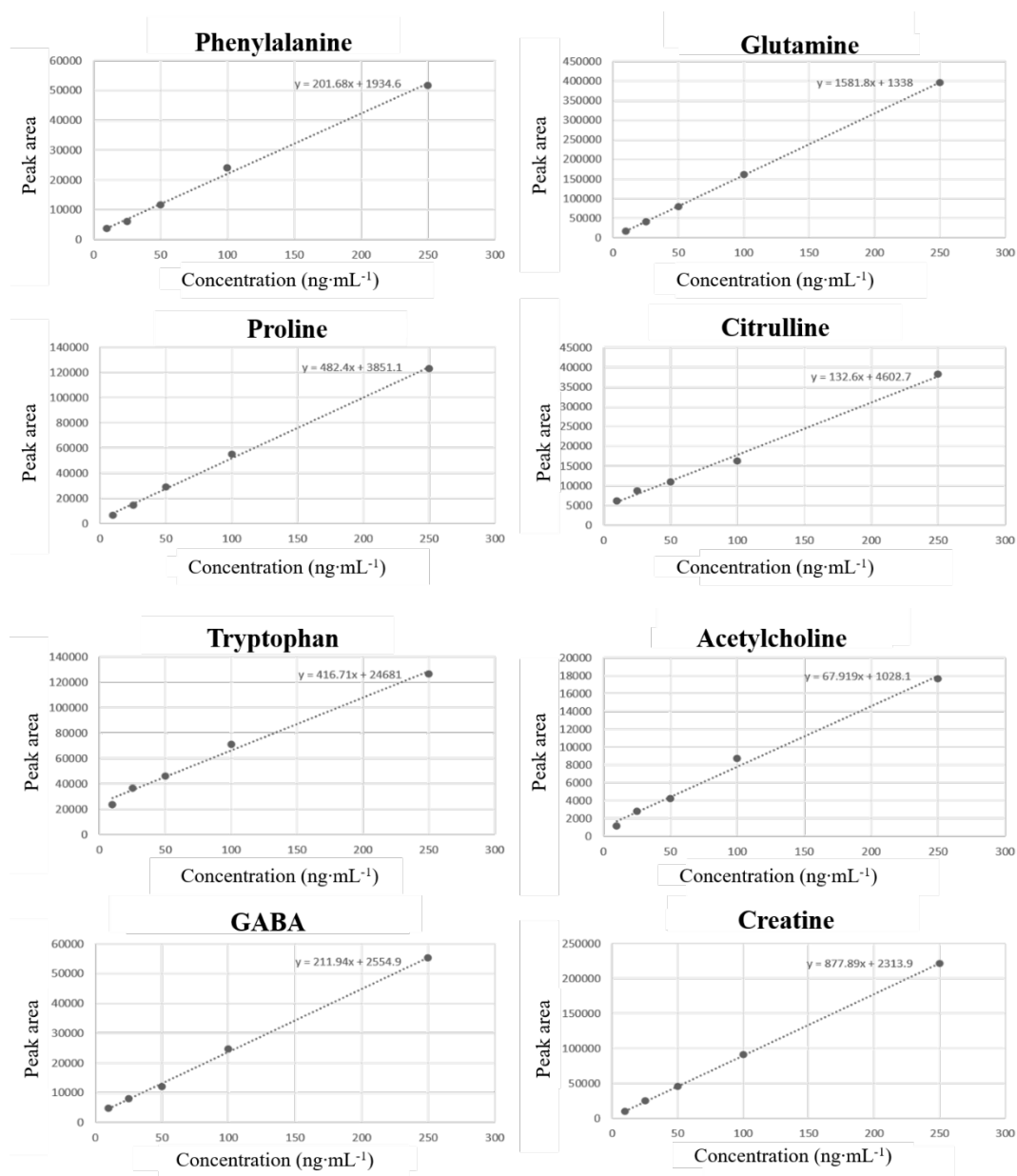


Figure B.1 Instrumental calibration curves for polar analytes (continued)

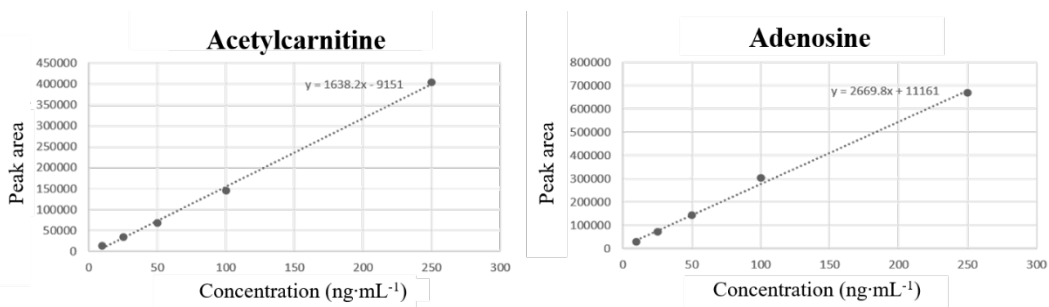


Figure B.1 Instrumental calibration curves for polar analytes (continued)

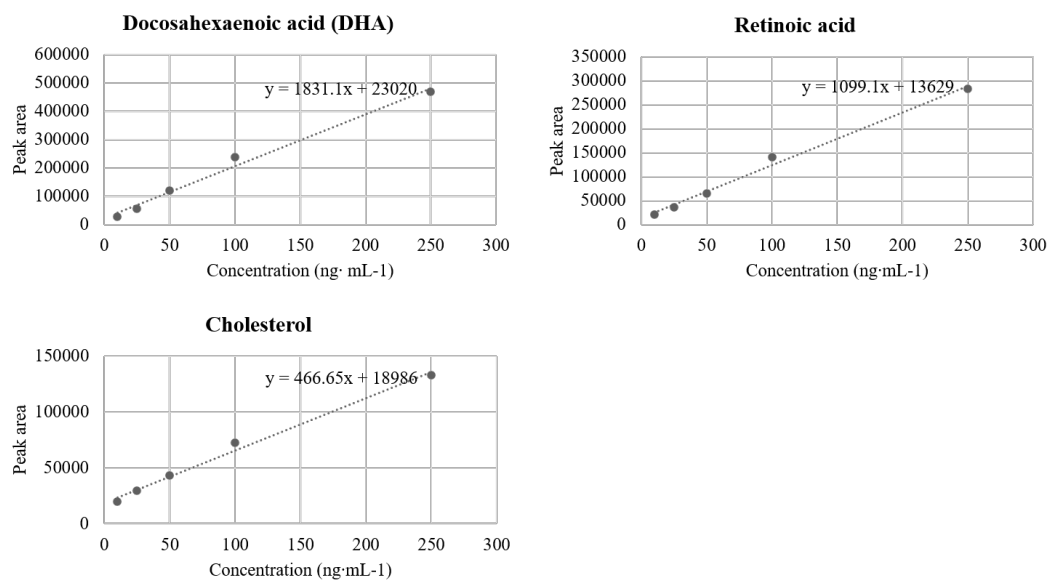


Figure B.2 Instrumental calibration curves for non-polar analytes